ADVANCEMENT OF ROTORDYNAMIC TOPICS

A Thesis

presented to

the Faculty of California Polytechnic State University,

San Luis Obispo

In Partial Fulfillment

of the Requirements for the Degree

Master of Science in Mechanical Engineering

by

Cameron Naugle

April 2018

COMMITTEE MEMBERSHIP

TITLE:	Advancement of Rotordynamic topics
AUTHOR:	Cameron Naugle
DATE SUBMITTED:	April 2018
COMMITTEE CHAIR:	Xi (Julia) Wu, Ph.D. Professor of Mechanical Engineering
COMMITTEE MEMBER:	Mohammad Noori Professor of Mechanical Engineering
COMMITTEE MEMBER:	Hemanth Porumamilla Professor of Mechanical Engineering
COMMITTEE MEMBER:	Peter Schuster Professor of Mechanical Engineering

ABSTRACT

Advancement of Rotordynamic topics

Cameron Naugle

In this thesis a basis for creating valuable rotordynamic models if formed. Theoretical models are formulated from the kinematic constraints to form a robust finite element model suited well for expansion. Analysis techniques for multiple degrees of freedom models with arbitrary damping are derived and demonstrated. These techniques include eigenvector and eigenvalue analysis of the complex state space equations. Furthermore, analysis techniques are developed for analyzing experimental data and comparing to theoretical models. All of the material is here to create a finite element model, compare its results to experimental results, and fine tune the design using stability analysis.

ACKNOWLEDGMENTS

Thanks to:

-

TABLE OF CONTENTS

LIST OF TABLES

LIST OF FIGURES

Chapter 1

FINITE ELEMENT METHOD FOR ROTORDYNAMIC SYSTEMS

In this chapter the Finite Element Method(FEM) will be employed in the simulation of rotordynamic systems. There are many advantages to using this discretizing method to solve problems of rotating machines. One of which is the generic form that the equation, and its parts take. The method lends itself to being able to easily create new matrices that can insert right into your equations of motion. Another, is the ability to move components around in space without the need to reevaluate the physics. Finally, the analysis techniques for Multiple Degree Of Freedom (MDOF) systems is wide reaching, and will serve to richly enhance our understanding of a complex system made of simple parts.

First, the beam element commonly refered to as the Timoshenko Beam Element will be derived from the kinematic and constitutive constraints. Then the solution to the resulting equation of motion will be discretized and variables separated in position and time to give the finite element equations of motion. Further, an extension to the beam element model is presented that will consider the viscous damping effects in the beam element. Equations for disks, bearings, and complex versions of all equations will be presented. Finally, the assembly and analysis of the model will result in intuitive figures that will be shown to compare well to experimental data.

1.1 Beam Element FE Equation

1.1.1 Timoshenko Beam Finite Element

The Timoshenko beam element allows for the beam cross section plane at any axis location to differ from normal with the axis of the beam. In other words, the element

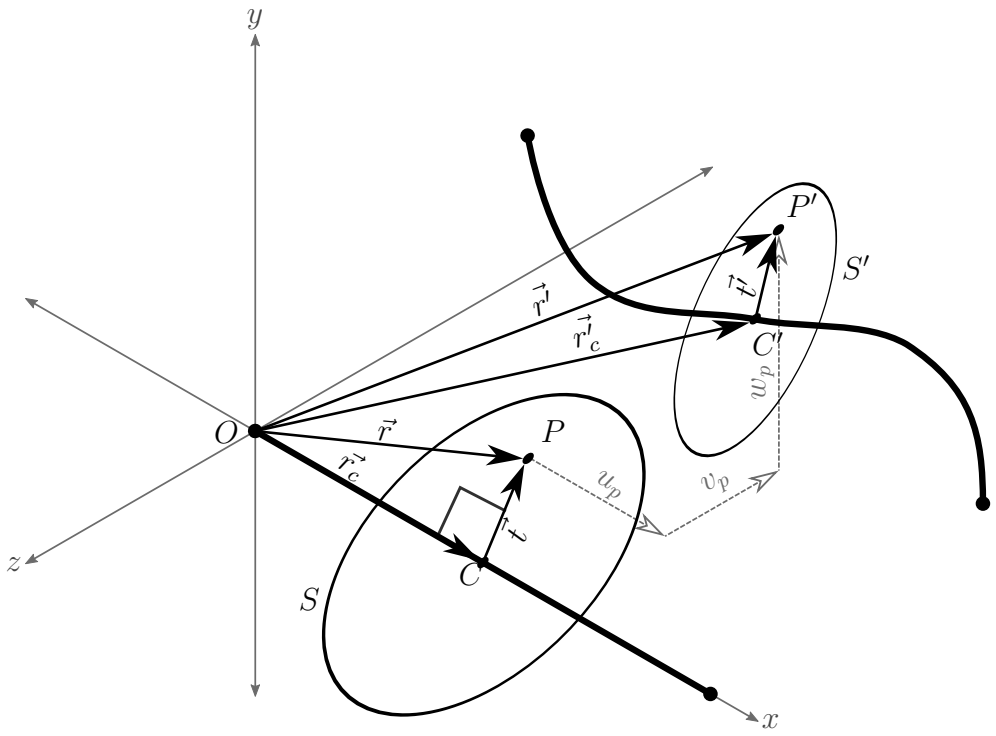

Figure 1.1: Beam Element with nodal displacements.

allows for shear stresses. This element often also includes the effects of rotary inertia and gyroscopic moments, as it will in this derivation. Generalized displacements used are assumed to be variable in both time and space. The element has six degrees of freedom. Three translation and three rotations all defined on the beam axis. So then all displacements are functions of time, t, and the axial spacial coordinate, x.

1.1.1.1 Kinematic Relationships

In order to develop the stresses and strains internal to the beam, and subsequently the equations of motion, the motion of some arbitrary point on the beam must be defined in terms of the generalized coordinates. Motion of two points is taken into consideration to assist in dividing the motion into a translation and a rotation. These points are shown in Figure 1.1. The first point, C, falls on the beam axis at location

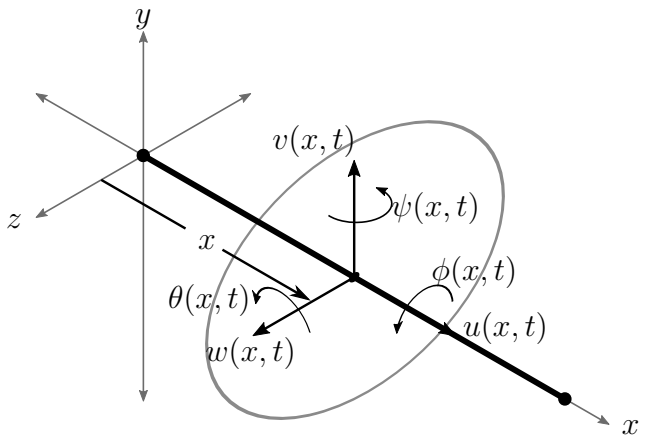

Figure 1.2: Timoshenko beam section with degrees of freedom at some point x along beam axis.

x, and in the undeformed configuration, the vector $\vec{r_c'} = \overrightarrow{OC}$ forms a right angle with the surface of the cross section. The second point, P is at some arbitrary (y, z) location on the cross section. The vecor $\vec{t} = \overrightarrow{CP}$ points from the beam axis to the point along the cross section. If we follow this point P we will be able to define the motion of the cross section as a whole, or more succinctly, to define the displacements u_p, v_p, w_p in terms of the coordinates $u, v, w, \psi, \theta,$ & ϕ. The motion of point P is split into translation and rotation, where $\vec{t}$ is rotated and $\vec{r_c}$ is translated to point to the deformed location P'. The vector pointing to P in the undeformed state is defined as

$$\vec{r} = \vec{r_c} + \vec{t} \tag{1.1}$$

Rotations are represented with a rotation transformation matrix,

$$\vec{t'} = \underline{R}\vec{t} \tag{1.2}$$

The linearized first order rotational matrix for small angles is represented by

$$\underline{R} = \begin{bmatrix} 1 & -\theta & \psi \\ \theta & 1 & -\phi \\ -\psi & \phi & 1 \end{bmatrix} \tag{1.3}$$

and the translation with a displacement vector

$$\vec{r_c'} = \vec{r_c} + \vec{u} \tag{1.4}$$

Combined motion from P to P' can be defined by

$$\vec{u}_p = \vec{r'} - \vec{r} \tag{1.5}$$

where $\vec{u}_p$ is the vector containing u_p, v_p, & w_p. The vector definitions for $\vec{r'}$ and $\vec{r}$ are substituted to the above equation to obtain

$$\vec{u}_p = \vec{r'_c} + \vec{t'} - \vec{r}_c + \vec{t} \tag{1.6}$$

and now using the definition for $\vec{u}$ and $\vec{t'}$ leads to the simplified expression for the motion of P

$$\vec{u}_p = \vec{u} + (\underline{R} - \underline{I})\vec{t} \tag{1.7}$$

expanding matrices reveals the equation

$$\vec{u}_p = \begin{Bmatrix} u_p \\ v_p \\ w_p \end{Bmatrix} = \begin{Bmatrix} u \\ v \\ w \end{Bmatrix} + \begin{bmatrix} 0 & -\theta & \psi \\ \theta & 0 & -\phi \\ -\psi & \phi & 0 \end{bmatrix} \begin{Bmatrix} 0 \\ y \\ z \end{Bmatrix} \tag{1.8}$$

Therefore, the motion of any point on the beam may be approximated with

$$\vec{u}_p = \begin{Bmatrix} u - \theta y + \psi z \\ v - \phi z \\ w + \phi y \end{Bmatrix} \tag{1.9}$$

1.1.1.2 Internal Constitutive Relationship

Stresses are assumed to exist in the beam in the axial direction, and in shear on the face of the beam section. Stresses in the transverse, or the y and z, directions are assumed negligible. Shear stresses out of the plane section are assumed to be vanishing as the differential element shrinks. Internal damping is to be considered independently from this material constitutive relationship. Written out, these stresses

are represented by the matrix

$$\sigma_{ij} = \begin{bmatrix} \sigma_{xx} & \sigma_{xy} & \sigma_{xz} \\ \sigma_{xy} & 0 & 0 \\ \sigma_{xz} & 0 & 0 \end{bmatrix} \tag{1.10}$$

using the Hooke's Law for a linear elastic isotropic material, expressed as

$$\epsilon_{ij} = \frac{1}{E}[(1+\nu)\sigma_{ij} - \nu\delta_{ij}\sigma_{kk}] \tag{1.11}$$

allows the determination of the stress strain relationship in engineering notation as

$$\begin{Bmatrix} \sigma_{xx} \\ \sigma_{xy} \\ \sigma_{xz} \end{Bmatrix} = \begin{bmatrix} E & 0 & 0 \\ 0 & 2G & 0 \\ 0 & 0 & 2G \end{bmatrix} \begin{Bmatrix} \epsilon_{xx} \\ \epsilon_{xy} \\ \epsilon_{xz} \end{Bmatrix} \tag{1.12}$$

where, $G = \frac{E}{2(1+\nu)}$. Strains are derived from displacements of equation (1.9) using a linear strain-displacement relationship for infinitesimal strains: $2\epsilon_{ij} = u_{i,j} + u_{j,i}$.

$$\begin{cases} \epsilon_{xx} = u' - \theta' y + \psi' z \\ \epsilon_{xy} = \frac{1}{2}(v' - \phi' z - \theta) \\ \epsilon_{xz} = \frac{1}{2}(w' + \phi' y + \psi) \end{cases} \tag{1.13}$$

Note that in the case of the Euler-Bernoulli beam derivation the slope in a transverse direction displacement is equal to the rotation angle about the orthogonal transverse axis, i.e., $v' = \theta$ and $w' = \psi$. Application of those would reduce the system to the Euler-Bernoulli beam.

It will be proven useful to introduce generalized strains that group strain contributions above as axial, bending, torsion, and shear, represented by the symbols ε, ρ,

φ, γ,respectively.

$$\begin{cases} \varepsilon = u' \\ \rho_y = -\theta' \\ \rho_z = \psi' \\ \varphi = \phi' \\ \gamma_y = v' - \theta \\ \gamma_z = w' + \psi \end{cases} \tag{1.14}$$

allowing the representation of the strains from eq (1.13) using the generalized strains as:

$$\begin{cases} \epsilon_{xx} = \varepsilon + \rho_y y + \rho_z z \\ \epsilon_{xy} = \frac{1}{2}(\gamma_y - \varphi z) \\ \epsilon_{xz} = \frac{1}{2}(\gamma_z + \varphi y) \end{cases} \tag{1.15}$$

Now the stresses in equation (1.12) can be represented with the displacements as

$$\begin{Bmatrix} \sigma_{xx} \\ \sigma_{xy} \\ \sigma_{xz} \end{Bmatrix} = \begin{Bmatrix} E(u' - \theta' y + \psi' z) \\ G(v' - \phi' z - \theta) \\ G(w' + \phi' y + \psi) \end{Bmatrix} = \begin{Bmatrix} E(\varepsilon + \rho_y y + \rho_z z) \\ G(\gamma_y - \varphi z) \\ G(\gamma_z + \varphi y) \end{Bmatrix} \tag{1.16}$$

$$U = \int_V \sigma_{ij} \epsilon_{ij} dV \tag{1.17}$$

Now the inner product of the total virtual strain energy can be expanded

$$U = \int_V \left[\sigma_{xx} \epsilon_{xx} + 2\sigma_{xy} \epsilon_{xy} + 2\sigma_{xz} \epsilon_{xz} \right] dV \tag{1.18}$$

Then expand virtual strains into the generalized strains corresponding to the degrees of freedom of the beam element and collect terms on generalized strains

$$U = \int_V \left[\sigma_{xx} \varepsilon + \sigma_{xx} y \rho_y + \sigma_{xx} z \rho_z + \sigma_{xy} \gamma_y + \sigma_{xz} \gamma_z + (\sigma_{xz} y - \sigma_{xy} z) \varphi \right] dV \tag{1.19}$$

this internal mechanical energy expression allows us to recognize stresses conjugate with each generalized strain as the corresponding stress for that phenomena. Integration allows the determination of the forces and moments related to each generalized

strain as

$$\begin{cases} N = & \int_A \sigma_{xx} dA & = E(A\varepsilon + S_y\rho_y + S_z\rho_z) \\ M_y = & \int_A \sigma_{xx} z dA & = E(S_z\varepsilon + I_{xy}\rho_y + I_y\rho_z) \\ M_z = & \int_A \sigma_{xx} y dA & = E(S_y\varepsilon + I_z\rho_y + I_{xy}\rho_z) \\ Q_y = & \int_A \sigma_{xy} dA & = \kappa G(A\gamma_y - S_z\varphi) \\ Q_z = & \int_A \sigma_{xz} dA & = \kappa G(A\gamma_z + S_y\varphi) \\ M_x = & \int_A (\sigma_{xz} y - \sigma_{xy} z) dA & = \kappa G\left(A_y\gamma_z - A_z\gamma_y + J_x\varphi\right) \end{cases} \tag{1.20}$$

$$\text{where, } \begin{cases} \kappa = \frac{6(1+\nu)}{7+6\nu}, \textit{for circular cross sections.} \\ A = \int_A dA \quad S_y = \int_A y dA \\ S_z = \int_A z dA \quad I_y = \int_A z^2 dA \\ I_z = \int_A y^2 dA \quad J_x = I_y + I_z \end{cases}$$

κ is the shear coefficient which attempts to correct for the fact that the shear strain is not constant over the beam cross section. Assuming the central axis of the beam is coincident with the shear center, then $A_y = A_z = I_{xy} = 0$. Which simplifies the conjugate forces to

$$\begin{cases} N = EA\varepsilon & = EAu' \\ M_y = EI_y\rho_z & = EI_y\psi' \\ M_z = EI_z\rho_y & = -EI_z\theta' \\ Q_y = \kappa GA\gamma_y & = \kappa GA(v' - \theta) \\ Q_z = \kappa GA\gamma_z & = \kappa GA(w' + \psi) \\ M_x = \kappa GJ_x\varphi & = \kappa GJ_x\phi' \end{cases} \tag{1.21}$$

1.1.1.3 Differential Equations of Motion

Now the equations are motion are derived for the Timoshenko beam element. External forces are not included in this derivation. Though they may easily be added to the

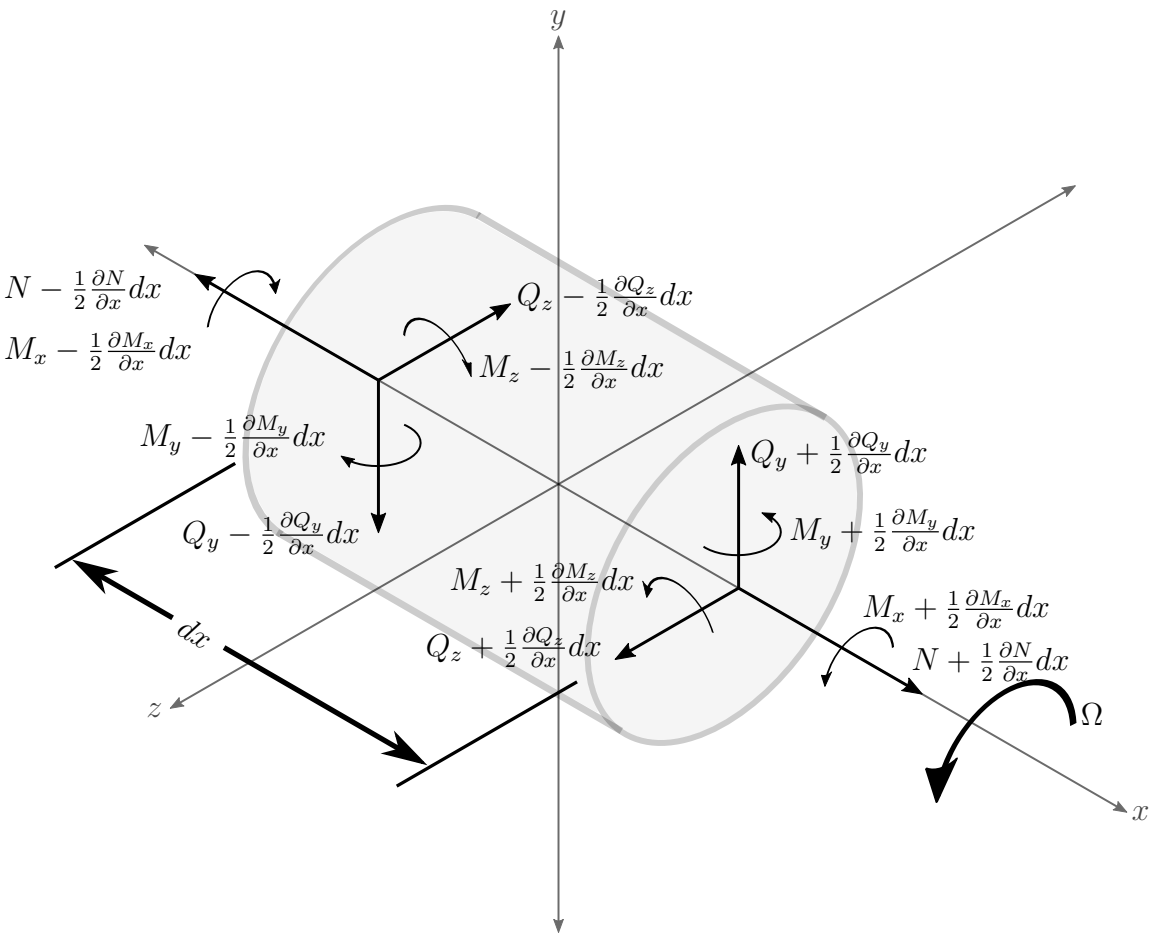

Figure 1.3: Beam differential element with generalized forces.

diagram of figure 1.3 and included in the analysis. It is also assumed that the cross section remains planar during deformation and the material properties are homogeneous through time and space. The derivation is the same as for a Euler-Bernoulli beam with the exception of the constitutive relations used at the end and the inclusion of torsion and axial degrees of freedom. Using conservation of momentum and conservation of the moment of momentum a relationship between inertia and internal forces is developed. Applying summation of forces in the x-direction

$$(N + \frac{1}{2}\frac{\partial N}{\partial x}dx) - (N - \frac{1}{2}\frac{\partial N}{\partial x}dx) = \rho A dx \frac{\partial^2 u}{\partial x^2} \tag{1.22}$$

by Simplifying the above equation, and performing the same steps for the other directions and moments we get

$$\begin{cases} \frac{\partial N}{\partial x} = \rho A \frac{\partial^2 u}{\partial x^2} \\ \frac{\partial Q_y}{\partial x} = \rho A \frac{\partial^2 v}{\partial x^2} \\ \frac{\partial Q_z}{\partial x} = \rho A \frac{\partial^2 w}{\partial x^2} \\ \frac{\partial M_y}{\partial x} - Q_z = \rho I_y \frac{\partial^2 \psi}{\partial x^2} + \rho J_x \Omega \frac{\partial \theta}{\partial x} \\ \frac{\partial M_z}{\partial x} + Q_y = \rho I_z \frac{\partial^2 \theta}{\partial x^2} - \rho J_x \Omega \frac{\partial \psi}{\partial x} \\ \frac{\partial M_x}{\partial x} = \rho J_x \frac{\partial^2 \phi}{\partial x^2} \end{cases} \tag{1.23}$$

Gyroscopic moments have been explicitly added to the summations in the appropriate equations. The generalized forces of equation (1.21) are substituted in the equilibrium equations (1.23)

$$\begin{cases} EAu'' = \rho A \ddot{u} & \text{(1.24a)} \\ \kappa GA(v'' - \theta') = \rho A \ddot{v} & \text{(1.24b)} \\ \kappa GA(w'' + \psi') = \rho A \ddot{w} & \text{(1.24c)} \\ EI_y \psi'' - \kappa GA(w' + \psi) = \rho I_y \ddot{\psi} + \rho J_x \Omega \dot{\theta} & \text{(1.24d)} \\ EI_z \theta'' + \kappa GA(v' - \theta) = \rho I_z \ddot{\theta} - \rho J_x \Omega \dot{\psi} & \text{(1.24e)} \\ \kappa GJ_x \phi'' = \rho J_x \ddot{\phi} & \text{(1.24f)} \end{cases}$$

In matrix form, this system of equations can be represented by this equation

$$\underline{\mathcal{M}}^e \ddot{\vec{\mathbf{u}}} + \Omega \underline{\mathcal{G}}^e \dot{\vec{\mathbf{u}}} - \left(\frac{\partial()}{\partial x} \underline{\mathcal{S}}^e - \underline{\mathcal{P}}^e \underline{\mathcal{S}}^e \right) \vec{\mathbf{u}} = 0 \tag{1.25}$$

where,

$$\begin{cases} \underline{\mathcal{M}}^e = \begin{bmatrix} \rho A & 0 & 0 & 0 & 0 & 0 \\ 0 & \rho A & 0 & 0 & 0 & 0 \\ 0 & 0 & \rho I_y & 0 & 0 & 0 \\ 0 & 0 & 0 & \rho I_z & 0 & 0 \\ 0 & 0 & 0 & 0 & \rho A & 0 \\ 0 & 0 & 0 & 0 & 0 & \rho J_x \end{bmatrix} \quad \underline{\mathcal{G}}^e = \begin{bmatrix} 0 & 0 & 0 & 0 & 0 & 0 \\ 0 & 0 & 0 & 0 & 0 & 0 \\ 0 & 0 & 0 & \rho J_x & 0 & 0 \\ 0 & 0 & -\rho J_x & 0 & 0 & 0 \\ 0 & 0 & 0 & 0 & 0 & 0 \\ 0 & 0 & 0 & 0 & 0 & 0 \end{bmatrix} \\ \underline{\mathcal{P}}^e = \begin{bmatrix} 0 & 0 & 0 & 0 & 0 & 0 \\ 0 & 0 & 0 & 0 & 0 & 0 \\ 0 & 1 & 0 & 0 & 0 & 0 \\ -1 & 0 & 0 & 0 & 0 & 0 \\ 0 & 0 & 0 & 0 & 0 & 0 \\ 0 & 0 & 0 & 0 & 0 & 0 \end{bmatrix} \quad \underline{\mathcal{S}}^e = \begin{bmatrix} \kappa GA\frac{\partial()}{\partial x} & 0 & 0 & -\kappa GA & 0 & 0 \\ 0 & \kappa GA\frac{\partial()}{\partial x} & \kappa GA & 0 & 0 & 0 \\ 0 & 0 & EI_y\frac{\partial()}{\partial x} & 0 & 0 & 0 \\ 0 & 0 & 0 & EI_z\frac{\partial()}{\partial x} & 0 & 0 \\ 0 & 0 & 0 & 0 & EA\frac{\partial()}{\partial x} & 0 \\ 0 & 0 & 0 & 0 & 0 & \kappa GJ_x\frac{\partial()}{\partial x} \end{bmatrix} \end{cases} \tag{1.26}$$

and $\vec{\mathbf{u}} = [v, w, \psi, \theta, u, \phi]^\intercal$ The principle of virtual displacements is utilized on the equations of motion to obtain the weak for of the equations of motion and integrated over the length of the beam.

$$\int_0^l \delta\vec{\mathbf{u}}^\intercal \underline{\mathcal{M}}^e \ddot{\vec{\mathbf{u}}} dx + \int_0^l \delta\vec{\mathbf{u}}^\intercal \Omega \underline{\mathcal{G}}^e \dot{\vec{\mathbf{u}}} - \int_0^l \delta\vec{\mathbf{u}}^\intercal \frac{\partial()}{\partial x} \underline{\mathcal{S}}^e \vec{\mathbf{u}} dx + \int_0^l \delta\vec{\mathbf{u}}^\intercal \underline{\mathcal{P}} \underline{\mathcal{S}}^e \vec{\mathbf{u}} dx = 0 \tag{1.27}$$

integration by parts on the third term and replacing $\underline{\mathcal{S}}$ with $\underline{\mathcal{D}}^e\underline{\mathcal{B}}$, and making use of the Identity matrix, $\underline{\mathbf{I}}$ where $\frac{\partial()}{\partial x}\underline{\mathbf{I}}$ is interpreted here as if the partial was a scalar

$$\int_0^l \delta\vec{\mathbf{u}}^\intercal \underline{\mathcal{M}}^e \ddot{\vec{\mathbf{u}}} dx + \Omega \int_0^l \delta\vec{\mathbf{u}}^\intercal \underline{\mathcal{G}}^e \dot{\vec{\mathbf{u}}} + \int_0^l \delta\vec{\mathbf{u}}^\intercal \left(\frac{\partial()}{\partial x}\underline{\mathbf{I}} + \underline{\mathcal{P}} \right) \underline{\mathcal{D}}^e \underline{\mathcal{B}} \vec{\mathbf{u}} dx = 0 \tag{1.28}$$

$$\underline{\mathcal{D}}^e = \begin{bmatrix} \kappa GA & 0 & 0 & 0 & 0 & 0 \\ 0 & \kappa GA & 0 & 0 & 0 & 0 \\ 0 & 0 & EI_y & 0 & 0 & 0 \\ 0 & 0 & 0 & EI_z & 0 & 0 \\ 0 & 0 & 0 & 0 & EA & 0 \\ 0 & 0 & 0 & 0 & 0 & \kappa GJ_x \end{bmatrix} \quad \& \quad \underline{\mathcal{B}} = \begin{bmatrix} \frac{\partial()}{\partial x} & 0 & 0 & -1 & 0 & 0 \\ 0 & \frac{\partial()}{\partial x} & 1 & 0 & 0 & 0 \\ 0 & 0 & \frac{\partial()}{\partial x} & 0 & 0 & 0 \\ 0 & 0 & 0 & \frac{\partial()}{\partial x} & 0 & 0 \\ 0 & 0 & 0 & 0 & \frac{\partial()}{\partial x} & 0 \\ 0 & 0 & 0 & 0 & 0 & \frac{\partial()}{\partial x} \end{bmatrix} \tag{1.29}$$

Notice that $\frac{\partial()}{\partial x}\underline{I} + \underline{\mathcal{P}} = \underline{\mathcal{B}}^\intercal$ so the equation of motion becomes

$$\int_0^l \delta\vec{\mathbf{u}}^\intercal \underline{\mathcal{M}}^e \ddot{\vec{\mathbf{u}}} dx + \Omega \int_0^l \delta\vec{\mathbf{u}}^\intercal \underline{\mathcal{G}}^e \dot{\vec{\mathbf{u}}} + \int_0^l \delta\vec{\mathbf{u}}^\intercal \underline{\mathcal{B}}^\intercal \underline{\mathcal{D}}^e \underline{\mathcal{B}} \vec{\mathbf{u}} dx = 0 \tag{1.30}$$

$\underline{\mathcal{M}}^e$ is the inertia of the element, $\underline{\mathcal{G}}^e$ is the rotating inertia, $\underline{\mathcal{D}}^e$ is the material stress-strain relationship, and $\underline{\mathcal{B}}^e$ is the strain-displacement operator. The solution of this differential system motivates a separation of variables that will be discussed in the next section.

1.1.1.4 Shape Functions

The displacements thus far have been assumed to be functions of both position and time. Now the total displacement is separated into functions that depend on time and functions that depend on position. This is a fundamental part of the discretization of the beam element, and the use the finite element method.

$$\begin{cases} \vec{\mathbf{u}}(x,t) &= \underline{\mathbf{N}}(x)\vec{\mathbf{q}}(t) \\ \dot{\vec{\mathbf{u}}}(x,t) &= \underline{\mathbf{N}}(x)\dot{\vec{\mathbf{q}}}(t) \\ \ddot{\vec{\mathbf{u}}}(x,t) &= \underline{\mathbf{N}}(x)\ddot{\vec{\mathbf{q}}}(t) \\ \delta\vec{\mathbf{u}}(x,t) &= \underline{\mathbf{N}}(x)\delta\vec{\mathbf{q}}(t) \end{cases} \tag{1.31}$$

where, $\vec{\mathbf{u}} = [v, w, -\psi, \theta, u, \phi]^\intercal$ & $\vec{\mathbf{q}} = [v_1, w_1, -\psi_1, \theta_1, v_2, w_2, -\psi_2, \theta_2, u_1, \phi_1, u_2, \phi_2]^\intercal$. This specfic order of $\vec{\mathbf{q}}$ is chosen with u and ϕ at the end to ease the condensation of the axial and torsional degrees of freedom out of the system if their use is not necessary for the system of interest. ψ angles are defined as negative to allow for the same stiffness matrix to define the motion in both planes, and more importantly, to allow for the use of the complex plane to simplify the problem. The shape functions $\underline{\mathbf{N}}(x)$ interpolate the displacements between the beam ends. These functions must must solve the static portion of the differential equations (1.24). These shape functions are chosen as a polynomials that satisfy the boundary nodal displacements and rotations at the ends of a beam element. These nodal degrees of freedom, depicted in Figure 1.4 are considered to be interpolated through the beam element by the shape functions. Interpolation functions chosen are listed in Equation (1.32). Axial displacement, u, and torsional rotation, ϕ are independent, so their shape functions are

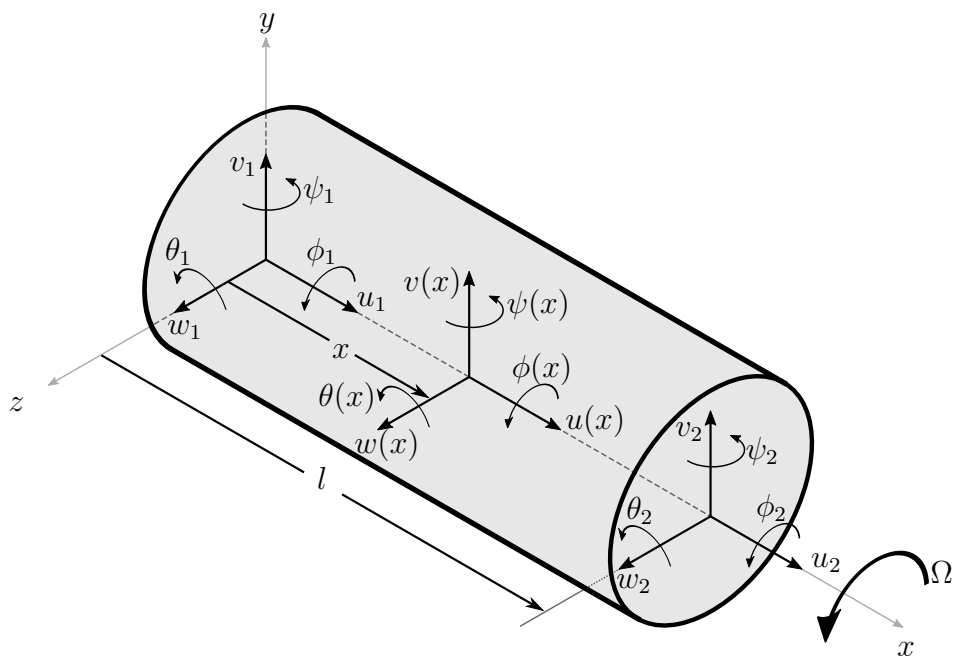

Figure 1.4: Beam Element with nodal displacements.

chosen as polynomials that satisfy the differential equation. Conversely, transverse displacements, v & w, and bending rotations, ψ & θ are coupled. Coupling of the shape functions has been proven to reduce some negative effects of linearly interpolated elements [25]. Polynomial functions are chosen for v & w and their rotational counterparts are derived using the differential relations.

$$\begin{cases} u = c_1 + c_2 x & \text{(1.32a)} \\ v = c_3 + c_4 x + c_5 x^2 + c_6 x^3 & \text{(1.32b)} \\ w = c_7 + c_8 x + c_9 x^2 + c_{10} x^3 & \text{(1.32c)} \\ \phi = c_{11} + c_{12} x & \text{(1.32d)} \end{cases}$$

$c_{1,2,\ldots}$ are the unknown constants of the polynomial solutions. Using transverse displacement of equations (1.32b) & (1.32c) in the differential equations (1.24b), (1.24c),

(1.24d), (1.24e) the interpolation functions of bending rotations are derived as:

$$\begin{cases} \psi = K_y c_{10} - c_8 - 2c_9 x - 3c_{10} x^2 & \text{(1.33a)} \\ \theta = K_z c_6 + c_4 + 2c_5 x + 3c_6 x^2 & \text{(1.33b)} \end{cases}$$

where, $K_y = \frac{6EI_y}{\kappa GA}$& $K_z = \frac{6EI_z}{\kappa GA}$ Boundary Conditions Boundary conditions for the interpolation polynomials of equations (1.32) & (1.33) are defined as the components of the vector $\vec{\mathbf{q}} u_j = u(x_j)$ and similarily for other degrees of freedom. Where, $j = 1, 2$ and defines the two states. In this derivation, $x_1 = 0$ and $x_2 = l$. Application of these boundary condition results in this relation between the polynomial constants and the boundary conditions.

$$\begin{Bmatrix} u_1 \\ u_2 \\ v_1 \\ v_2 \\ w_1 \\ w_2 \\ \psi_1 \\ \psi_2 \\ \theta_1 \\ \theta_2 \\ \phi_1 \\ \phi_2 \end{Bmatrix} = \begin{bmatrix} 1 & 0 & 0 & 0 & 0 & 0 & 0 & 0 & 0 & 0 & 0 & 0 \\ 1 & l & 0 & 0 & 0 & 0 & 0 & 0 & 0 & 0 & 0 & 0 \\ 0 & 0 & 1 & 0 & 0 & 0 & 0 & 0 & 0 & 0 & 0 & 0 \\ 0 & 0 & 1 & l & l^2 & l^3 & 0 & 0 & 0 & 0 & 0 & 0 \\ 0 & 0 & 0 & 0 & 0 & 0 & 1 & 0 & 0 & 0 & 0 & 0 \\ 0 & 0 & 0 & 0 & 0 & 0 & 1 & l & l^2 & l^3 & 0 & 0 \\ 0 & 0 & 0 & 0 & 0 & 0 & 0 & -1 & 0 & -K_y & 0 & 0 \\ 0 & 0 & 0 & 0 & 0 & 0 & 0 & -1 & -2l & -K_y - 3l^2 & 0 & 0 \\ 0 & 0 & 0 & 1 & 0 & K_z & 0 & 0 & 0 & 0 & 0 & 0 \\ 0 & 0 & 0 & 1 & 2l & K_z + 3l^2 & 0 & 0 & 0 & 0 & 0 & 0 \\ 0 & 0 & 0 & 0 & 0 & 0 & 0 & 0 & 0 & 0 & 1 & 0 \\ 0 & 0 & 0 & 0 & 0 & 0 & 0 & 0 & 0 & 0 & 1 & l \end{bmatrix} \begin{Bmatrix} c_1 \\ c_2 \\ c_3 \\ c_4 \\ c_5 \\ c_6 \\ c_7 \\ c_8 \\ c_9 \\ c_{10} \\ c_{11} \\ c_{12} \end{Bmatrix} \quad \text{(1.34)}$$

Inversion of this matrix results in a system of equations defining the constant c_1 through c_{12}. These constants are then substituted in to the polynomial expressions

(1.32) & (1.33) giving the interpolations as functions of the nodal displacements.

$$\begin{cases} u = N_1 u_1 + N_2 u_2 \\ v = T_{t_1 y} v_1 + T_{t_2 y} v_2 + T_{r_1 y} \theta_1 + T_{r_2 y} \theta_2 \\ w = T_{t_1 z} w_1 + T_{t_2 w} w_2 + T_{r_1 z} \psi_1 + T_{r_2 z} \psi_2 \\ \psi = R_{t_1 z} w_1 + R_{t_2 w} w_2 + R_{r_1 z} \psi_1 + R_{r_2 z} \psi_2 \\ \theta = R_{t_1 y} v_1 + R_{t_2 y} v_2 + R_{r_1 y} \theta_1 + R_{r_2 y} \theta_2 \\ \phi = N_1 \phi_1 + N_2 \phi_2 \end{cases} \tag{1.35}$$

with;

$$\begin{cases} N_1 = 1 - \zeta & N_2 = \zeta \\ T_{t_1 y,z} = \frac{1}{1+\alpha_{y,z}}(2\zeta^3 - 3\zeta^2 - \alpha_{y,z}\zeta + 1 + \alpha_{y,z}) & T_{t_2 y,z} = \frac{1}{1+\alpha_{y,z}}(-2\zeta^3 + 3\zeta^2 + \alpha_{y,z}\zeta) \\ T_{r_1 y,z} = \frac{l}{1+\alpha_{y,z}}[\zeta^3 - (2 + \frac{1}{2}\alpha_{y,z})\zeta^2 + (1 + \frac{1}{2}\alpha_{y,z})\zeta] & T_{r_2 y,z} = \frac{l}{1+\alpha_{y,z}}[\zeta^3 - (1 - \frac{1}{2}\alpha_{y,z})\zeta^2 - \frac{1}{2}\alpha_{y,z}\zeta] \\ R_{t_1 y,z} = \frac{6/l}{1+\alpha_{y,z}}(\zeta^2 - \zeta) & R_{t_2 y,z} = \frac{6/l}{1+\alpha_{y,z}}(-\zeta^2 + \zeta) \\ R_{r_1 y,z} = \frac{1}{1+\alpha_{y,z}}(3\zeta^2 - (4 + \alpha_{y,z})\zeta + 1 + \alpha_{y,z}) & R_{r_2 y,z} = \frac{1}{1+\alpha_{y,z}}(3\zeta^2 - (2 - \alpha_{y,z})\zeta) \end{cases} \tag{1.36}$$

where, $\alpha_y = 2K_y/l^2 = \frac{12EI_y}{\kappa GAl^2}$, $\alpha_z = 2K_z/l^2 = \frac{12EI_z}{\kappa GAl^2}$, & $\zeta = x/l$. (1.35) is expressed in matrix form as it appears in (1.31) where

$$\underline{\mathbf{N}}(x) = \begin{bmatrix} T_{t_1 y} & 0 & 0 & T_{r_1 y} & T_{t_2 y} & 0 & 0 & T_{r_2 y} & 0 & 0 & 0 & 0 \\ 0 & T_{t_1 z} & T_{r_1 z} & 0 & 0 & T_{t_2 z} & T_{r_2 z} & 0 & 0 & 0 & 0 & 0 \\ 0 & R_{t_1 z} & R_{r_1 z} & 0 & 0 & R_{t_2 z} & R_{r_2 z} & 0 & 0 & 0 & 0 & 0 \\ R_{t_1 y} & 0 & 0 & R_{r_1 y} & R_{t_2 y} & 0 & 0 & R_{r_2 y} & 0 & 0 & 0 & 0 \\ 0 & 0 & 0 & 0 & 0 & 0 & 0 & 0 & N_1 & 0 & N_2 & 0 \\ 0 & 0 & 0 & 0 & 0 & 0 & 0 & 0 & 0 & N_1 & 0 & N_2 \end{bmatrix} \tag{1.37}$$

still with the generalized displacement vector $\vec{\mathbf{q}} = [v_1, w_1, -\psi_1, \theta_1, v_2, w_2, -\psi_2, \theta_2, u_1, \phi_1, u_2, \phi_2]^{\intercal}$

Shape functions depend on the term α which is sometimes called the shear correction factor. This shear correction factor is proportional to the square of the ratio of radius to length of the beam element. So, as the length increases relative to the radius, α tends to zero. It will be evident in the following section that as α approaches

zero, the equations of motion approach the equations of the Bernoulli-Euler beam. A spatial representation of the shape functions of equation (1.36) is given in figure 1.5. Shape functions plotted with respect to the non-dimensional length lend a visu-

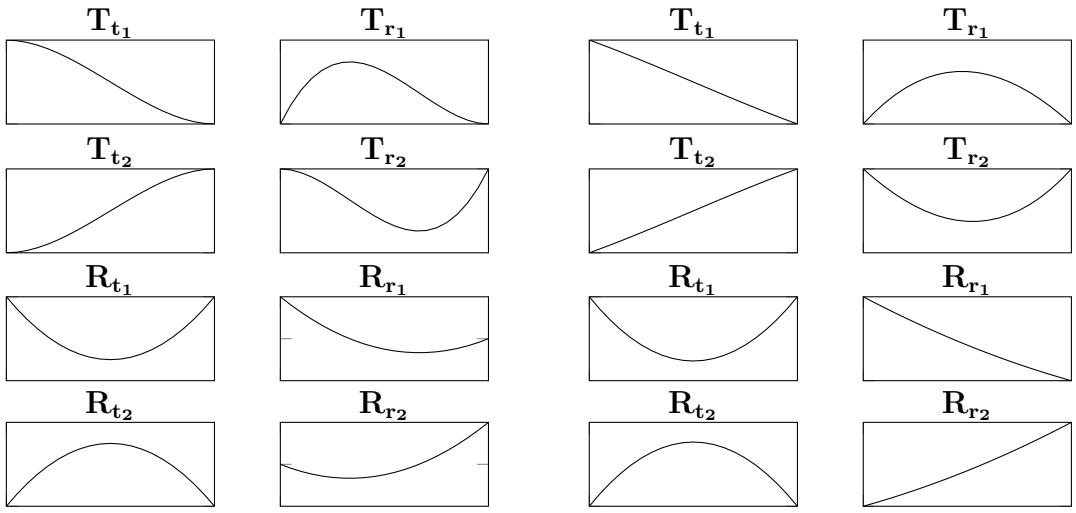

(a) length to radius ratio of 100. (b) length to radius ratio of 1.

Figure 1.5: Shape Functions as they vary with ζ using two different ratios of length to radius of beam element.

alization to the contribution of each shape function. Shape functions for axial and torsion are omitted since they are just linear polynomials. Each individual plot can be interpreted as a transformation from the input, being the coordinate multiplied to it, to the output of the variable function. For instance, the first shape function plot is the output of $v(x)$ with an input of v_1 while all other coordinates are zero. The shape makes sense under this interpretation, as the translation starts at some value, v_1 and decreases to zero at the end since v_2 is zero. Also, the expected shape breaks as the radius approaches the length as in Figure 1.5b. All shapes this beam will make in the model is a linear combination of the shapes shown here.

1.1.1.5 Finite Equations of Motion

To obtain the equations of motion in terms of the generalized coordinates, $\vec{\mathbf{q}}$, displacement variables $\vec{\mathbf{u}}$ are replaced with definitions in equation 1.31.

$$\int_0^l \underline{\mathbf{N}}^{\intercal}\delta\vec{\mathbf{q}}^{\intercal}\underline{\mathcal{M}}^e\underline{\mathbf{N}}\ddot{\vec{\mathbf{q}}}dx + \Omega\int_0^l \underline{\mathbf{N}}^{\intercal}\delta\vec{\mathbf{q}}^{\intercal}\underline{\mathcal{G}}^e\underline{\mathbf{N}}\dot{\vec{\mathbf{q}}}dx + \int_0^l \underline{\mathbf{N}}^{\intercal}\delta\vec{\mathbf{q}}^{\intercal}\underline{\mathcal{B}}^{\intercal}\underline{\mathcal{D}}^e\underline{\mathcal{B}}\underline{\mathbf{N}}\vec{\mathbf{q}}dx = 0 \tag{1.38}$$

Note that $\vec{\mathbf{q}}$ is not dependent on x so it, and it's derivatives, may be pulled out of the integrals. Define $\underline{\mathbf{B}} = \underline{\mathcal{B}}\underline{\mathbf{N}}$ and substitute in, noting that $\underline{\mathbf{B}}$ interpolates strains from discrete displacements $\vec{\mathbf{q}}$. The motion equations are then

$$\int_0^l \underline{\mathbf{N}}^{\intercal}\underline{\mathcal{M}}^e\underline{\mathbf{N}}dx\ddot{\vec{\mathbf{q}}} + \Omega\int_0^l \underline{\mathbf{N}}^{\intercal}\underline{\mathcal{G}}^e\underline{\mathbf{N}}dx\dot{\vec{\mathbf{q}}} + \int_0^l \underline{\mathbf{B}}^{\intercal}\underline{\mathcal{D}}^e\underline{\mathbf{B}}dx\vec{\mathbf{q}} = 0 \tag{1.39}$$

Define

$$\begin{cases} \underline{\mathbf{M}}^e = \displaystyle\int_0^l \underline{\mathbf{N}}^{\intercal}\underline{\mathcal{M}}^e\underline{\mathbf{N}}dx & \text{(1.40a)} \\ \underline{\mathbf{G}}^e = \displaystyle\int_0^l \underline{\mathbf{N}}^{\intercal}\underline{\mathcal{G}}^e\underline{\mathbf{N}}dx & \text{(1.40b)} \\ \underline{\mathbf{K}}^e = \displaystyle\int_0^l \underline{\mathbf{B}}^{\intercal}\underline{\mathcal{D}}^e\underline{\mathbf{B}}dx & \text{(1.40c)} \end{cases}$$

so that, the general equations of motion for the timoshenko beam element are

$$\underline{\mathbf{M}}^e\ddot{\vec{\mathbf{q}}} + \Omega\underline{\mathbf{G}}^e\dot{\vec{\mathbf{q}}} + \underline{\mathbf{K}}^e\vec{\mathbf{q}} = 0 \tag{1.41}$$

Notwithstanding the inclusion of viscous and hysteretic internal damping phenomena. Derivations, and inclusion of these phenomena in the equations of motion are to be included in the following section.

1.1.1.6 Rotating Internal Damping

Rotating damping is the main cause of instability in rotating machines. Non-rotating damping, such as the damping contributions from bearing supports, introduce a stabilizing effect. But, as rotating damping is dependent on rotation, its direction of force

can contribute to destabilization. Typically, friction components such as bearings with shrink fits or oil bearings are responsible for this destabilizing force. Due to the inherent complexity of modeling loose bearing components, or shrink fit dynamics, the analysis of the internal damping in the shaft elements is considered alone. This will allow for the study of the destabilizing effect in general, and the factors that may contribute stability such as structural damping and anisotropy of supports. Another area of interest is the design of components for specific rotor geometry to maximize the stability in the system. This stability analysis is only possible with the inclusion of some destabilizing force, [16],[15],[22],[36].

To motivate understanding of this force a simple derivation is provided with a rotating damping whose force is proportional to the flex of rate of change of the flex of the shaft. Obviously this is easier to define in the rotating reference frame, as the variables in this coordinate system directly represent the flex of the shaft from its neutral position. This relationship is as follows:

$$\vec{\mathcal{F}}_{\xi\eta} = -c_r \begin{Bmatrix} \dot{\xi}_c \\ \dot{\eta}_c \end{Bmatrix} \tag{1.42}$$

Now to translate this force back to the stationary reference frame, we will see the rotation transformation matrix

$$\underline{\mathcal{R}} = \begin{bmatrix} \cos\Omega t & \sin\Omega t \\ -\sin\Omega t & \cos\Omega t \end{bmatrix} \tag{1.43}$$

transforms stationary into rotating coordinates

$$\begin{cases} \begin{Bmatrix} \xi_c \\ \eta_c \end{Bmatrix} = \underline{\mathcal{R}} \begin{Bmatrix} y_c \\ z_c \end{Bmatrix} \\ \begin{Bmatrix} \dot{\xi}_c \\ \dot{\eta}_c \end{Bmatrix} = \underline{\mathcal{R}} \begin{Bmatrix} \dot{y}_c \\ \dot{z}_c \end{Bmatrix} + \dot{\underline{\mathcal{R}}} \begin{Bmatrix} y_c \\ z_c \end{Bmatrix} \end{cases} \tag{1.44}$$

where,

$$\underline{\dot{\mathcal{R}}} = \Omega \begin{bmatrix} -\sin\Omega t & \cos\Omega t \\ -\cos\Omega t & -\sin\Omega t \end{bmatrix} \tag{1.45}$$

substituting the second equation in 1.44 for the velocities in 1.42

$$\vec{\mathcal{F}}_{xy} = -c_r \begin{Bmatrix} \dot{y}_c \\ \dot{z}_c \end{Bmatrix} - c_r\Omega \begin{bmatrix} 0 & 1 \\ -1 & 0 \end{bmatrix} \begin{Bmatrix} y_c \\ z_c \end{Bmatrix} \tag{1.46}$$

From the equation (1.46) we see a dependence on both velocity and position. The portion dependent on the velocity is inherently stable as pulls opposite the motion. Conversely, the portion dependent on position cross couples the two displacements. This causes a destabilizing effect that grows as Ω increases. A net destabilizing force is produced once the latter portion of the exceeds the former. Without the presence of other structural damping forces, the system will destabilize.

For the beam element, the constitutive relationship[36] is comprised of both viscous and hysteretic forms of damping, η_v & η_h respectively.

$$\sigma_{xx} = E\left\{ \frac{\epsilon_{xx}}{\sqrt{1+\eta_h^2}} + \left(\eta_v + \frac{\eta_h}{\omega\sqrt{1+\eta_h^2}} \right) \dot{\epsilon}_{xx} \right\} \tag{1.47}$$

through the use of kinematics to obtain strain-displacement relations,

$$\begin{cases} \epsilon_{xx} &= -r\cos(\Omega-\omega)\, t\frac{\partial^2 R}{\partial x^2} \\ \dot{\epsilon}_{xx} &= (\Omega-\omega) r\sin(\Omega-\omega) t\frac{\partial^2 R}{\partial x^2} - r\cos(\Omega-\omega) t\frac{\partial}{\partial t}\frac{\partial^2 R}{\partial x^2} \end{cases} \tag{1.48}$$

and inspection to obtain moment equations,

$$\begin{cases} M_y &= \int_0^{2\pi}\int_0^a [w + r\sin\Omega t]\sigma_{xx} dr(rd(\Omega t)) \\ M_z &= \int_0^{2\pi}\int_0^a -[v + r\cos\Omega t]\sigma_{xx} dr(rd(\Omega t)) \end{cases} \tag{1.49}$$

we can complete a moment bending relationship to be used in the equations of motion

$$\begin{Bmatrix} M_y \\ M_z \end{Bmatrix} = EI \begin{bmatrix} \eta_a & \Omega\eta_v + \eta_b \\ \Omega\eta_v + \eta_b & -\eta_a \end{bmatrix} \begin{Bmatrix} v'' \\ w'' \end{Bmatrix} + EI \begin{bmatrix} \eta_v & 0 \\ 0 & -\eta_v \end{bmatrix} \begin{Bmatrix} \dot{v}'' \\ \dot{w}'' \end{Bmatrix} \tag{1.50}$$

where, $\eta_a = \frac{1+\eta_h}{\sqrt{1+\eta_h^2}}$ & $\eta_b = \frac{\eta_h}{\sqrt{1+\eta_h^2}}$

Now use the same strategy followed when solving for the weak form of the beam differential equations using the Principle of Virtual Displacements starting at equation (1.27). Then use the seperation of variables of defined by equation (1.31) to arrive at the total beam element equations of motion including internal damping as

$$\underline{\mathbf{M}}^e\ddot{\vec{\mathbf{q}}} + (\eta_v\underline{\mathbf{K}}^e + \Omega\underline{\mathbf{G}}^e)\dot{\vec{\mathbf{q}}} + [\eta_a\underline{\mathbf{K}}^e + (\Omega\eta_v + \eta_b)\underline{\mathbf{C}}^e]\vec{\mathbf{q}} = 0 \tag{1.51}$$

where,

$$\underline{\mathcal{I}} = \begin{bmatrix} 0 & 1 & 0 & 0 & 0 & 0 \\ -1 & 0 & 0 & 0 & 0 & 0 \\ 0 & 0 & 0 & 1 & 0 & 0 \\ 0 & 0 & -1 & 0 & 0 & 0 \\ 0 & 0 & 0 & 0 & 0 & 0 \\ 0 & 0 & 0 & 0 & 0 & 0 \end{bmatrix} \quad \& \quad \underline{\mathbf{C}}^e = \int_0^l \underline{\mathbf{B}}^\intercal \underline{\mathcal{I}}\underline{\mathcal{D}}\underline{\mathbf{B}} dx \tag{1.52}$$

$\underline{\mathbf{C}}^e$ is the "Circulation matrix", or the skew symmetric stiffness matrix.

1.1.1.7 Beam Element in Complex Coordinates

Complex coordinates collapse the equations of each plane into one set of equations. This lends properties to a axisymmetric rotor systems that will be exploited in the analysis of the model. For the complex analysis in this body of work, the system is assumed to be axisymmetric and the torsional and axial degrees of freedom are omitted. Since the contributions from axial and torsional degrees of freedom are uncoupled from the system, there condensation has no effect on the remainder of system matrices. Complex coordinates used here are defined as:

$$\vec{\mathbf{s}} = \begin{Bmatrix} \vec{r} \\ \vec{p} \end{Bmatrix} = \begin{Bmatrix} v + iw \\ \theta - i\psi \end{Bmatrix} \tag{1.53}$$

Because the element is axisymmetric, and the special form of coordinates is used, symmetric beam equations in one plane hold for the complex plane and skew symmetric matrices become complex versions of the same matrix. Elemental matrices

can be formed using the collapsed version of the shape functions matrix

$$\underline{\mathbf{N}}^c = \begin{bmatrix} T_{t_1 y} & T_{r_1 y} & T_{t_2 y} & T_{r_2 y} \\ R_{t_1} & R_{r_1} & R_{t_2} & R_{r_2} \end{bmatrix} \tag{1.54}$$

in

$$\vec{\mathbf{s}} = \underline{\mathbf{N}}^c \vec{\mathbf{q}}^c \tag{1.55}$$

where $\vec{\mathbf{q}}^c = [\vec{\mathbf{s}}_1, \vec{\mathbf{s}}_2]^\intercal$.

To convince this property of the system in the complex plane, a proof for the elemental equations of motion will be made. Taking equation (1.24b), adding equation (1.24c) multiplied by the imaginary unit i and using the definition for complex variables $\vec{p}$ and $\vec{r}$ leads to the transverse equation of motion in the complex plane

$$\kappa GA(\vec{r}'' - \vec{p}') = \rho A \ddot{\vec{r}} \tag{1.56}$$

and taking equation (1.24e) and subtracting equation (1.24d) multiplied by i gives the rotation equation in the complex plane

$$EI\vec{p}'' - \kappa GA(\vec{r}' - \vec{p}) = \rho I \ddot{\vec{p}} + i\rho J\Omega\dot{\vec{p}} \tag{1.57}$$

which by inspection of both of these equations it is evident that the form is the same as equations (1.24b) and (1.24e) except for the imaginary unit on the cross coupled parts of the equation. Now that this idea is motivated, the finite element equations of motion analogous to equation (1.51) are

$$\underline{\mathbf{M}}^{ec}\ddot{\vec{\mathbf{q}}}^c + (\eta_v \underline{\mathbf{K}}^{ec} - i\Omega \underline{\mathbf{G}}^{ec})\dot{\vec{\mathbf{q}}}^c + [\eta_a \underline{\mathbf{K}}^{ec} - i(\Omega\eta_v + \eta_b)\underline{\mathbf{C}}^{ec}]\vec{\mathbf{q}}^c = 0 \tag{1.58}$$

1.2 Disk Nodal Equations

Since the beam element has been discretized into nodal degrees of freedom, so long as the locations of disks in the model are chosen to coincide with one of these nodal locations, the expressions for stiffness and inertia can be directly combined with the

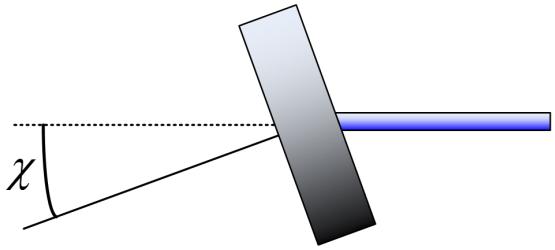

Figure 1.6: Depiction of skew angle χ

global matrices at that node. The mass element is considered as a body at a point with inertia, gyroscopic moments, and unbalance considered as external forces.

$$\underline{\mathbf{M}}^d\ddot{\vec{\mathbf{q}}}_k + \Omega\underline{\mathbf{G}}^d\dot{\vec{\mathbf{q}}}_k = \Omega^2\vec{\mathbf{F}}^d \tag{1.59}$$

the superscript d represents that the matrix or array is for a disk, and the subscript $_k$ on the displacement array indicates the array is only displacements for a single node, written out as: $\vec{\mathbf{q}}_k = [v, w, -\psi, \theta, u, \phi]^\intercal$. The matrices and forcing array of (3.6) are as follows,

$$\begin{cases} \underline{\mathbf{M}}^d = \begin{bmatrix} \rho Al & 0 & 0 & 0 & 0 & 0 \\ 0 & \rho Al & 0 & 0 & 0 & 0 \\ 0 & 0 & \rho I_z & 0 & 0 & 0 \\ 0 & 0 & 0 & \rho I_y & 0 & 0 \\ 0 & 0 & 0 & 0 & \rho Al & 0 \\ 0 & 0 & 0 & 0 & 0 & \rho J_x \end{bmatrix} \underline{\mathbf{G}} = \begin{bmatrix} 0 & 0 & 0 & 0 & 0 & 0 \\ 0 & 0 & 0 & 0 & 0 & 0 \\ 0 & 0 & 0 & \rho J_x & 0 & 0 \\ 0 & 0 & -\rho J_x & 0 & 0 & 0 \\ 0 & 0 & 0 & 0 & 0 & 0 \\ 0 & 0 & 0 & 0 & 0 & 0 \end{bmatrix} \\ \vec{\mathbf{F}}^d = \begin{Bmatrix} \rho Al\epsilon\cos(\Omega t + \delta_\varepsilon) \\ \rho Al\epsilon\sin(\Omega t + \delta_\varepsilon) \\ -\rho(I_y - J_x)\chi\sin(\Omega t) \\ \rho(I_z - J_x)\chi\cos(\Omega t) \\ 0 \\ 0 \end{Bmatrix} \end{cases} \tag{1.60}$$

Disk unbalance is caused by an eccentricity, or a geometrical distance between the axis of rotation and the center of mass of the disk. Eccentricity is represented here

as ϵ and is equivalent to that geometric distance. The moment unbalance forces, the third and fourth equations of $\vec{\mathbf{F}}^d$ in (1.60), are caused by the skew angle, χ, which is the angle the disk major axis forms with the axis of rotation as in Figure 1.6. The major axis is the axis normal from the disk face from which the polar moment of inertia, J_x is defined.

1.2.1 Disk in complex coordinates

Disk equations of motion (3.6) are converted to the complex plane in the same manner the beam element was derived in §1.1.1.7

$$\underline{\mathbf{M}}^{dc}\ddot{\vec{\mathbf{q}}}_k^c - i\Omega\underline{\mathbf{G}}^{dc}\dot{\vec{\mathbf{q}}}_k^c = \Omega^2\vec{\mathbf{F}}^{dc} \tag{1.61}$$

where,

$$\underline{\mathbf{M}}^{dc} = \begin{bmatrix} \rho Al & 0 \\ 0 & \rho I \end{bmatrix}, \quad \underline{\mathbf{G}}^{dc} = \begin{bmatrix} 0 & 0 \\ 0 & \rho J_x \end{bmatrix}, \quad \vec{\mathbf{F}}^{dc} = \begin{Bmatrix} \rho Al\epsilon e^{i\delta_\epsilon} e^{i\Omega t} \\ \rho(I - J_x)\chi e^{i\Omega t} \end{Bmatrix}$$

1.3 Bearing Nodal Equations

Bearings in this work are to be considered massless points of stiffness and damping acting at a node. Represented by the local equations of motion

$$\underline{\mathbf{D}}^b\dot{\vec{\mathbf{q}}}_k + \underline{\mathbf{K}}^b\vec{\mathbf{q}}_k = 0 \tag{1.62}$$

The superscript ^{b} indicates the matrix is for a bearing. A simple model for the stiffness and damping is used. Structural damping of the bearing is considered to be proportional to the stiffness, Raleigh Damping for the local bearing system. The

stiffness matrix is comprised of only transverse stiffness terms, as

$$\underline{\mathbf{K}}^b = \begin{bmatrix} k_{yy} & k_{yz} & 0 & 0 & 0 & 0 \\ k_{zy} & k_{zz} & 0 & 0 & 0 & 0 \\ 0 & 0 & 0 & 0 & 0 & 0 \\ 0 & 0 & 0 & 0 & 0 & 0 \\ 0 & 0 & 0 & 0 & 0 & 0 \\ 0 & 0 & 0 & 0 & 0 & 0 \end{bmatrix} \quad \underline{\mathbf{D}}^b = a\underline{\mathbf{K}}^b \tag{1.63}$$

The stiffness is typically simplified further to represent an orthotropic bearing, where $k_{yz} = k_{zy} = 0$ or further yet as a isotropic bearing, where $k_{yz} = k_{zy} = 0$ & $k_{yy} = k_{zz} = k$. Generally, these unknown parameters of stiffness are determined by changing the values to achieve the correct natural frequencies of the system.

1.3.1 Bearing in Complex Coordinates

Following the same methodology as sections §1.1.1.7 & §1.2.1, the equation of motion in the complex plane is

$$\underline{\mathbf{D}}^{bc}\dot{\vec{\mathbf{q}}}_k^c + \underline{\mathbf{K}}^{bc}\vec{\mathbf{q}}_k^c = 0 \tag{1.64}$$

where,

$$\underline{\mathbf{K}}^{bc} = \begin{bmatrix} k & 0 \\ 0 & k \end{bmatrix}, \quad \underline{\mathbf{D}}^{bc} = a\underline{\mathbf{K}}^{bc}$$

k is the isotropic bearing stiffness. It is possible to define the complex system with anisotropic terms of stiffness, but the complexity added to the system outweighs the benefit of using the complex plane in the first place.

1.4 Assembly of the Global Systems of Equations

The matrices in the global system of equations are determined using the direct approach of taking the summation of the inertia, damping, stiffness, or force at each degree of freedom.

1.4.1 In the Real Coordinate System

$$\underline{\mathbf{M}}\ddot{\vec{\mathbf{q}}} + \underline{\mathbf{G}}\dot{\vec{\mathbf{q}}} + \underline{\mathbf{K}}\vec{\mathbf{q}} = \Omega^2\vec{\mathbf{F}} \tag{1.65}$$

Each summation is defined as

$$\begin{cases} \underline{\mathbf{M}} = \underline{\mathbf{M}}^e_G + \underline{\mathbf{M}}^b_G + \underline{\mathbf{M}}^d_G & \underline{\mathbf{D}} = \eta_v\underline{\mathbf{K}}^e_G + \Omega\underline{\mathbf{G}}^e_G + \Omega\underline{\mathbf{G}}^d_G + \underline{\mathbf{D}}^b_G \\ \underline{\mathbf{K}} = \eta_a\underline{\mathbf{K}}^e_G + (\Omega\eta_v + \eta_b)\underline{\mathbf{C}}^e_G + \underline{\mathbf{K}}^b_G & \vec{\mathbf{F}} = \vec{\mathbf{F}}^d_G \end{cases}$$

Subscript $_G$ indicates the matrix is in the global coordinate system that contains all of the degrees of freedom. Care must be taken here to associate the correct degrees of freedom, and recognize that some of the matrices are elemental and others are nodal.

1.4.2 In the Complex Coordinate System

$$\underline{\mathbf{M}}\ddot{\vec{\mathbf{q}}}^c + \underline{\mathbf{D}}\dot{\vec{\mathbf{q}}}^c + \underline{\mathbf{K}}\vec{\mathbf{q}}^c = \Omega^2\vec{\mathbf{F}} \tag{1.66}$$

where,

$$\begin{cases} \underline{\mathbf{M}} = \underline{\mathbf{M}}^{ec}_G + \underline{\mathbf{M}}^{dc}_G + \underline{\mathbf{M}}^{bc}_G & \underline{\mathbf{D}} = \eta_v\underline{\mathbf{K}}^{ec}_G - i\Omega(\underline{\mathbf{G}}^{ec}_G + \underline{\mathbf{G}}^{dc}_G) + \underline{\mathbf{D}}^{bc}_G \\ \underline{\mathbf{K}} = \eta_a\underline{\mathbf{K}}^{ec}_G - i(\Omega\eta_v + \eta_b)\underline{\mathbf{C}}^{ec}_G + \underline{\mathbf{K}}^{bc}_G & \vec{\mathbf{F}} = \vec{\mathbf{F}}^{dc}_G \end{cases}$$

1.5 Model Analysis

The benefit of the finite element model is the general linear ordinary differential equation that is left to solve in equations (1.65), & (1.66). Many techniques exist to provide frequency and time domain information on the solution to this system of equations. In rotordynamic analysis many of the analyses are interested in the dependence of the system on the spin speed Ω. The inclusion of this parameter as a time dependent variable would make the solutions to the system much more difficult. In this work, the spin speed is considered to be constant in each operation taken in a series of operation as the value is changed. In this way, the effect of spin acceleration

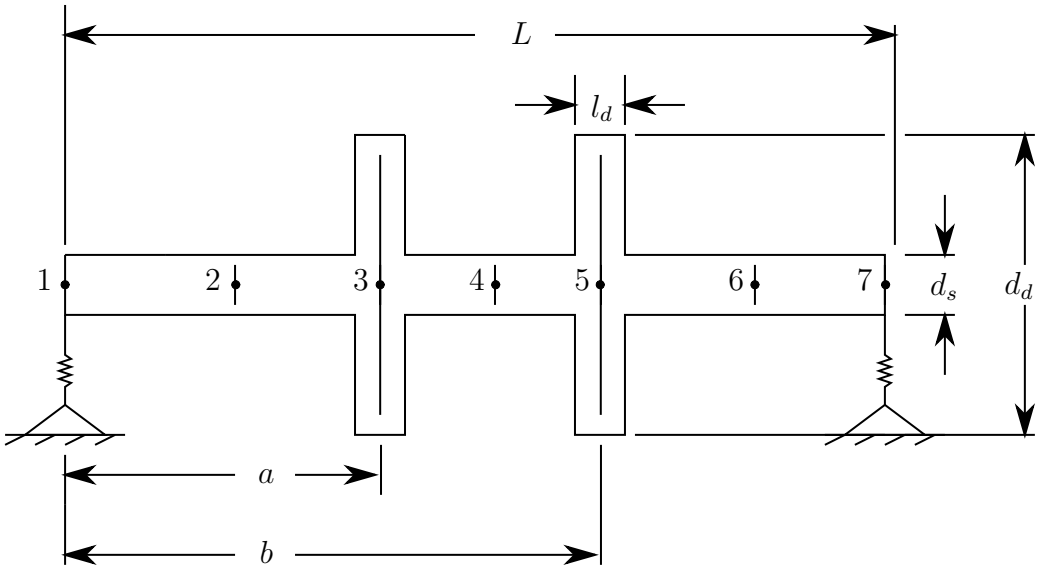

Figure 1.7: Diagram of Two disk model example problem.

is not taken into account, but the dependence on spin speed is approximated. For the vast majority of rotordynamic systems this approximation is sufficiently accurate. For a simple critical speed computation without dependence on spin speed, Ω, the homogeneous solution, using $\vec{\mathbf{q}} = e^{i\Omega t}$ while neglecting all damping and forcing, will provide the free whirling dynamic equation. In the case that the critical speeds need to be calculated with the inclusion of spin speed, like in the Campbell diagram, a solution of the form $\vec{\mathbf{q}}_0 e^{i\omega t}$ is used so that the spin speed and whirl speed can vary freely. Unbalance response is calculated using the particular integral as well.

Details of the different analyses to follow will be accompanied by an example problem to demonstrate the results. The problem of interest is a simple two disk rotor system depicted in Figure 1.7. The geometry and material properties are listed in Table 1.1. The Beam is discretized as in figure 1.7 with 6 elements. With geometry of $L = 1.8[m]$, $a = \frac{1}{3}L$, & $b = \frac{2}{3}L$ and bearing located at the ends of the shaft.

Table 1.1: Properties of disks, shaft elements, and bearings of the example problem.

	$\rho[\frac{kg}{m^3}]$	$r[m]$	ν	$E[Pa]$	$\eta_v[s]$	η_h
Shaft	7850	0.5	0.3	210×10^9	0.0002	0
	$\rho[\frac{kg}{m^3}]$	$r[m]$	$l[m]$			
Disks	7850	0.3	0.1			
	$k_x[\frac{N}{m}]$	$k_y[\frac{N}{m}]$	$c_x[\frac{Ns}{m}]$	$c_y[\frac{Ns}{m}]$		
Bearings	1×10^7	1×10^7	100	100		

1.5.1 State Space Representation and the Eigenvalue Problem

The system can be represented in state space where,

$$\dot{\vec{\mathbf{z}}} = \underline{\mathbf{A}}\vec{\mathbf{z}} + \underline{\mathbf{B}}\vec{\mathbf{w}}, \quad \vec{\mathbf{z}} = \begin{Bmatrix} \dot{\vec{\mathbf{q}}} \\ \vec{\mathbf{q}} \end{Bmatrix} \tag{1.67}$$

$\underline{\mathbf{B}}\vec{\mathbf{w}}$ is an input into the system, which here will represent the forces due to unbalance. Solving for $\underline{\mathbf{A}}$ & $\underline{\mathbf{B}}\vec{\mathbf{w}}$

$$\underline{\mathbf{A}} = \begin{bmatrix} -\underline{\mathbf{M}}^{-1}\underline{\mathbf{D}} & -\underline{\mathbf{M}}^{-1}\underline{\mathbf{K}} \\ \underline{\mathbf{I}} & \underline{\mathbf{0}} \end{bmatrix} \quad \& \quad \underline{\mathbf{B}}\vec{\mathbf{w}} = \Omega^2 \begin{Bmatrix} \underline{\mathbf{M}}^{-1}\vec{\mathbf{F}} \\ 0 \end{Bmatrix} \tag{1.68}$$

This equation is valid in both the complex and real coordinate plane. With the use of complex coordinates, the state vector is represented by $\vec{\mathbf{z}} = [\dot{\vec{\mathbf{q}}}^c, \vec{\mathbf{q}}^c]^\intercal$. $\underline{\mathbf{I}}$ & $\underline{\mathbf{0}}$ are appropriately sized to match the matrices in the system of choice. $\underline{\mathbf{A}}$ is the dynamic matrix of the system, which represents the dynamics in a single expression. Now in the form of a first order linear differential equation, numerical integration and many other numerical analysis techniques may be applied.

Using equation (1.67) and assuming a solution of $\vec{\mathbf{z}} = \vec{\mathbf{\Theta}}e^{st}$ leads to the eigenvalue problem

$$(\underline{\mathbf{A}} - s)\vec{\mathbf{\Theta}} = \underline{\mathbf{0}} \tag{1.69}$$

$\vec{\mathbf{\Theta}}$ is the vector containing the eigenvectors. Since the state in which these equations are defined is the combination of displacement and velocity, the eigenvectors are defined as a set corresponding to both displacement and velocity. This effectively duplicates the set as

$$\vec{\mathbf{\Theta}} = \left\{ \begin{array}{c} \vec{\theta}_{\dot{\vec{\mathbf{q}}}} \\ \vec{\theta}_{\vec{\mathbf{q}}} \end{array} \right\} = \left\{ \begin{array}{c} s\vec{\theta}_{\vec{\mathbf{q}}} \\ \vec{\theta}_{\vec{\mathbf{q}}} \end{array} \right\}$$

1.5.2 Unbalance Response

The unbalance response of the dynamic system can be achieved by substituting the particular integral $\vec{\mathbf{q}} = \vec{\mathbf{q}}_0 e^{i\Omega t}$ into the equation of motion (1.65),(1.66).

$$\vec{\mathbf{q}}_0 = (-\Omega^2 \underline{\mathbf{M}} + i\Omega \underline{\mathbf{D}} + \underline{\mathbf{K}})^{-1} \Omega^2 \vec{\mathbf{F}} \tag{1.70}$$

where the matrix in the parenthesis is called the dynamic response of the system. The dynamic response acts as a transfer matrix that converts inputs, $\vec{\mathbf{F}}$ into outputs $\vec{\mathbf{q}}_0$. The result is complex with the absolute part of the result representing the magnitude of the response, and the angle of the result as representing the phase delay of the response from the input. If the input phase is known in terms of shaft angle, then the phase delay of the response angle can be interpreted as a shaft angle.

The Unbalance response can also be calculated using the particular integral $\vec{\mathbf{q}} = \vec{\mathbf{q}}_0 e^{i\omega t}$ where ω is the independent whirl frequency. Then the response is found as the transfer response of the oscillation $e^{i(\Omega-\omega)t}$.

For the example problem defined in §1.5 the unbalance response to a disk b unbalance of $2 \times 10^{-5}[m]$ is depicted in Figure 1.8. We may enhance the frequency response figure by associating a plot of the phase angle with the response. This is called the Bode diagram and is presented in figure 1.9

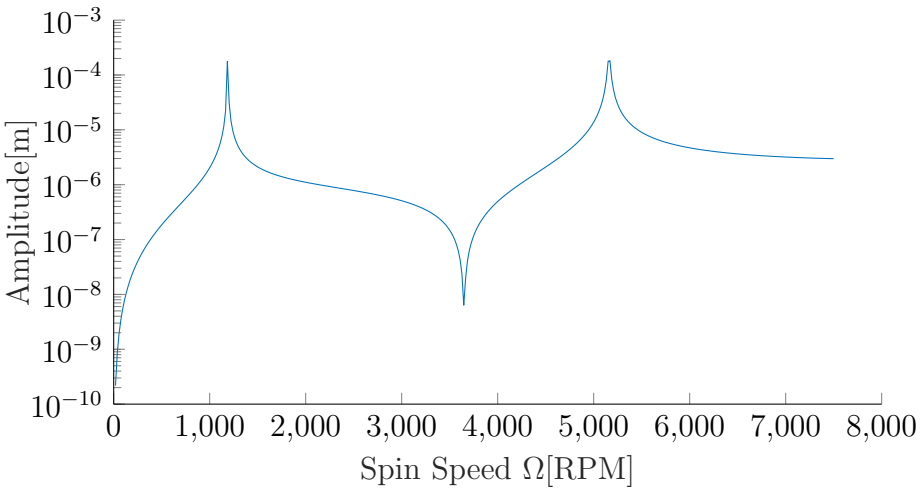

Figure 1.8: Frequency response of the second disk subject to an unbalance at the second disk.

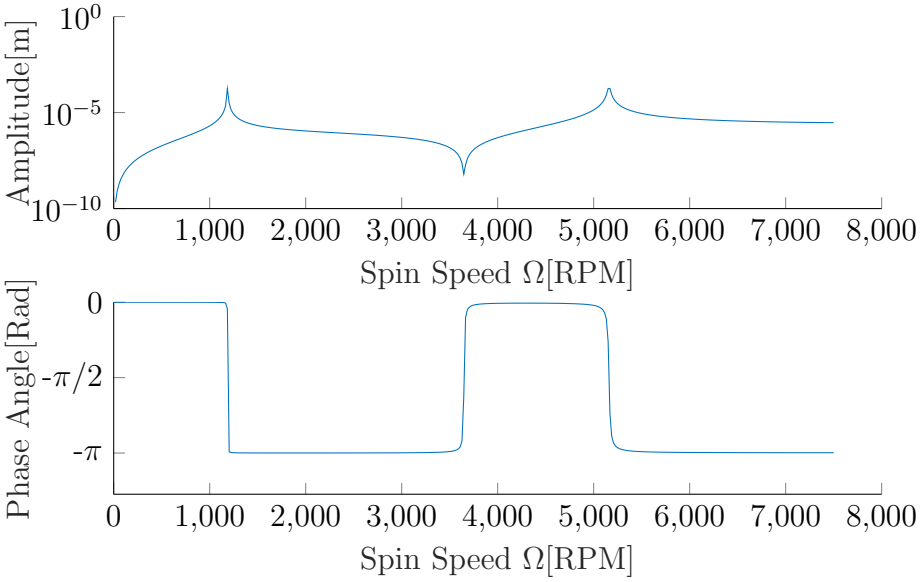

Figure 1.9: Bode diagram of the second disk subject to an unbalance at the second disk.

1.5.3 Roots Locus and Stability Analysis

One of the most valuable facets of a rotordynamic model is its ability to predict instability. unstable operation can lead to rotor failures and unsafe operating conditions. Before the advent of modern mathematical models for rotating machinery, it was not common to operate a machine above the first critical speed. Internal damping and other rotating damping can cause a subsynchronous whirl when operating above the first critical speed. This effect is worse for machines with stiff bending modes, and is often instigated by loose fittings, shrink fits, and couplings. As mentioned in §1.1.1.6, the effect of external damping sources will not be investigated here. Rather, the stability will be tested by modeling the internal damping of the rotor due to viscous heat production during loading and unloading of the beam in bending. See §1.1.1.6 for a more detailed explanation and derivation.

Roots Locus is the plot of the eigenvalues on the $\Re - \Im$ plane as some value they are dependent on changes. In rotordynamic analysis the dependent variable is often the spin speed Ω. In this plane, the eigenvalues s represent the complex set of which the real part is the damping ans the imaginary is the damped natural frequency. The roots locus is useful in determining stability of the system, and which mode is responsible for the instability. Using the eigenvalues s of the eigenvalue problem defined in equation (1.69) on the example problem defined in §1.5 a plot of the roots locus can be found as in figure 1.10. Internal damping coefficient, η_v, is added to the system at the value of $0.0002[s]$. The first three modes are presented with the negative complex couple joining each positive mode of vibration. In completely symmetric systems, the eigenvalue problem It is evident by looking at figure 1.10 that the system becomes unstable at some point, as many of the eigenvalues are in the positive real region of the plane. Since this example system is symmetric about the axis, the positive and negative pairs for each mode start at the same point when

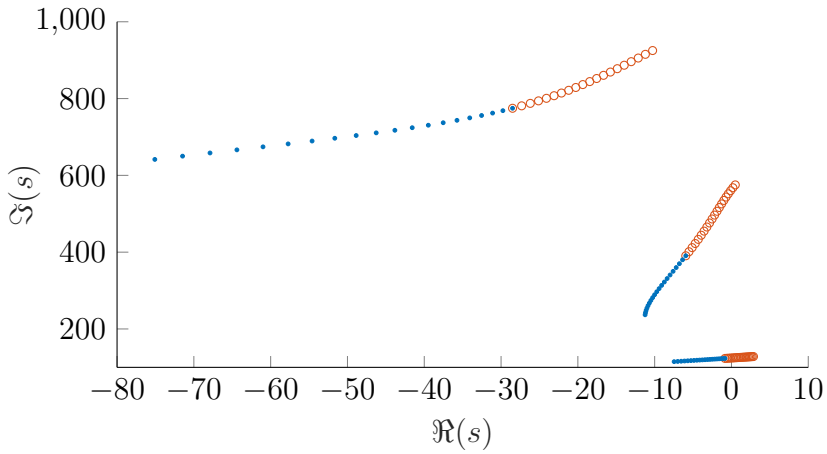

Figure 1.10: Roots Locus of the example problem with an internal damping coefficient of 0.0002. Red circles represent positive frequencies, while blue dots represent negative ones.

the spin speed is zero. The positive modes then move in the positive real direction–becoming more unstable. On the other hand, the negative frequencies move in the negative real direction–becoming more stable. This phenomena of the positive modes becoming more unstable and the negative becoming more stable is a general trend, but not a rule, and the rotating damping assists defined in §1.1.1.6 assists in this trend. Also, Gyroscopic effects tend to increase the whirl frequency (Imaginary part of eigenvalue) of the positive mode, while the opposite effect is seen in the negative mode.

The Roots Locus for the example problem is also presented in three dimensions to lend in the understanding of the relationship with spin speed. This can be seen in Figure 1.11. A direct method of measuring the stability of the system is to observe the real part of the eigenvalues of the dynamic matrix. Since the solution was assumed the be of the form $\vec{\mathbf{z}} = \vec{\mathbf{\Theta}} e^{st}$, then the eigenvalues represent the values of the complex exponent s. Splitting s into its real and complex components as $s = \sigma + i\omega_d$, and plugging into $\vec{\mathbf{z}}$ gives: $\vec{\mathbf{z}} = \vec{\mathbf{\Theta}} e^{\sigma + i\omega_d}$. By inspection, it is evident that when the real part is positive, the response will grow without bound–an unstable system.

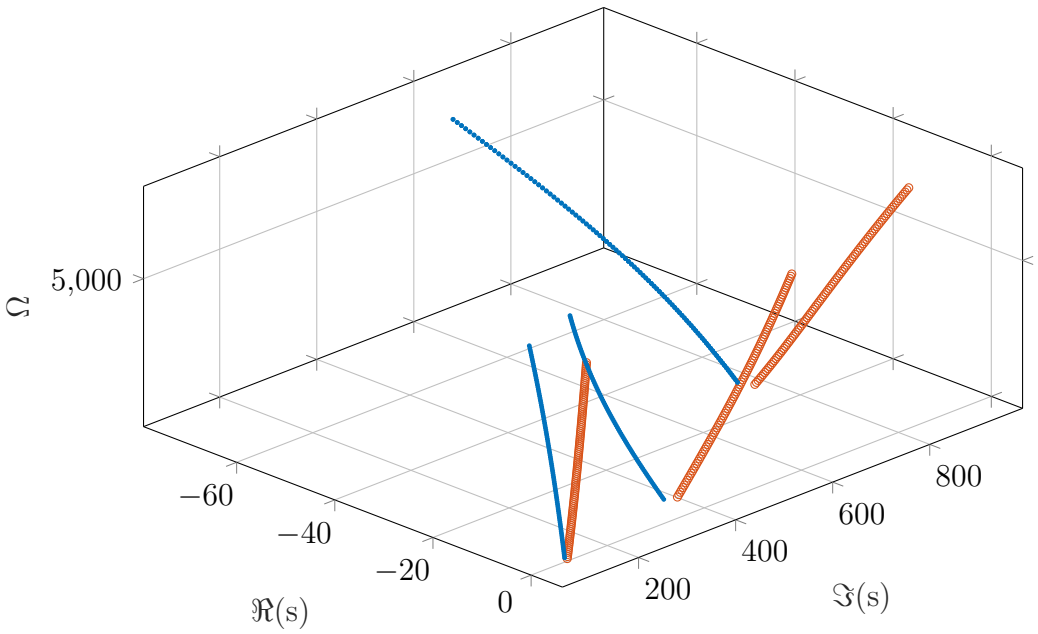

Figure 1.11: Roots Locus of the example problem in 3-D with an internal damping coefficient of 0.0002. Red circles represent positive frequencies, while blue dots represent negative ones.

Damping is Commonly represented as a the ratio of the real part of the eigenvalue to the natural frequency as

$$\zeta = \frac{-\sigma}{\omega_n} \ , \ \omega_n = \sqrt{\sigma^2 + \omega_d^2} \tag{1.71}$$

where ζ is the damping ratio, and ω_n is the natural frequency. The stability margin, or the range of speeds through which the system remains stable can be determined by plotting the maximum real part, $\Re(s)$, of the set against spin speed. The point at which $\Re(s)$, or σ, crosses the real axis is the threshold of stability. The plot which represents this is termed the Stability Margin plot, and is shown in 1.12 for the example problem defined in §1.5.

Finally, the stability can be analyzed using the damping coefficients(ζ) plotted against speed. This figure, shown in 1.13, indicates instability as when ζ drops below zero.

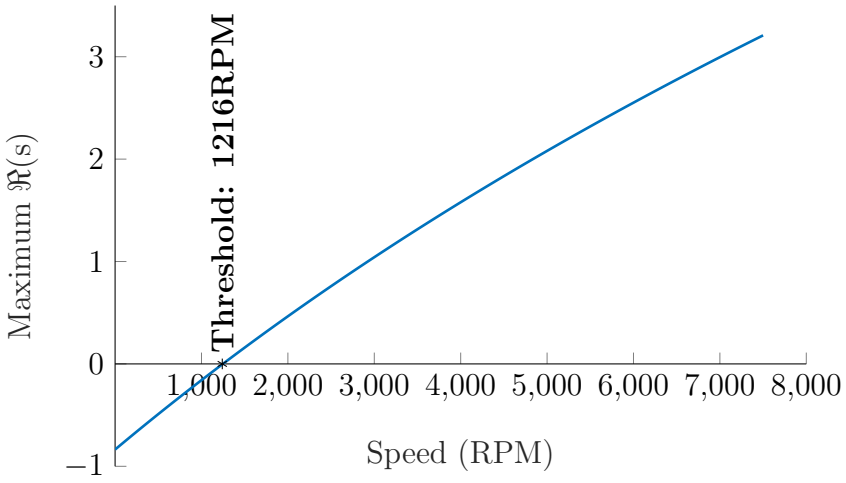

Figure 1.12: length to radius ratio of 1.

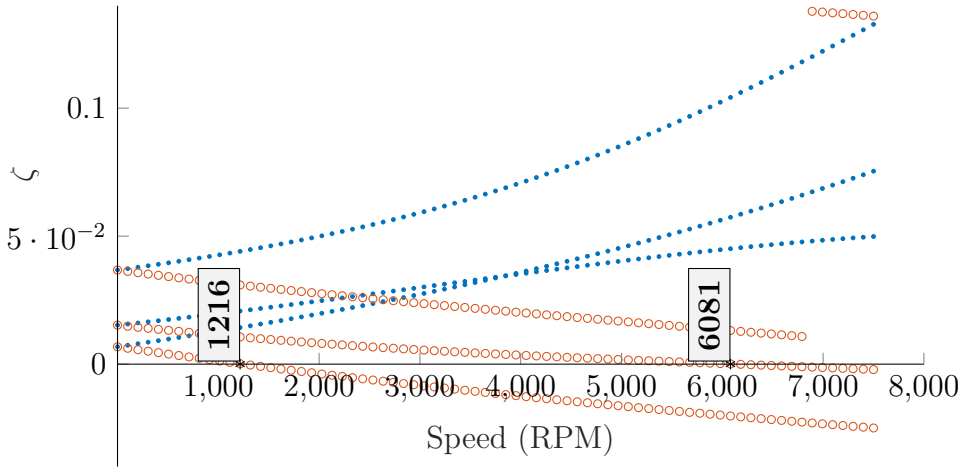

Figure 1.13: Damping ratio vs. spin speed with indication of threshold of stability.

1.5.4 Shapes

Deformed shape can be predicted using the eigenvectors of the eigenvalue problem 1.69. Eigenvectors contain displacement arrangement that corresponds to a natural frequency; this includes phase and relative amplitude of the generalized displacements from one another. For a simple model to conceptualize this idea, consider a rigid rod that can only translate in one plane at each end. The eigenvectors will contain all linearly independent combinations of the movement of the left side relative to the

right. This would be in general; opposite left to right (one up, one down), and same left and right(both up, or both down). The bending modes of the beam operate in a similar manner but scaled up, and just like in the simple case, including the same number of modes as there are degrees of freedom in the system. Since the state space representation used for eigenanalysis contains $\dot{\vec{\mathbf{q}}}$, & $\vec{\mathbf{q}}$ the eigenvector will contain $2N$ modes. For a general ith mode of vibration, the eigenvector $\vec{\mathbf{\Theta}}_i$ contains the displacement information. But, since the portion of $\vec{\mathbf{\Theta}}_i$ pertaining to velocities, $\vec{\theta}_{\dot{\vec{\mathbf{q}}}i}$, is a linear combination of $\vec{\theta}_{\vec{\mathbf{q}}i}$, all of the information is contained in one of these arrays. Therefore, the interpolation of displacements for the ith mode is given by

$$\vec{\mathbf{u}}_i = \underline{\mathbf{N}}\vec{\theta}_{\vec{\mathbf{q}}i} \tag{1.72}$$

where, the value of $\vec{\mathbf{u}}_i$ is now a function of x. So, through the choice of an array of positions that span the length of the beam element the displacement, and phase angle distribution of the ith mode of vibration is determined. Phase angle and amplitude of an transverse pair may be used to for an orbit of a beam axis location x.

Shape figures for the first 3 modes of the example problem are presented in Figures 1.14a,1.14b, and 1.14c. Note that the real and imaginary parts of the eigenvalues are listed along with the shapes. Also, note that the speed is chosen to coincide with the damped natural frequency so that this is the critical speed bending shape.

1.5.5 Campbell

The Campbell diagram correlates the spin speed and the whirl speed. The whirl speed is calculated as the imaginary part of the complex eigenvalue of the dynamic matrix (1.67). Spin speed is varied while calculating all of the critical speeds at each step of spin speed. The campbell diagram for the example problem is given in figure 1.15. This diagram can be used to discerne the critical speeds of the system. As can be seen in figure 1.15 the $\omega = \Omega$ synchronous line passes through 3 different complex modes

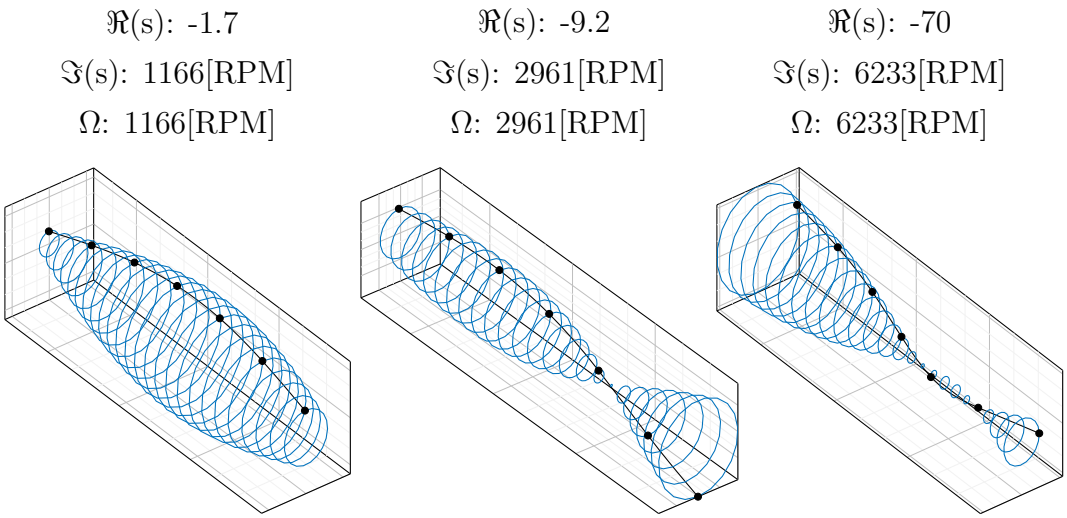

(a) Mode Shape 1. (b) Mode Shape 2. (c) Mode Shape 3.

Figure 1.14: Modal shapes of the example problem.

in this speed range. Note: with the large influence of the gyroscopic effect in the example problem presented here, the positive and negative frequencies for the second and third modes diverge from one another rath quickly. A physical interpretation of th selective effect of the gyroscopic moments can be presented by taking the mode shapes into account. Recall that the disks in the example are mounted at nodal locations 2 & 3. In figure 1.14 it is evident that in the first mode, Figure 1.14a, both disks are translating together. As a matter of fact, most of all the points of the system are translating in sync. This type of mode is called a cylindrical mode for the fact that as the whirl is traced, as it is in 1.14a, it forms a cylinder. The consequence of this type of motion is limiting on the transverse rotation angle of the mass elements. Since the gyroscopic moments are proportional to these angles, their magnitude is very low compared to transverse effects. On the contrary, in mode 2 & 3 of figures 1.14b & 1.14c respectively, the angle of the disks and other mass elements is changing significantly through rotation. Because of this, large gyroscopic moments induce an out of phase force that stiffens positive whirl and softens negative whirl tendencies. Gyroscopic moments are larger in these types of modes where there is

a point of inflection on the beam, commonly called an antinode of vibration. This mode is called a conical mode, as analogous with the cylindrical mode, the shape of the path forms one or many cones.

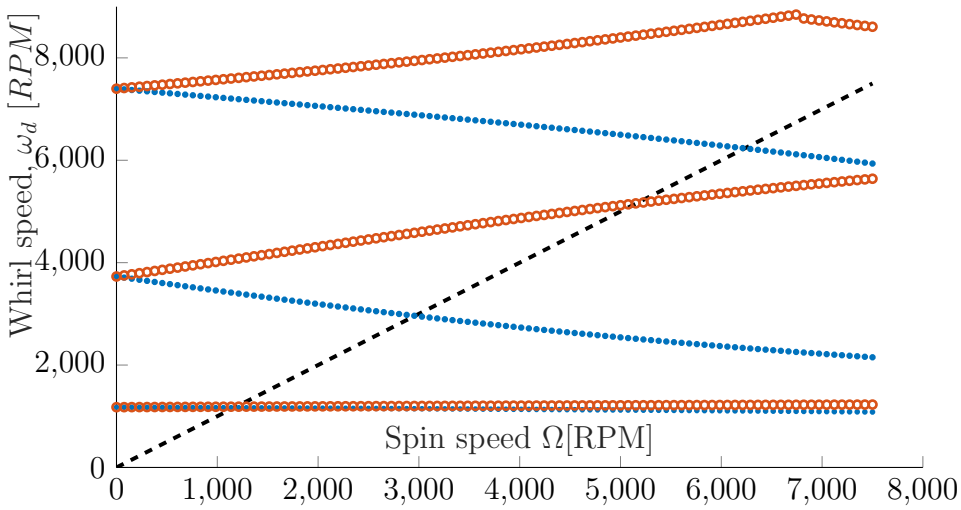

Figure 1.15: Campbell Diagram of the example problem.

Chapter 2

EXPERIMENTAL ANALYSIS

2.1 Data Collection and Analysis

The most important measurement to be made in order to perform significant analysis is the vibration signal. Improvements on this would be to collect some speed information and preferably some reference point on a turn of the shaft in the system. This is often performed using a once per turn reference mark on the shaft. Additionally, a spin speed measurement independent of the spin speed and with more time precision will aid in filtering and providing accuracy of frequency spectrum. An orthogonal vibration signal can help in characterizing non-symmetric systems, and allow for the visualization of the shaft centerline orbit path. For the correct characterization of the signals metioned thus far, it is important to also retain the sampling rates of the various signals.

There are two main figures that form the basis for other rotordynamic analysis techniques and figures. These are the Bode diagram and the Frequescy Spectrum. The Bode diagram plots the amplitude of vibration against speed alongside the phase angle against speed. Frequency spectrum plots encapsulate frequency domain information gathered from the time domain amplitude data. A derivation of the Bode diagram, the Polar plot, plots the amplitude and phase of the signal as a vector on the polar plane as speed changes. Finally, the cascade plot cascades frequency spectrum plots as speed changes.

A difficulty in rotordynamic analysis arises in the change of speed of the system forcing much of the analysis to be performed in a short window in time. The window is typically made small enough to where the operation performed would be the same

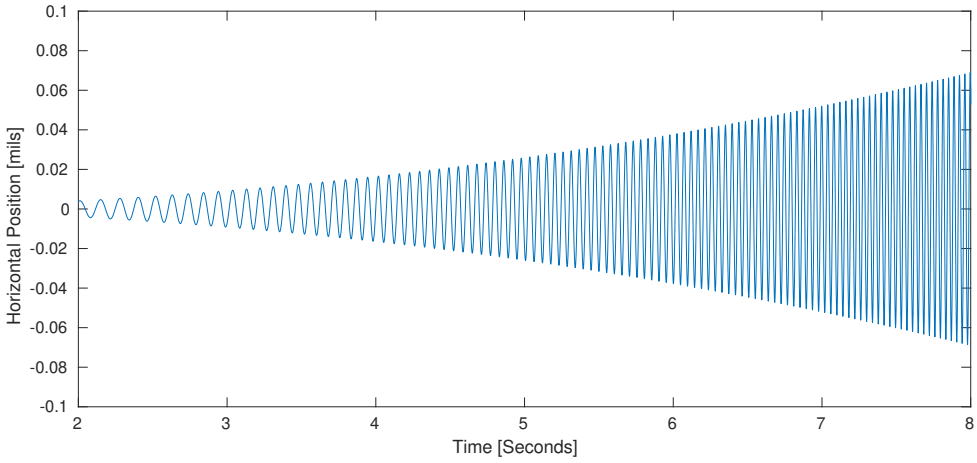

Figure 2.1: Position of the rotor shaft over a certain timespan.

or similar if it had been performed on a stationary system. A generic ramping of speed, and inherently vibration, is depicted in Figure 2.1. The time domain signals will be represented as $v(t)$ & $w(t)$ for an orthogonal set of transducers.

To combat the dynamic nature of the system, a windowing approach is taken as depicted in figures 2.2a and 2.2b Approaching the problem this way Inside of a window of vibration, as the one shown in Figure 2.3the Speed, Amplitude and Phase all approach constant the smaller the window gets.The Frequency Response has a twofold proportionality to window size; as the window gets smaller the frequency content of the signal itself approaches constant, but the resolution of the transform to approximate those frequencies decreases.

The variables $v(t)$ & $w(t)$ will now take the form $v(n)$ & $w(n)$ inside the window in fig. 2.3, where n is sample number. All of the plots to be presented here will be functions of two or more of the following variables: Amplitude[mils],Phase[Rad],Frequency Spectrum[mils], and Rotation Speed[RPM]. The Speed comes from the system so no analysis is necessary. Amplitude, Phase, and Frequency Spectrum must be calculated in windows of the data. Amplitude, Phase and speed are often combined into an array of vectors where speed is the index and Amplitude and Phase are the magnitude and

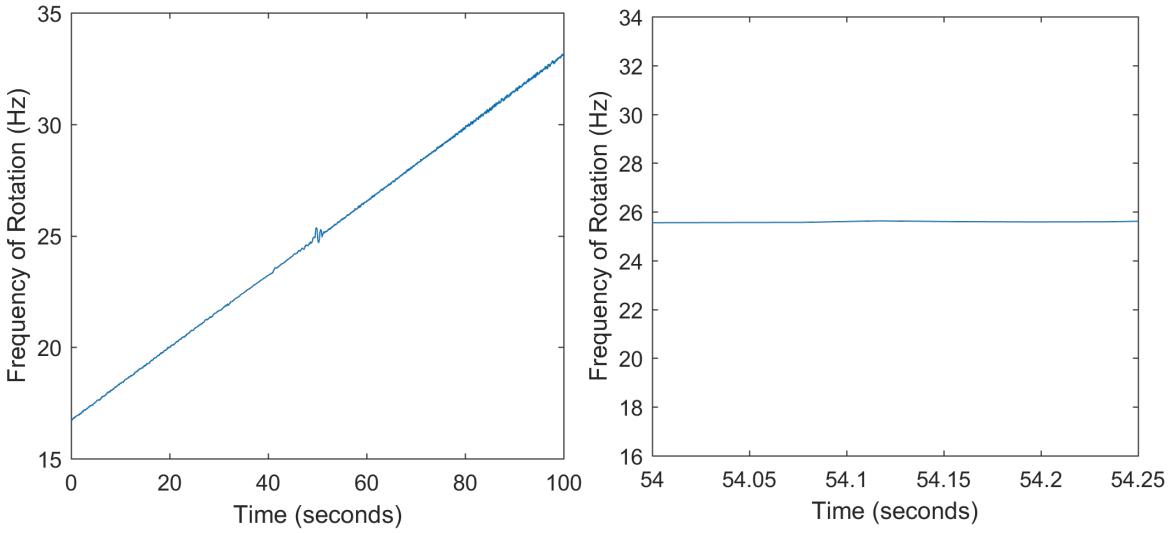

(a) Rotor speed change over time during a ramp up.

(b) Rotor speed change over time during a ramp up.

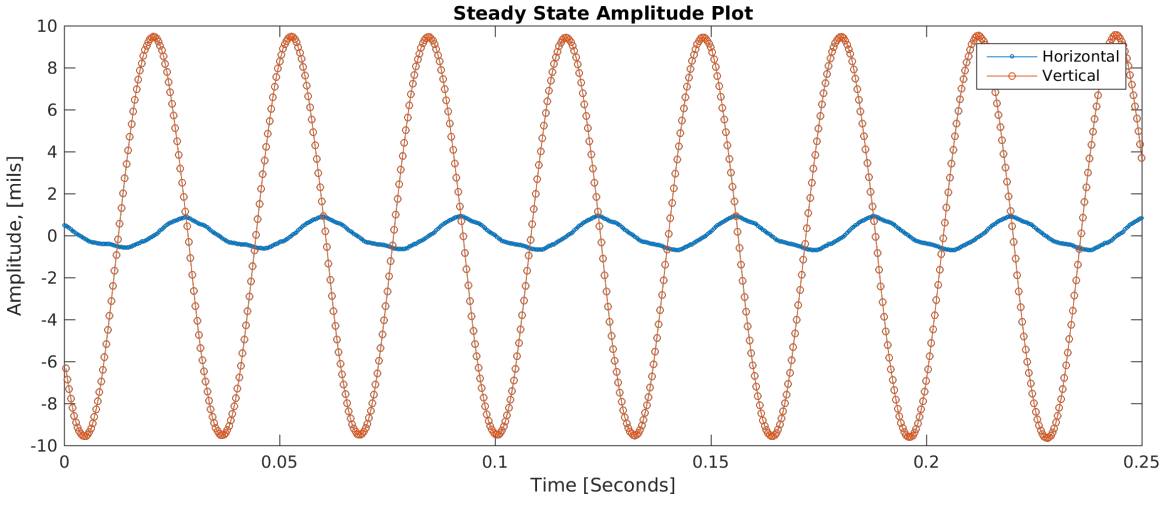

Figure 2.3: A window in time of the transient vibration signal in orthogonal directions.

angle of a vector, respectively.

2.1.1 Amplitude

Amplitude calculation is fairly straightforward within the window of 2.3. One approach to calculate the peak to peak vibration is to take the $A_v = max(v) - min(v)$ over the whole sample, where A is the amplitude. Another is to use a peak-finding algorithm to determine the height of each peak and average them all over the sample length.

2.1.2 Frequency Spectrum

The frequency spectrum of the signal is calculated inside the window using the Fourier Transform. In MATLAB the Fast Fourier Transform has been preprogramed allowing easy working between time and frequency domains.

$$Y = \text{fft}(v), \ \& \ Z = \text{fft}(w) \tag{2.1}$$

where X and Y must be scaled by the length of v and w to represent amplitude of vibration.

A useful way to represent the data is using complex variable to compact the two orthogonal displacements v & w as

$$z = v + iw \tag{2.2}$$

now the frequency spectrum of this complex value represents both equations in one

$$Z = \text{fft}(z) \tag{2.3}$$

Thus far, the frequency spectrum in the real coordinates and in the complex is in terms of samples on the dependent axis. The frequency vector to which the fft()

coresponds must be calculated. It is known that the slop of the frequency vector is $df = Fs/N$, where Fs is the sampling rate of the time domain signals. It is also known that the frequency vector is the same length as the time domain signal

$$f = df(0 : N - 1)$$

but the spectrum needs to be centered at 0

$$Q = (N + 1)/2$$
$$f_Q = df(Q - 1)$$
$$f_c = f - fQ$$

where f_c is the frequency vector that pairs with the real or complex frequency spectrum.

2.1.3 Phase Angle

2.1.3.1 Time Domain Approach

A rather direct way of calculating the phase angle comes from the interpretation of the time domain signal. If some once per turn reference is available, then using either a zero-crossing, peak-finding, or threshold algorithm can be employed to reference a specific angle of the shaft rotation. If the vibration signal is mostly synchronous, that is vibrating at the same frequency as the rotation of the shaft, then a peak-finding or zero-crossing algorithm can be used to determine the number of samples from the shaft reference angle to the peak of the vibration.

$$\beta_i = 2\pi \frac{\#ref_i - \#peak_i}{\#ref_i - \#ref_{i-1}} \tag{2.4}$$

where β_i is the phase lag of the signal of interest from the reference signal at the ith reference cycle, $\#ref_i$ is the sample number of the reference trigger, and $\#peak_i$ is the sample number of the peak of the signal of interest. One large advantage to

this brute force method is that is can run continuously and provide current phase information on just the last rotation of the shaft. In the application to the window of vibration data, fig. 2.3, the measurements of each cycle would be averaged across the window to provide just one phase lag data point to match the one amplitude data point and the one speed data point.

2.1.3.2 Frequency Domain Approach

Alternatively, the phase angle can be determined using the frequency domain signals.

If the speed of the rotor is known and the time domain signals v & w are known to be synchronous, or filtered to synchronous, then the spectrums of the signals of interest can be used to calculate the phase delay. calculate the fft of the time domain signal of interest and reference signals

$$Y = \text{fft}(v)$$
$$K = \text{fft}(k)$$

where K and k are the freq. domain and time domain signals of the reference signal respectively. Now using the speed of synchronous vibration, find the bin that is a peak nearest to that speed. Calculate the angle of the complex number corresponding to that bin for both the reference and signal of interest

$$\varphi_Y = atan2(Y(max_bin))$$
$$\varphi_K = atan2(K(max_bin))$$

and finally, the phase delay $\beta_y = \varphi_K - \varphi_Y$

2.2 Experimental Plots

In the previous section Amplitude, Phase, and frequency spectrum were calculated for the interior of a window on the data as a whole. Each of the data then need to be

indexed on the speed for that window and continue until the entire signal has been exhausted. The Bode, and the Cascade plots can now be formed.

for the visualization of the plots, experimental data from a overhung rotor system with one disk will used to calculate the figures.

2.2.1 Bode

The Bode diagram is the stacked plot containing amplitude as a function of speed on top of phase as a function of speed. A Bode plot for the system mentioned in the §2.2 is given in Figure 2.4. Notice how the Vertical plane undergoes a critical speed before the horizontal plane. This is an indication of high anisotropy of stiffness in the system. By observing the phase lag of each the vertical and the horizontal, it is evident that the orbit direction is opposite the spin speed between speeds 1280-1350[RPM]. This is due to the phase angles switching polarity with one another. If normally horizontal lags vertical, as is suggested by the sub-synchronous and super-synchronous range, then during the critical speed the orbit is reversed since vertical begins to lag horizontal.

2.2.2 Cascade

The Cascade plot is a cascade, or waterfall of the spectrum at either various spin speeds, or in the case of the waterfall plot, at various times. A Cascade plot is demonstrated with the experimental system described in §2.2, as Figure 2.5. Now using this figure it is easy to detect the portion of the start-up in which the orbit is opposite the spin speed. A sharp dip in positive resonances correlated with a sharp rise in negative ones leads to this phenomena caused by the anisotropy in the stiffness matrix.

The Cascade plot is particularly useful in characterizing non-synchronous vibra-

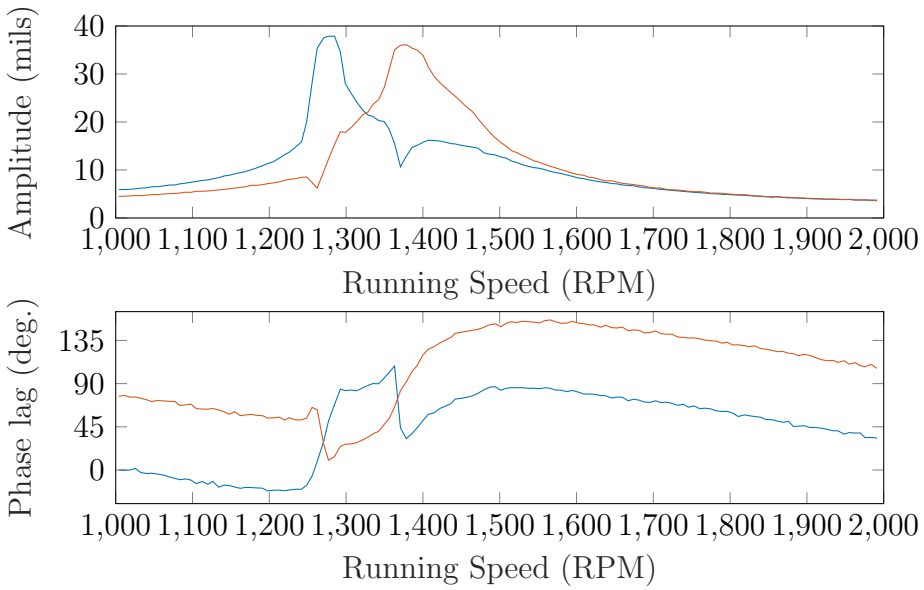

Figure 2.4: Bode diagram of the experimental system described in §2.2. Red is horizontal plane, and blue is vertical.

tion. Slightly evident in the example cascade of figure 2.5 is the super-synchronous vibration at twice the spin speed, this is often called the 2X vibration and likewise and other non-synchronous whirl can be referenced as nX. The cascade plot is an indispensable tool for the analysis of fluid film bearing as they are characterized by sub-synchronous whirl that is difficult to identify in a Bode Diagram.

2.2.3 Orbit

Now in the "real" space, the actual orbit or trace of the centerline of the shaft is observed. In this work, the orbit is visualized in two ways; as a path in 2D space at a specific spin speed, or as a 3D orbit with a cascade of orbits as spin speed is increased. The 3D Orbit allows for the visualization of complex phenomena in a unique physical way where the shapes feel more real. Figure 2.6 3D Orbit is given for the experimental example described in §2.2. Appearing, once again is evidence of the negative whirl in the critical speed range. In the 3D orbit a necking of the shape can be seen between the speeds of 1200-1400[RPM] indicating the orbit has reversed its direction.

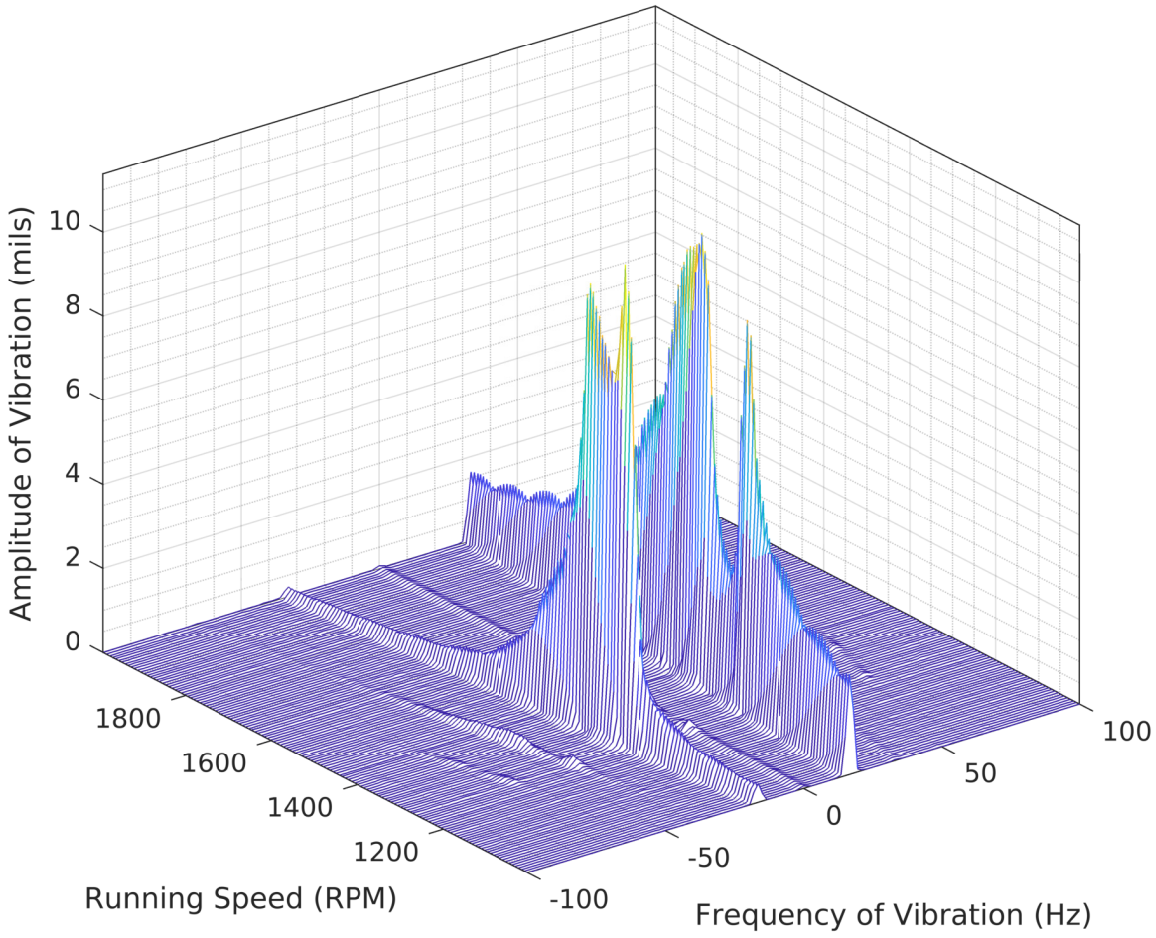

Figure 2.5: Cascade of the experimental system described in §2.2.

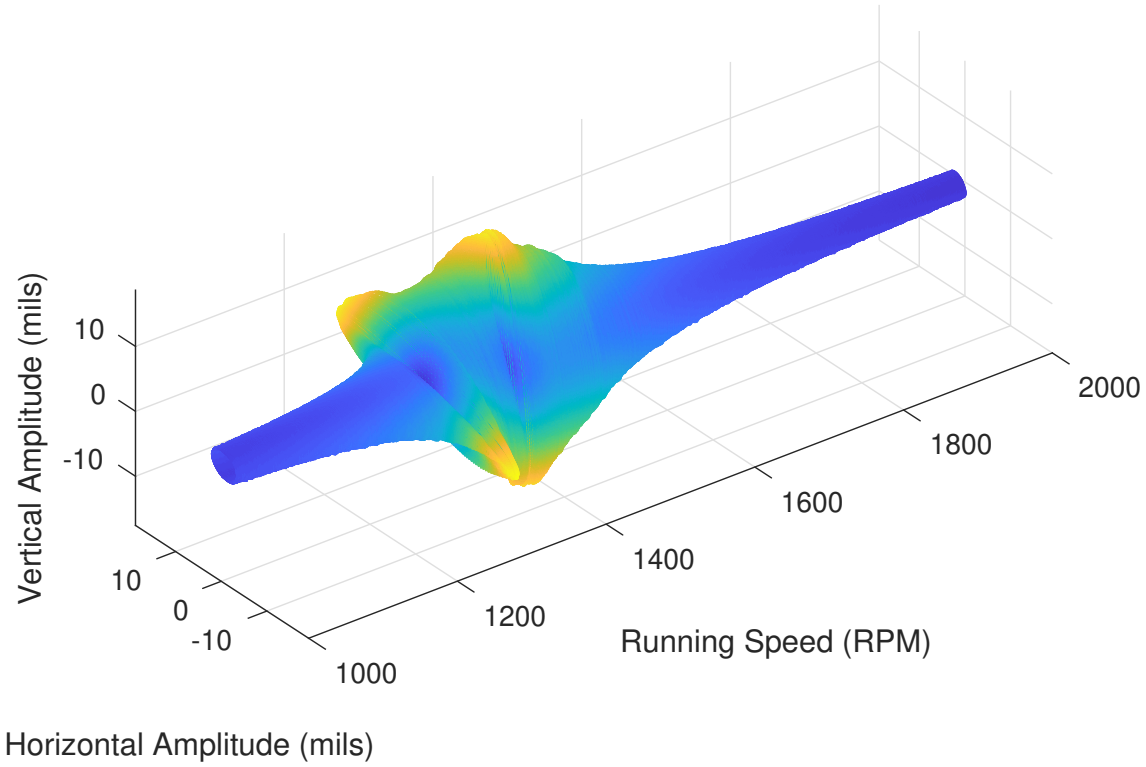

Figure 2.6: 3DOrbit of the experimental system described in §2.2.

Looking at independent orbits at specific speeds should explicitly demonstrate the orbit necking and turning negative.

Inspection of the orbits of Figure 2.7 reveals that the orbit is whirling backward between the speeds 1205-1280[RPM].

2.2.4 Filtering

Correlating phase angles between real signals can be extremely difficult due to the noise and harmonic frequencies that may disrupt the measurement. Furthermore, it can be useful to decompose a real signal into specific harmonic components of the spin speed. One such instance is in the analysis of a fluid film bearing. Often the fluid film bearing will cause an unbalance at the subsynchronous frequency of just under 0.5X. Using a filter, the response of the system to this specific frequency can

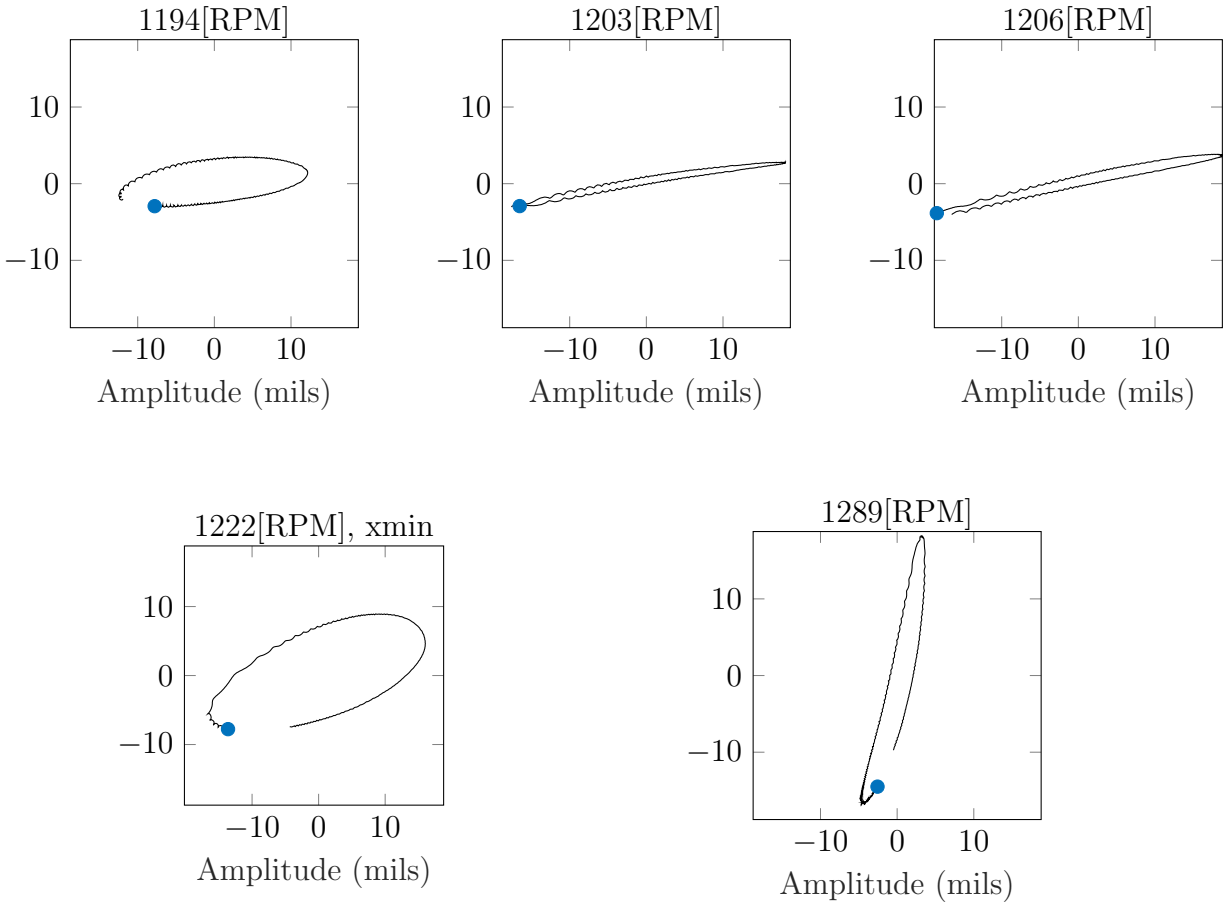

Figure 2.7: Orbits of the experimental example. Spin speed is counter-clockwise.

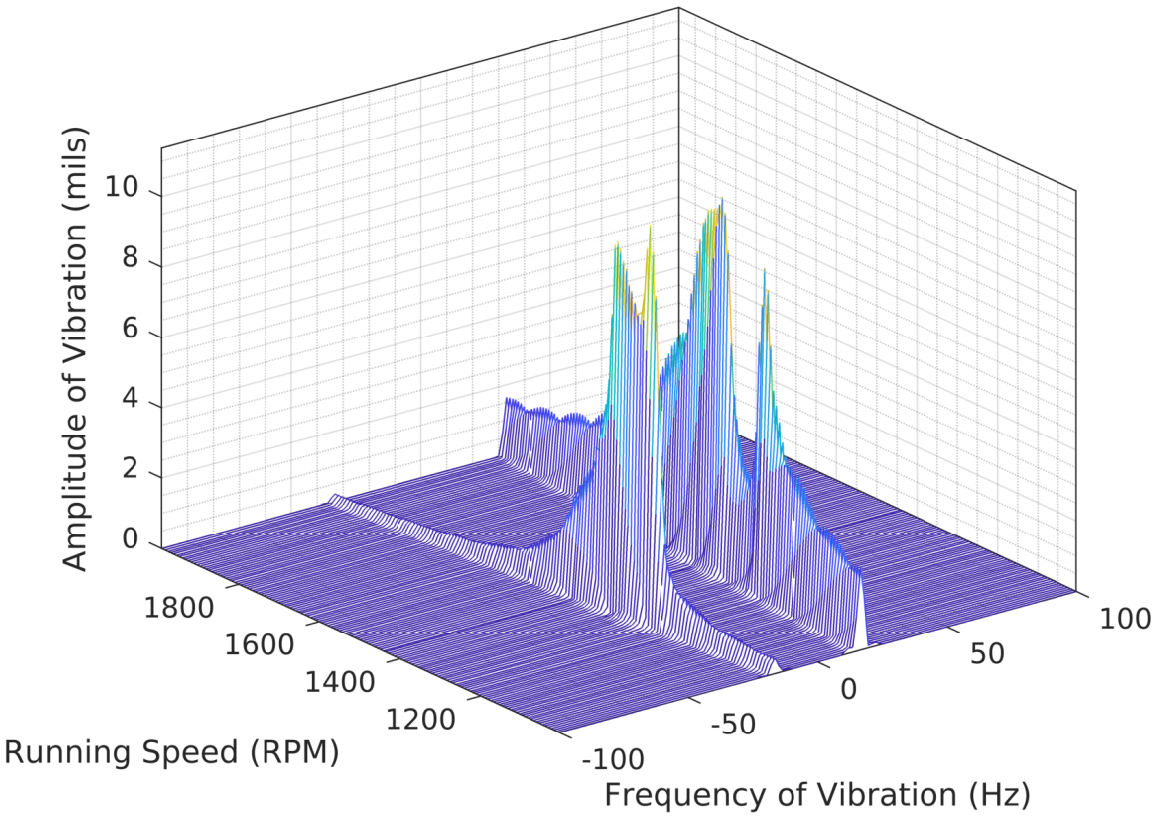

Figure 2.8: Cascade of the experimental system witha synchronous filter applied.

be extracted, allowing the analysis of phase angle and amplitude directly due to the influence of interest.

MATLAB has an extensive library of digital filters that can be adjusted to filter specific frequency ranges with no phase delay, and recall the states from the previous window as to not loose dynamic information from one step to the next.

A synchronous filter was applied the experimental example and the cascade plot is shown in Figure 2.8. All amplitudes of frequencies other than the synchronous frequencies have been eliminated. This system did not have strong super- or sub-synchronous response, so this filtering does not make an appreciable effect to the Bode plot. But, with many real systems filtering will be necessary to analyze the system.

Chapter 3

SYNTHESIS IN EXAMPLE OF A MAGNETIC BEARING ON AN OVERHUNG ROTOR

Analysis and modeling techniques of the previous chapters will now be put to use in a practical example. The goal of which will be to reduce vibration on an overhung disk rotor system with the use of an Active Magnetic Bearing(AMB). An experimental test rig, not unlike the system used in the experimental example of §2.2, will be used to calibrate a finite element theoretical model. Then, the theoretical model will be extended to include an AMB near the overhung disk. The model will be evaluated for stability, and parameters of the control algorithm for the AMB will be varied to attempt to eliminate the first natural frequency and stabilize the system.

3.1 Physical System

The rotor system of interest is depicted in Figure 3.1. Geometric parameters are listed in Table 3.1. The springs at nodes 1 & 4 are intended to represent bushings, portion at node 6 is the rotating disk, and nodal numbers are shown as the rotor will be discretized for the finite element model.

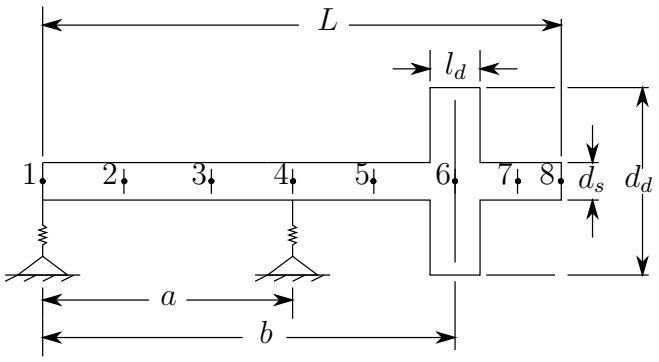

Figure 3.1: Overhung rotor system diagram.

Table 3.1: Geometric parameters of the overhung rotor system.

$L[m]$	$a[m]$	$b[m]$	$l_d[m]$	$d_d[m]$	$d_s[m]$
0.5	0.23	0.13	0.025	0.075	0.01

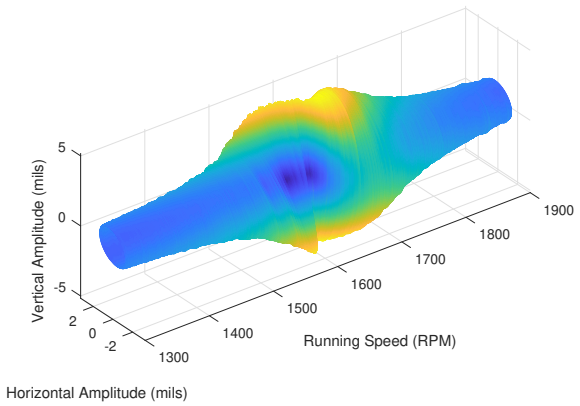

Figure 3.2: 3D Orbit of the experimental overhung rotor system.

3.2 Experimental Results

The rotor system was tested in a start-up from slow roll to 3000$[RPM]$. Data shown here is taken from 1000$[RPM]$ to 2000$[RPM]$. A set of orthogonal eddy current sensors placed near the disk on the outboard side were used to measure the position of the shaft throughout the start-up. Position data was recorded at a sampling rate of 128000$[Hz]$ with no processing applied. The resulting 3D orbit of the start-up is shown in Figure 3.2. Of note is the necking in the 3D orbit that is indicative of high anisotropy inducing a negative whirl during the first natural frequency. Also resulting from the experiment is the full spectrum cascade plot of Figure 3.3, in which it is evident that synchronous vibration dominates the spectra. Though, for the production of the bode diagram (Figure 3.4) there was a benefit in clarity from filtering the data to synchronous speed.

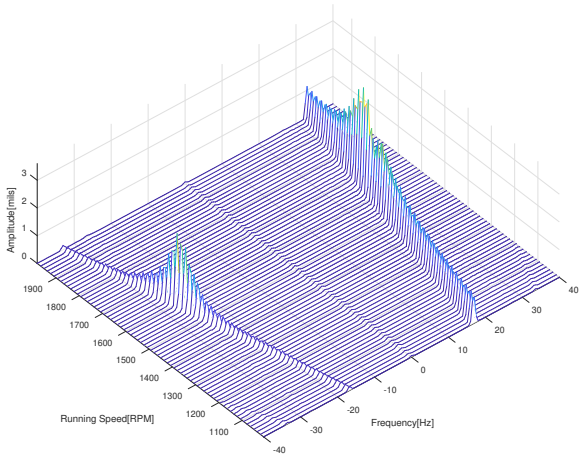

Figure 3.3: Cascade of the experimental overhung rotor system.

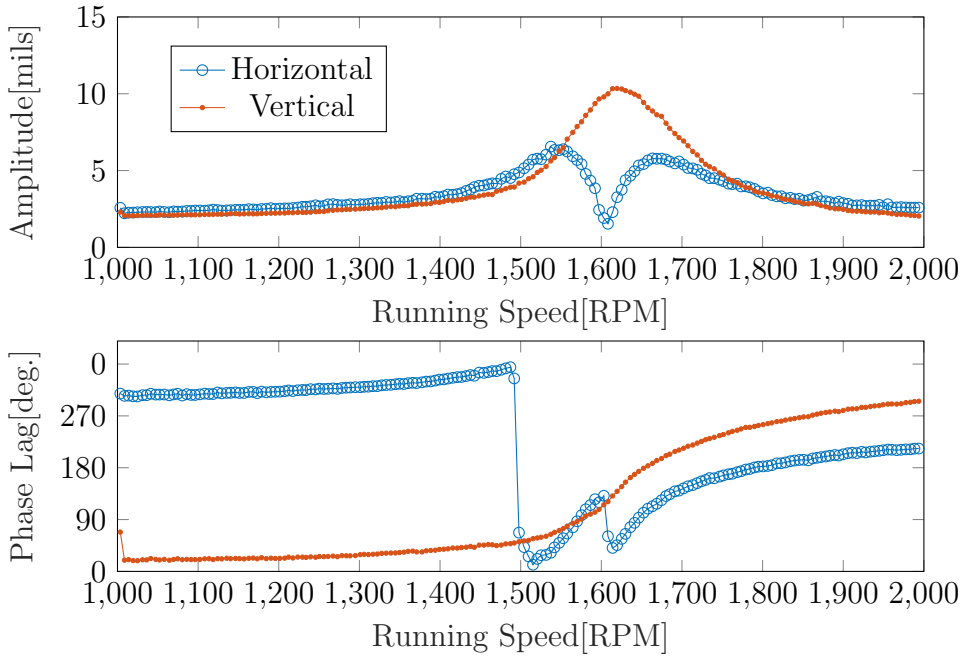

Figure 3.4: Bode diagram of the experimental overhung rotor filtered to 1X.

3.3 Theoretical Model

To create a theoretical model for this rotor system. The shaft will be discretized into 7 elements a disk at node 6 and bearings at nodes 1 and 4, as depicted in Figure 3.1. In the experiment, a small length of shaft continued after the overhung disk

Table 3.2: Properties of disks, shaft elements, and bearings of the theoretical model.

	$\rho\left[\frac{kg}{m^3}\right]$	$r[m]$	ν	$E[Pa]$	$\eta_v[s]$	η_h
Shaft	7850	0.005	0.3	210×10^9	0.0002	0
	$\rho\left[\frac{kg}{m^3}\right]$	$r[m]$	$l[m]$			
Disks	7850	0.0375	0.025			
	$k_y\left[\frac{N}{m}\right]$	$k_z\left[\frac{N}{m}\right]$	$c_y\left[\frac{Ns}{m}\right]$	$c_z\left[\frac{Ns}{m}\right]$		
Bearing A	1.7×10^5	2.2×10^5	68	88		
Bearing B	2.04×10^5	2.64×10^5	81.6	105.6		

and has been included in this model. The AMB will be included as a nodal point element with with stiffness and damping to be derived in §3.3.1. Parameter values for the finite element model are provided in Table 3.2. Discovered values such as η_v and the stiffnesses of bearing are listed here, but the process for their determination is discussed. First the model is formed to match the experimental results. Known parameters, such as beam lengths, beam diameters, density of the material, and geometry of the disk and rotor are used to begin construction of the model. Then, guesses are made for the stiffnesses in the rotor bearings. The first natural frequency is calculated with the resulting model and its value compared to the experimentally found natural frequency from the bode diagram (fig.3.4). Stiffness are then adjusted to better match the natural frequency, and this is repeated until the natural frequency of the model matches the experiment. After this process, the stiffness was determined to be around $2 \times 10^5\left[\frac{N}{m}\right]$.

It is evident by inspection of the Bode diagram for the experimental system (fig.3.4), and the 3D orbit, that there is anisotropy in the system, leading to the dip in amplitude of one plane of vibration. It is also known from inspection of the frequency spectrum in the cascade of figure 3.3 that in this speed range the orbit is in the opposite direction of the rotation–a phenomena only possible with anisotropy

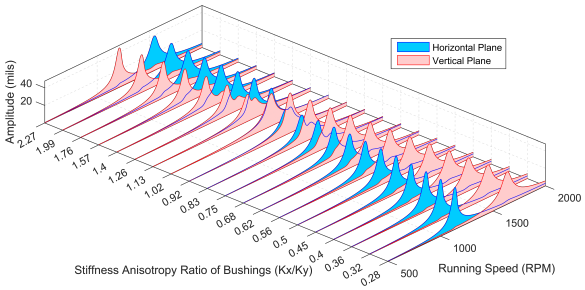

(a) 3D Orbit of the experimental overhung rotor system.

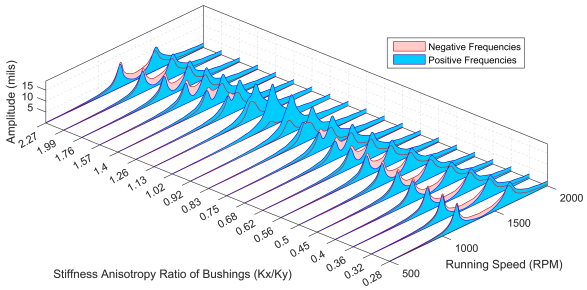

(b) 3D Orbit of the experimental overhung rotor system.

of the stiffness. Figures 3.5a&3.5b demonstrate this affect anisotropy has on both the real coordinates, as well as positive and negative whirl amplitudes.

Using the bode diagram, the stiffness anisotropy is adjusted until the shapes of the amplitudes and phases match the experimental results of figure 2.4. Then damping is added to the system to appropriately match the experimental results. The resulting bode diagram is Figure 3.6. Stiffnesses were determined to be $k_y = 1.7 \times 10^5[N/m]$ & $k_z = 2.2 \times 10^5[N/m]$. And now the resulting system is further

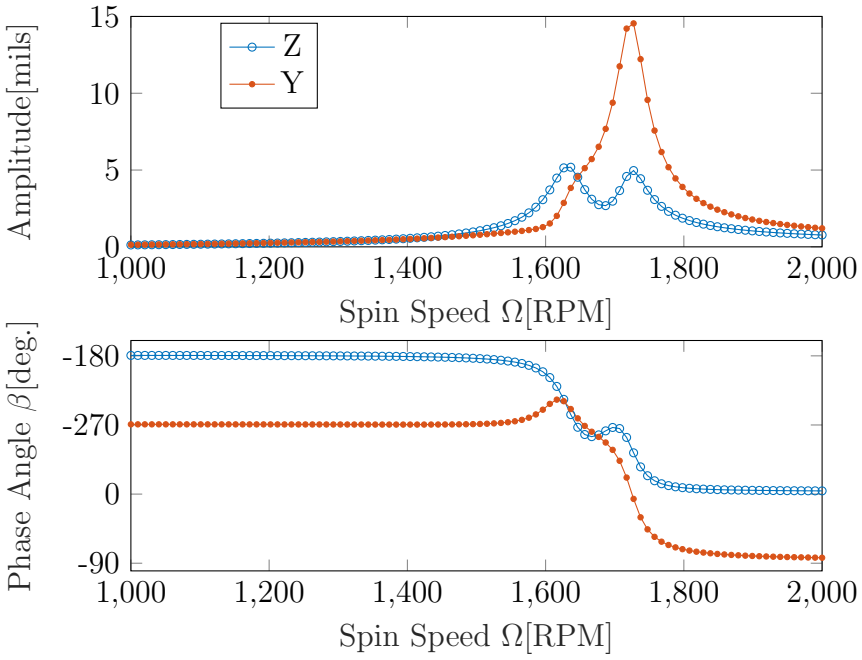

Figure 3.6: Damping ratio vs. spin speed with indication of threshold of stability.

described with an expanded speed range of 20000$[RPM]$. The new Campbell diagram of Figure 3.7, the roots locus of Figure 3.8. Additionally, the first three mode shapes are plotted for this theoretical model (Figures 3.9a, 3.9b, & 3.9c). Note that the first mode is conical in shape, but the disk is far from an antinode at node 6 so it does not experience significant gyroscopic moments. This idea is supported by the campbell diagram, fig. 3.7, as the first mode natural frequency does not change significantly over the speed range. On the other hand, the second mode has its antinode atode 6 so the disk experience maximum gyroscopic moments and the second mode critical speed is much more dependent on speed.

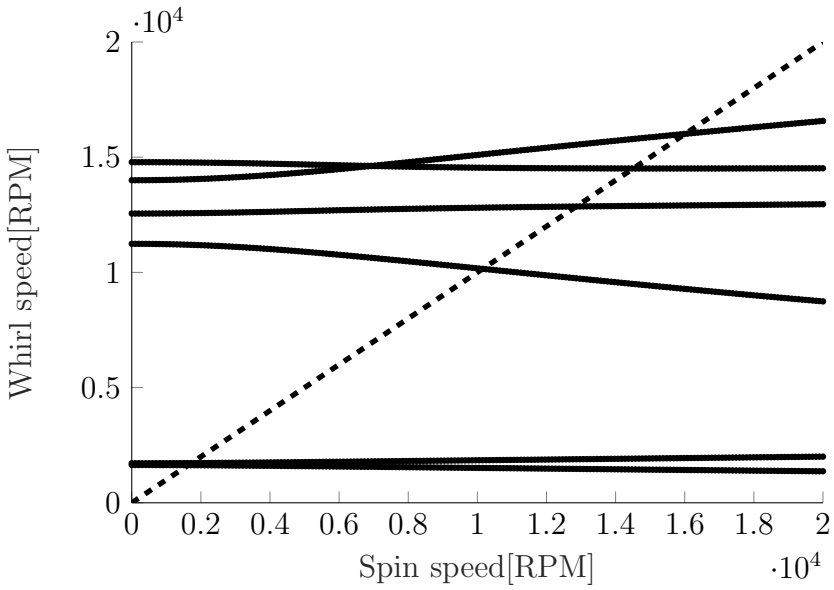

Figure 3.7: Damping ratio vs. spin speed with indication of threshold of stability.

3.3.1 Active Magnetic Bearing

Magnetic pole-rotor relationship will be derived based on the detailed derivation in [9]. Assumptions made in this model are:

- Air gap between the magnet pole face and the rotor is vanishingly small com-

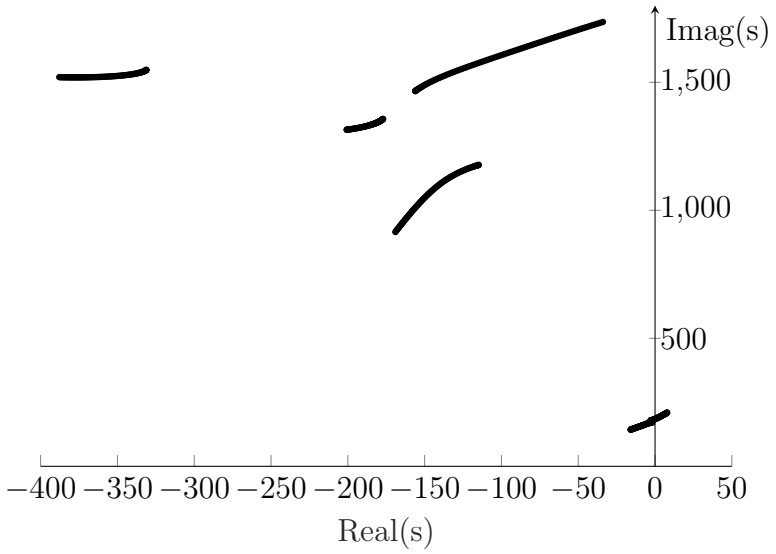

Figure 3.8: Damping ratio vs. spin speed with indication of threshold of stability.

pared to the diameter of the shaft.

- Flux leakage from the magnetic pole is negligible.
- Curvature of rotor surface under the pole face is ignored.
- A linear relationship of flux density and magnetic field is assumed.
- Hysteresis of the magnetic field is negligible.

These assumptions lead to a magnetic force due to coil current in the relationship of

$$F_m = \frac{-k_m i^2}{l_g^2} \tag{3.1}$$

where, $k_m = \frac{\mu_0 A_p N^2}{4}$, and $\mu_0 = 4\pi \times 10^{-7}$ is the absolute permeability in free air, N is the number of coil turns, A_p is the pole face area, i is the supplied electrical current, and l_g is the air gap.

Consider a set of magnetic pole pairs in each the y & z directions (i.e. One on the left and one on the right; one on top and one on bottom), where each pole pair has its own electrical circuit. There are 4 total magnets in this model, 2 in each direction,

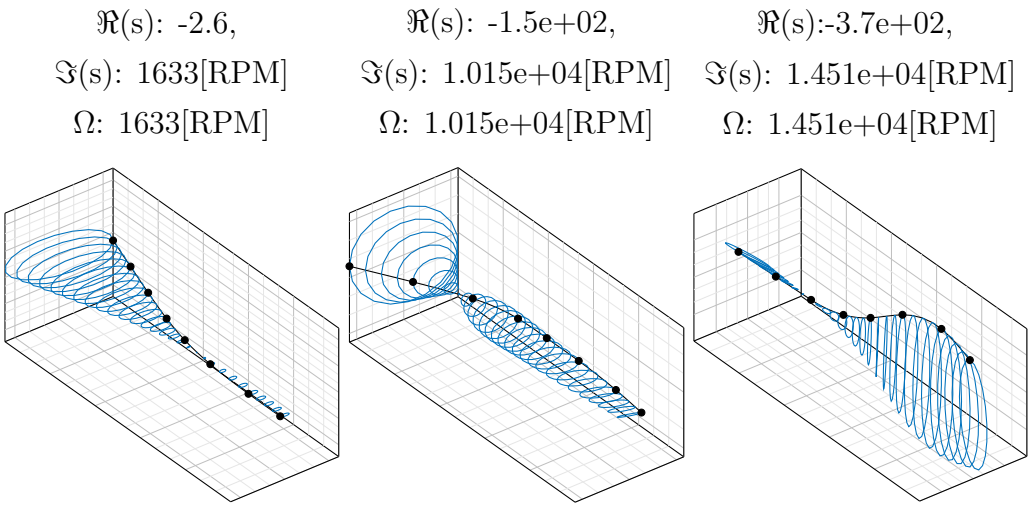

(a) Mode Shape 1. (b) Mode Shape 2. (c) Mode Shape 3.

and 8 total poles where 2 form a magnet. All poles in the neutral position of the system will have a nominal air gap of g_0 and will be supplied by a bias current of i_0. Deviations of the current from this bias will be considered as i_y and i_z. Deviations of the position from this neutral position are the displacements of the rotor at this beam axis location, v, & w. Therefore, total current will be $(i_0 \pm i_y)$ & $(i_0 \pm i_z)$ for opposing poles in the y & z directions respectively. Similarly, total gaps are given by $(g_0 \pm v)$ & $(g_0 \pm w)$. Using these new definitions for the gap and current, and summing forces in the y & z directions leads to the total forces

$$F_y = K_m \left\{ \left(\frac{i_0 + i_y}{g_0 + v} \right)^2 - \left(\frac{i_0 - i_y}{g_0 - v} \right)^2 \right\} \ \& \ F_z = K_m \left\{ \left(\frac{i_0 + i_z}{g_0 + w} \right)^2 - \left(\frac{i_0 - i_z}{g_0 - w} \right)^2 \right\} \tag{3.2}$$

where, $K_m = k_m \cos(\alpha)$, and α is half of the angle between the poles of a magnet. Linearizing the magnetic force equations (3.2), while assuming the operating point for the system is where all positions and control currents are zero, results in

$$F_y = k_i i_y + k_y v, \ \& \ F_z = k_i i_z + k_z w \tag{3.3}$$

where, $k_i = 4K_m \frac{i_0}{g_0^2}$ is the current stiffness developed by the bias current, and $k_y = k_z = k_s = -4K_m \frac{i_0^2}{g_0^3}$.

3.3.1.1 Proportional Derivative Control

A control algorithm is used to control the current sent to each pair of poles based on the position (proportional) and velocity (derivative) of the rotor. It is assumed that each set of pole pairs will receive opposite currents to act as a unit. Current control is given by

$$i_y = -k_g(k_p v + k_v \dot{v}),\ \&\ i_z = -k_g(k_p w + k_v \dot{w}) \tag{3.4}$$

where, k_g is the power amplifier gain, k_p is the proportional gain, and k_v is the derivative gain. The total linearized force becomes

$$F_y = -(k_g k_i k_p - k_s)v - k_g k_i k_v \dot{v},\ \&\ F_z = -(k_g k_i k_p - k_s)w - k_g k_i k_v \dot{w} \tag{3.5}$$

so then the stiffness of the AMB is $k_{mag} = (k_g k_i k_p - k_s)$ and the damping is $d_{mag} = k_g k_i k_v$. As an equation of nodal stiffness and damping in the finite element system it can be represented by

$$\underline{\mathbf{D}}^m \dot{\vec{\mathbf{q}}}_k + \underline{\mathbf{K}}^m \vec{\mathbf{q}}_k = 0 \tag{3.6}$$

where,

$$\underline{\mathbf{K}}^m = \begin{bmatrix} k_{mag} & 0 & 0 & 0 & 0 & 0 \\ 0 & k_{mag} & 0 & 0 & 0 & 0 \\ 0 & 0 & 0 & 0 & 0 & 0 \\ 0 & 0 & 0 & 0 & 0 & 0 \\ 0 & 0 & 0 & 0 & 0 & 0 \\ 0 & 0 & 0 & 0 & 0 & 0 \end{bmatrix} \quad \underline{\mathbf{D}}^m = \begin{bmatrix} d_{mag} & 0 & 0 & 0 & 0 & 0 \\ 0 & d_{mag} & 0 & 0 & 0 & 0 \\ 0 & 0 & 0 & 0 & 0 & 0 \\ 0 & 0 & 0 & 0 & 0 & 0 \\ 0 & 0 & 0 & 0 & 0 & 0 \\ 0 & 0 & 0 & 0 & 0 & 0 \end{bmatrix}$$

Knowing that the amplitude of vibration, A, in the experimental system peaks at about 10 mils, or $2.54 \times 10^{-4}[m]$, the greatest possible velocity for synchronous vibration is determined using the simple equation $v = (A/2)\omega$, where ω is the whirl speed in rad/s. Under the assumption of synchronous vibration, ω during the natural frequency is then $167.6[Rad/s]$. Leading to a velocity, v, of $0.02[m/s]$. Looking also at the velocity in the upper speed range, knowing that the amplitude of vibration

after the first natural frequency is equal to the eccentricity of the unbalance. With an eccentricity of 1×10^{-5} and an upper speed of 15000$[RPM]$, the velocity is calulated to be 0.008$[m/s]$. Since the estimated velocity during the natural frequency is higher, it will be used to limit the output of the AMB controller. Since the total voltage supply of most digital to analog converters is limited to 10$[V]$ the control voltage is calculated to be within this range for the given velocity and positions that will be seen under synchronous vibration. This results in a limitation of the term k_v, which is proportional to the voltage control signal that is sent to the amplifier for conversion to control current. A value of 480$[Vs/m]$ would max the converter, so the value to be determined must be less than this. With a similar, but separate, evaluation of the displacement leads to a cap of 500000$[V/m]$ for k_p–a value not anticipated to be necessary. The maximum force due to unbalance is $\epsilon m_d \Omega^2$, where ϵ is the eccentricity, and m_d is the mass of the disk. At the maximum speed expected of 15000$[RPM]$, the force will be 24$[N]$. To counteract this force with a single coil would require 1.25$[A]$, or 0.625$[A]$ per coil in a opposing pair. The amplifier gain is assumed to be programmable to $k_g = 1[A/V]$, this leads to a reasonable choice of bias current at 0.5$[A]$ to maintain a good resolution on the voltage output of the controller. The voltage should not need to peak above 1.25$[V]$, and will rest at an output of 0.5$[V]$. Now in the next section, control parameters k_v & k_p will be determined to maximize stability of the system while also minimizing vibration.

3.4 Addition of Magnetic Bearing to the Rotor Model

In order to measure the effectiveness of the AMB, the Stability of the theoretical model before the addition is shown in Figure 3.10a. The magnetic bearing added is modeled after a magnetic bearing that is currently in the lab at California Polytechnic State University. This theoretical exercise is intended to be followed by experimental

verification not included in this work. The parameters used are listed in 3.3 as well as the control values whose determinations will be evaluated.

First the position of the AMB must be determined. By inspection of the mode shapes, it is evident that in the first mode (the mode we are most concerned about suppressing) a conical mode shape exists with increasing amplitude toward the end of the beam after the second bearing. It is also known that the source of vibration, the rotating disk, is located at nodal index 6. With both these pieces of information, node 7 is chosen as a starting point for the AMB for two reasons: having the AMB closer to the source of vibration reduces the phase lag between the source and the bearing, increasing the effectiveness of control; amplitude of vibration, according to the mode shape, is higher on the outboard side of the disk and placing the AMB on this side will minimize more vibration.

To determine best derivative control, the proportional control was set to zero and the derivative increased until the first mode on the Roots locus(fig. 3.8) moved away from the imaginary axis, becoming more damped. The resulting movement of the Roots on the Roots Locus is given in Figure 3.11. Notice how none of the new modes that appear on the roots locus cross the real plane–this demonstrates the stability of the new system. Stability of the system with the AMB addition is confirmed in the stability plot of Figure 3.10b. In fact from the roots locus with $k_v = 1$ to the roots locus with $k_v = 10$ the first mode of vibration is completely relegated to the imaginary axis and not reaching break-away for this entire speed range–this indicates that the first mode has been over-damped.

Proportional control, k_p, was added after the ideal derivative control was determined, but it did not improve the performance of the controller. It is possible that the stiffness of the bearing inherent to the bias current is sufficient. In any case, proportional control in this scenario is only adding stiffness to the system, and with

Table 3.3: Active Magnetic Bearing Parameters.

$\alpha[rad]$	$g_0[m]$	$i_0[A]$	$k_p[\frac{V}{m}]$	$k_v[\frac{Vs}{m}]$	$k_g[\frac{A}{V}]$	$N[\#]$	$A_p[m^2]$
$\frac{\pi}{8}$	2.5×10^{-3}	0.5	0	10	1	800	$\frac{5}{100*100}$

the objective being to minimize vibration, k_p does not help. So the optimal control is determined to be with $k_v = 10[Vs/m]$. The remaining parameters for this resulting controller are listed in table 3.3. It is worthwhile to note that this optimal control is standing on the basis that the feedback is of synchronous vibration only. In a scenario where there is significant sub or super-synchronous vibrations, this controller may exceed its voltage limit. It is recommended that the feedback signal be filtered to match rotor speed to ensure this scenario does not take place. Furthermore, without at least low-pass filtering of the feedback signal the control would certainly provide out of range signals due to the volatile nature of derivatives of discrete signals.

The frequency spectrum is provided showing the result of the AMB application in the bode diagram of Figure 3.12. Certainly it can be concluded that the AMB is successfully performing the desired task of reducing the vibration while also inproving the stability of the system.

Now the result from this synthesis exercise can be implemented on the actual experimental test rig with the AMB set to the control parameters suggested. The power of the finite element method in this application is the ability to move components around with ease. For instance, with the changing of just two parmeters in the input file for this model, a new simulation is create for complete levitation of the overhung rotor. The AMB is put in place of bearing b and the resulting frequency spectrum is plotted in Figure 3.13

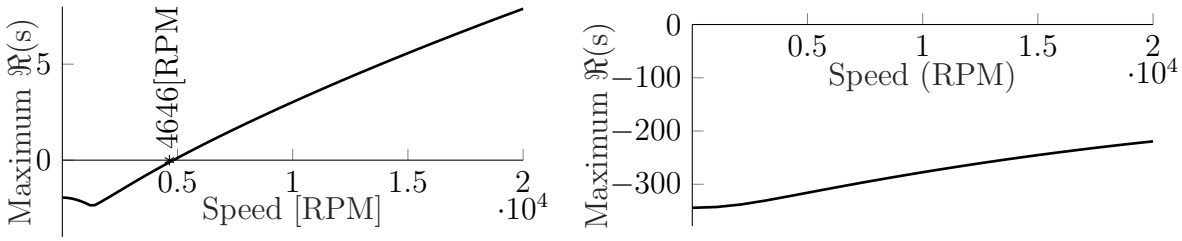

(a) Stability plot of rotor without AMB, threshold of stability: 4646[RPM].

(b) Stability plot of rotor with AMB, indicates complete stability through speed range.

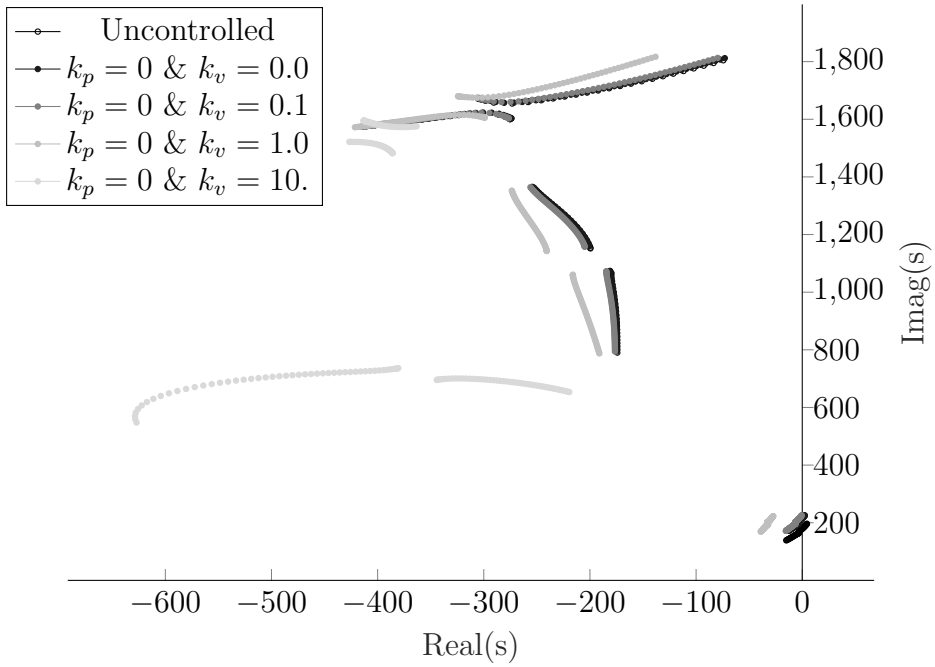

Figure 3.11: Roots locus of Overhung rotor system with varying k_v.

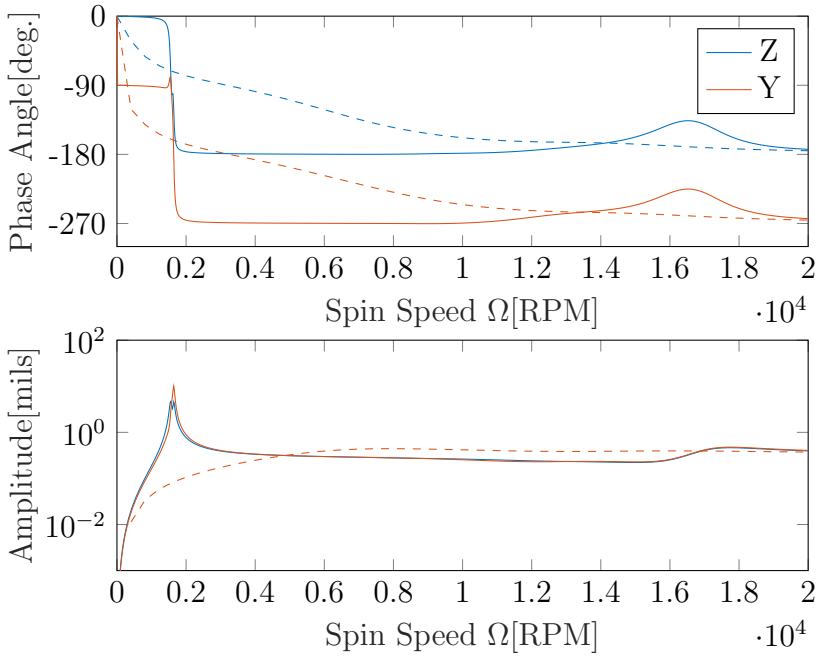

Figure 3.12: Bode diagram at node 6 comparing the rotor without AMB(solid) and with AMB(dashed).

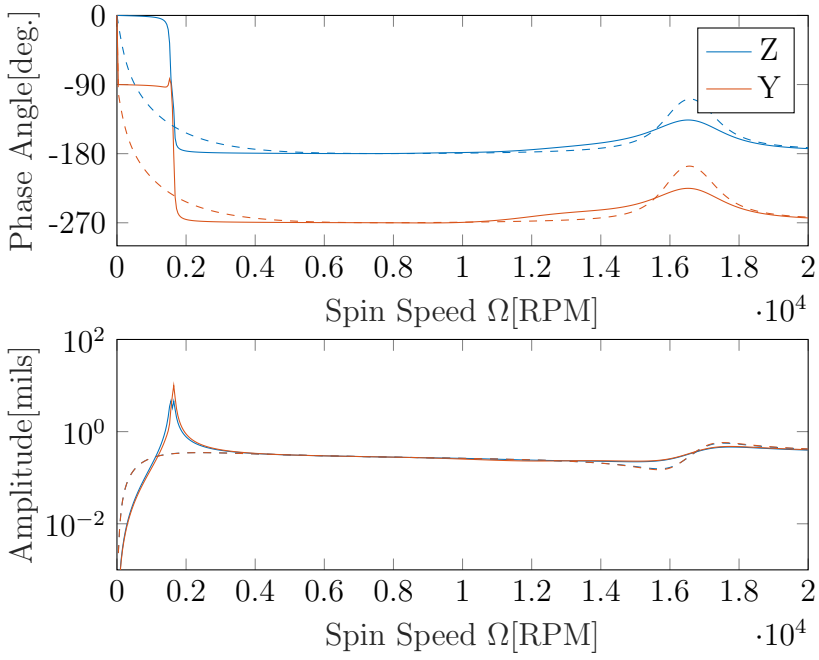

Figure 3.13: Bode diagram at node 6 comparing the rotor without AMB(solid) and with AMB(dashed) for complete levitation at node 4.

BIBLIOGRAPHY

[1] M. L. Adams. *Rotating machinery vibration: from analysis to troubleshooting*. CRC Press, 2009.

[2] L. Andersen and S. R. Nielsen. Elastic beams in three dimensions. *Aalborg University*, 2008.

[3] G. Barbaraci. Axial active magnetic bearing design. *Journal of Vibration and Control*, 22(5):1190–1197, 2016.

[4] D. E. Bently and T. Hatch'Charles. Fundamentals of rotating machinery diagnostics. *Mechanical Engineering-CIME*, 125(12):53–54, 2003.

[5] A. Bouaziz, S. Bouaziz, T. Hentati, J. Y. Cholley, and M. Haddar. Vibrations monitoring of high speed spindle with active magnetic bearings in presence of defects. *International Journal of Applied Electromagnetics and Mechanics*, 49(2):207–221, 2015.

[6] D. W. Childs. *Turbomachinery rotordynamics: phenomena, modeling, and analysis*. John Wiley & Sons, 1993.

[7] R. R. Craig and A. J. Kurdila. *Fundamentals of structural dynamics*. John Wiley & Sons, 2006.

[8] S. M. Darbandi, A. Habibollahi, M. Behzad, H. Salarieh, and H. Mehdigholi. Sensor runout compensation in active magnetic bearings via an integral adaptive observer. *Control Engineering Practice*, 48:111–118, 2016.

[9] A. Das, M. Nighil, J. Dutt, and H. Irretier. Vibration control and stability analysis of rotor-shaft system with electromagnetic exciters. *Mechanism and Machine Theory*, 43(10):1295–1316, 2008.

[10] A. Dimarogonas and S. Haddad. Vibration for engineers. *VhSˆ WI) IN914A R4 22k AWn 22kVAR5£ ilOuF 100k [ˆ. 2k 22k 22k*, page 252, 1993.

[11] B. Ertas and J. Vance. The influence of same-sign cross-coupled stiffness on rotordynamics. *Journal of Vibration and Acoustics*, 129(1):24–31, 2007.

[12] M. G. Farmakopoulos, M. D. Thanou, P. G. Nikolakopoulos, C. A. Papadopoulos, and A. P. Tzes. A control model of active magnetic bearings. In *Proceedings of the 3rd International Conference of Engineering Against Failure (ICEAF III)*, pages 26–28, 2013.

[13] L. Forrai. Stability analysis of symmetrical rotor-bearing systems with internal damping using finite element method. In *International Gas Turbine and AeroB engine Congress and Exhibition, Birmingham, UK*, 1996.

[14] G. Genta. Consistent matrices in rotor dynamic. *Meccanica*, 20(3):235–248, 1985.

[15] G. Genta. On a persistent misunderstanding of the role of hysteretic damping in rotordynamics. *TRANSACTIONS-AMERICAN SOCIETY OF MECHANICAL ENGINEERS JOURNAL OF VIBRATION AND ACOUSTICS*, 126(3):459–461, 2004.

[16] G. Genta. *Dynamics of rotating systems*. Springer Science & Business Media, 2007.

[17] T. Gmur and J. Rodrigues. Shaft finite elements for rotor dynamics analysis. *Journal of Vibration and Acoustics*, 113(4):482–493, 1991.

[18] U. Goerguelue. Beam theories the difference between euler-bernoulli and timoschenko. *Lecture Handouts*, 2009.

[19] P. Goldman and A. Muszynska. Application of full spectrum to rotating machinery diagnostics. *Orbit*, 20(1):17–21, 1999.

[20] N. Instruments. Ni labview for compactrio developer's guide. 2013.

[21] C. Jin, Y. Xu, J. Zhou, and C. Cheng. Active magnetic bearings stiffness and damping identification from frequency characteristics of control system. *Shock and Vibration*, 2016, 2016.

[22] M. A. Kandil. *On rotor internal damping instability*. PhD thesis, Imperial College London (University of London), 2005.

[23] B. Kirchgäßner. Finite elements in rotordynamics. *Procedia Engineering*, 144:736–750, 2016.

[24] A. Kuperman. Uncertainty and disturbance estimator-assisted control of a two-axis active magnetic bearing. *Transactions of the Institute of Measurement and Control*, 38(6):764–772, 2016.

[25] Y. Luo. An efficient 3d timoshenko beam element with consistent shape functions. *Adv. Theor. Appl. Mech*, 1(3):95–106, 2008.

[26] A. Muszynska. *Rotordynamics*. CRC press, 2005.

[27] V. Mykhaylyshyn. *Application of Active Magnetic Force Actuator for Control of Flexible Rotor System Vibrations*. PhD thesis, Cleveland State University, 2011.

[28] H. Nelson and J. McVaugh. The dynamics of rotor-bearing systems using finite elements. *Journal of Engineering for Industry*, 98(2):593–600, 1976.

[29] H. Roy, A. Das, and J. Dutt. An efficient rotor suspension with active magnetic bearings having viscoelastic control law. *Mechanism and Machine Theory*, 98:48–63, 2016.

[30] G. Schweitzer. Active magnetic bearings-chances and limitations. In *IFToMM Sixth International Conference on Rotor Dynamics, Sydney, Australia*, volume 1, pages 1–14, 2002.

[31] E. Swanson, C. D. Powell, and S. Weissman. A practical review of rotating machinery critical speeds and modes. *Sound and vibration*, 39(5):16–17, 2005.

[32] K. Tammi. *Active vibration control of rotor in desktop test environment*. VTT, 2003.

[33] J. M. Vance. *Rotordynamics of turbomachinery*. John Wiley & Sons, 1988.

[34] H. Wettergren and K.-O. Olsson. Dynamic instability of a rotating asymmetric shaft with internal viscous damping supported in anisotropic bearings. *Journal of sound and vibration*, 195(1):75–84, 1996.

[35] T. Yamamoto and Y. Ishida. *Linear and nonlinear rotordynamics: a modern treatment with applications*, volume 11. John Wiley & Sons, 2001.

[36] E. Zorzi and H. Nelson. Finite element simulation of rotor-bearing systems with internal damping. *Journal of Engineering for Power*, 99(1):71–76, 1977.

.1 Bernoulli-Euler Beam equation

Assumptions used to derive the Bernoulli-Euler beam equation are (Complete derivation in [7]):

1. Beam is bending in a plane, in this case in the y-direction, where the x-direction is along the length of the beam.

2. The neutral axis undergoes no deformation in the longitudinal direction.

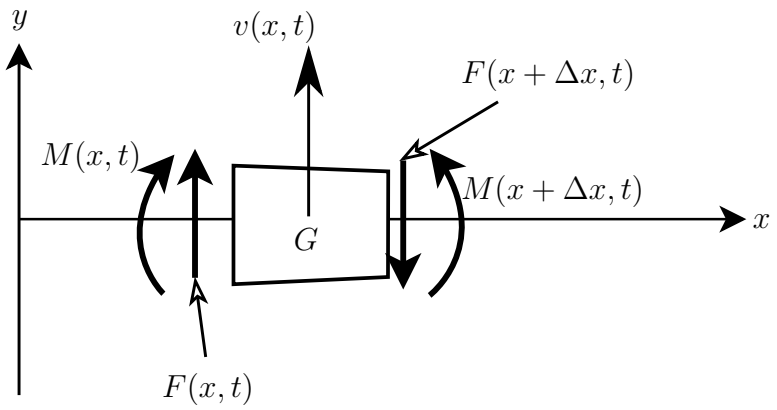

Figure .14: Free body diagram of a beam section in planar bending.

3. Cross sections remain plane and perpendicular to the nuetral axis.

4. The material is linear-elastic.

5. Stresses in the y and z direction are negligible compared to those in the x direction.

6. Rotary inertial effects are not considered.

7. Mass density is constant at each cross section, so that each mass center is coincident with the centroid of that section.

Using kinematics and assumptions 2 & 3, the strain in the x direction may be related to the curvature of the beam, $\mu(x,t)$, and the distance from the neutral axis by

$$\epsilon = -\frac{y}{\mu} \tag{.7}$$

then, with assumption 4 & 7 the relation from curvature to moment is

$$M(x,t) = \frac{EI}{\mu} \tag{.8}$$

where E, Young's modulus, and I, area moment of inertia are constant in cross sections. By using Newton's laws and the free body diagram of a single beam element,

see Figure .14, the equations of motion are summarized as:

$$\sum F_y = \Delta m \ddot{v} \quad \& \quad \sum M_G = 0 \tag{.9}$$

Moment equation is represented as moments summarized at the center of mass, G. The right hand side of moment equation of EOM (.9) is know to be null due to assumption 6. Applying Newton's equations (.9) to the FBD of Figure .14 results in the force equation

$$F(x,t) - F(x+\Delta x,t) = \rho A \Delta x \frac{\partial^2 v}{\partial t^2} \tag{.10}$$

and moment equation

$$-M(x,t) + M(x+\Delta x,t) + F(x,t)\left(\frac{-\Delta x}{2}\right) + [-F(x+\Delta x,t)]\left(\frac{\Delta x}{2}\right) = 0 \tag{.11}$$

Taking the limit of equations (.10) & (.11) as $\Delta x \to 0$ results in equations (.12) & (.13) respectively.

$$\frac{\partial F}{\partial x} = -\rho A \frac{\partial^2 v}{\partial t^2} \tag{.12}$$

$$\frac{\partial M}{\partial x} - F = 0 \tag{.13}$$

Assuming the beam slope, $\frac{\partial v}{\partial x}$, remains relatively small, then linearized curvature of the beam is inversely related to $\frac{\partial^2 v}{\partial x^2}$. Substituting this linearized curvature in (.8) produces

$$M(x,t) = EI \frac{\partial^2 v}{\partial x^2} \tag{.14}$$

Using linearized moment equation (.14), combined with (.12) & (.13) lends the Euler beam equation

$$\frac{\partial^2}{\partial x^2}\left(EI \frac{\partial^2 v}{\partial x^2}\right) = -\rho A \frac{\partial^2 v}{\partial t^2} \tag{.15}$$

This is the governing differential equation for transverse motion of a slender beam. This equation is not suitable for an application involving lengths that are not much greater than the width of the beam [16].

```
classdef RotorFEM< handle
    %MODEL Summary of this class goes here
    %   Detailed explanation goes here

    properties
        M
        C
        K
        F
        input_file
        npos

    end
    properties (Access = private)

    end
    methods
        function obj = Model(input_filename)
            if nargin == 1
                obj.Assem(input_filename);
                obj.input_file = input_filename;
            end
        end
    end

end
```

```
function Assem(obj,input_file)
run(input_file)

nodes = size(elems,1)+1;
npos = zeros(nodes,1);
for ii = 1:nodes-1
    npos(ii+1) = npos(ii) + elems(ii,2);
end
obj.npos = npos;

K = zeros(nodes*DOF,nodes*DOF);
C = zeros(nodes*DOF,nodes*DOF);
M = zeros(nodes*DOF,nodes*DOF);
F = zeros(nodes*DOF,1);
for ii = 1:1:size(elems,1)
    E = mate(elems(ii,1),2);
    l = elems(ii,2);
    do = elems(ii,3);
    if size(elems(ii,:))<4
        di=0;
    else
        do=elems(ii,4);
    end
    I = obj.AInert(do,di);
    A = obj.Area(do,di);
    rho = mate(elems(ii,1),3);
```

```
27      nuv = mate(elems(ii,1),4);
28      poi = mate(elems(ii,1),5);
29      Id = obj.DiaInert(do,l,rho,di);
30      Ip = obj.PolInert(do,l,rho,di);
31      [kbe, cbe, mbe] = obj.TBeam(E,I,l,A,rho,Id,Ip,nuv,poi,DOF
            );
32      K = obj.Add(K,kbe,(ii-1)*DOF+1:(ii+1)*DOF);
33      C = obj.Add(C,cbe,(ii-1)*DOF+1:(ii+1)*DOF);
34      M = obj.Add(M,mbe,(ii-1)*DOF+1:(ii+1)*DOF);
35  end
36
37  if exist('disks', 'var')
38      for ii = 1:1:size(disks,1)
39          do = disks(ii,3);
40          l = disks(ii,2);
41          rho = mate(disks(ii,1),3);
42          a = disks(ii,4);
43          Ki = disks(ii,5);
44          if size(disks(ii,:))<7
45              di=0;
46          else
47              di=disks(ii,7);
48          end
49          md = obj.Mass(do,l,rho,di);
50          Ip = obj.PolInert(do,l,rho,di);
51          Id = obj.DiaInert(do,l,rho,di);
52          [mi,gi,fi] = obj.Disk(md,Id,Ip,a,Ki,DOF);
```

```
53          M = obj.Add(M,mi,(disks(ii,6)*DOF-DOF+1:disks(ii,6)*
                DOF));
54          C = obj.Add(C,gi,(disks(ii,6)*DOF-DOF+1:disks(ii,6)*
                DOF));
55          F = obj.AddVect(F,fi,(disks(ii,6)*DOF-DOF+1:disks(ii
                ,6)*DOF));
56      end
57  end
58
59  for ii = 1:1:size(bears,1)
60      kx = beartypes(bears(ii,1),2);
61      ky = beartypes(bears(ii,1),3);
62      c = beartypes(bears(ii,1),4);
63      [ki,ci] = obj.Bear(kx,ky,c,DOF);
64      K = obj.Add(K,ki,(bears(ii,2)*DOF-DOF+1:bears(ii,2)*DOF))
            ;
65      C = obj.Add(C,ci,(bears(ii,2)*DOF-DOF+1:bears(ii,2)*DOF))
            ;
66
67  end
68  if exist('mags', 'var')
69      for ii = 1:1:size(mags,1)
70          olddir = pwd;
71          cd(char(magfile(mags(ii,1),2)))
72          Magfn = str2func(char(magfile(mags(ii,1),3)));
73          [ki, ci] = Magfn();
74          cd(olddir)
```

```
75          K = obj.Add(K, ki, (mags(ii,2)*DOF-DOF+1:mags(ii,2)*DOF
                ));
76          C = obj.Add(C, ci, (mags(ii,2)*DOF-DOF+1:mags(ii,2)*DOF
                ));
77
78      end
79  end
80  obj.M = M;
81  obj.C = C;
82  obj.K = K;
83  obj.F = F;
```

```
1   function [ K,D,M ] = TBeam( obj, E,I,l,A,rho,Id,Ip,nuv,poi,
        DOF )
2   %TBeam Timoshenko beam element
3   % disp1y disp1z ang1y ang1z disp2y disp2z ang2y ang2z disp1x
        ang1x disp2x ang2x
4   %
        ----------------------------------------------------------------
5   %|
        |disp1y
6   %|
        |disp1z
7   %|
```

```
    |ang1y
%|
    |ang1z
%|
    |disp2y
%|
    |disp2z
%|
    |ang2y
%|
    |ang2z
%|
    ------------------------------------------------------------
    |ang2x
%% Properties %%
k = 6*(1+poi)/(7+6*poi);
G = E/2/(1+poi);
alph = 12*E*I/k/G/A/l^2;
%% Variables %%
syms x
z = x/l;
```

```
%% Shape Functions %%
N1 = 1-z;
N2 = z;
Tt1 = (1/(1+alph))*(2*z^3 - 3*z^2 - alph*z + 1 + alph);
Tt2 = (1/(1+alph))*(-2*z^3+3*z^2+alph*z);
Tr1 = (l/(1+alph))*(z^3 - (2+1/2*alph)*z^2 + (1+1/2*alph)*z);
Tr2 = (l/(1+alph))*(z^3 - (1-1/2*alph)*z^2 - 1/2*alph*z);
Rt1 = 6/l*(1/(1+alph))*(z^2-z);
Rt2 = -Rt1;
Rr1 = (1/(1+alph))*(3*z^2 - (4+alph)*z + 1 + alph);
Rr2 = (1/(1+alph))*(3*z^2 - (2-alph)*z);
%% Transformation Matricies %%
P = [0   0 0 0 0 0;
     0   0 0 0 0 0;
     0 -1 0 0 0 0;
     1   0 0 0 0 0;
     0   0 0 0 0 0;
     0   0 0 0 0 0];
Di = [12*E*I/alph/l^2          0       0    0    0              0;
     0          12*E*I/alph/l^2 0    0    0              0;
     0                  0       E*I  0    0              0;
     0                  0       0    E*I  0              0;
     0                  0       0    0    E*A            0;
     0                  0       0    0    0    12*E*I/alph/l^2/A
        *2*I];
Mi = diag([rho*A*l,rho*A*l,Id,Id,rho*A*l,Ip])./l;
Gi = kron(diag([0,1,0]),[0, Ip;-Ip,0])./l;
```

```
T = kron(diag([1,1,0]),[0,1;-1,0]);
N = [   Tt1   0    0   Tr1  Tt2   0    0   Tr2  0   0   0   0;
    0   Tt1   Tr1   0   0   Tt2   Tr2   0   0   0   0   0;
    0   Rt1   Rr1   0   0   Rt2   Rr2   0   0   0   0   0;
    Rt1   0    0   Rr1  Rt2   0    0   Rr2  0   0   0   0;
    0    0    0    0    0    0    0    0   N1  0   N2  0;
    0    0    0    0    0    0    0    0   0   N1  0   N2];
%% DOF Modifications%%
switch DOF
    case 6
        I = diag([1,1,-1,1,1,1]);
        N = I*N*[I,zeros(6);zeros(6),I]; % Adjust for use of
            -angy,-ang1,2y definitions in shape functions
    case 4
        P = P(1:4,1:4);
        Di = Di(1:4,1:4);
        Mi = Mi(1:4,1:4);
        Gi = Gi(1:4,1:4);
        T = T(1:4,1:4);
        I = diag([1,1,-1,1]); % Adjust for use of -angy,-ang1
            ,2y definitions in shape functions
        N = I*N(1:4,1:8)*[I,zeros(4);zeros(4),I];
    case 2
        P = P(2:3,2:3);
        Di = Di(2:3,2:3);
        Mi = Mi(2:3,2:3);
        Gi = Gi(2:3,2:3);
```

```
72          T = T(2:3,2:3);
73          N = N(2:3,[2,3,6,7]);
74  end
75  %% Elemental Integration %%
76  B = diff(N.',x) - N.'*P;
77  B = B.';
78  K_B = int(B.'*Di*B,x,0,l);
79  K_C = int(B.'*T*Di*B,x,0,l);
80  G = int(N.'*Gi*N,x,0,l);
81  M = int(N.'*Mi*N,x,0,l);
82  %% Case of symbolic Integration %%
83  if isa(l,'sym') || isa(E,'sym') || isa(I,'sym') || isa(nuv,'
        sym')
84  else
85      K_B = double(K_B);
86      K_C = double(K_C);
87      G = double(G);
88      M = double(M);
89  end
90  K =       K_B + nuv.*1i.*K_C;
91  D = nuv.*K_B +       1i.*G;
92
93  end
```

```
1  function [Md,Gd,Fd] = Disk(obj,md,Id,Ip,a,Ki,DOF)
2  %% Creates Disk nodal stiffness matrix in the form:
3  % disp1x disp1y ang1x ang1y
```

```
4  % -------------------------
5  %|                         |disp1x
6  %|                         |disp1y
7  %|                         |ang1x
8  %| ------------------------|ang1y
9
10 %% Begin Function
11 Fx = md*a;
12 Fy = md*a;
13 Mx = (Id-Ip)*Ki;
14 My = (Id-Ip)*Ki;
15 Gi=[0,Ip;-Ip,0];
16 switch DOF
17     case 6
18         Md = diag([md,md,Id,Id,md,Ip]);
19         Gd = 1i*kron(diag([0,1,0]),Gi);
20         Fd = [Fx; Fy; Mx; My; 0; 0];
21     case 4
22         Md = diag([md,md,Id,Id]);
23         Gd = 1i*kron(diag([0,1]),Gi);
24         Fd = [Fx; Fy; Mx; My];
25     case 2
26         Md = diag([md,Id]);
27         Gd = 1i*[0,0;0,Ip];
28         Fd = [Fx; My];
29 end
30 % Fx = md*a*(w^2*cos(theta+phi1)-alph*sin(theta+phi1)); %N,
```

```
    Forcing funtion at disk 1
% Fy = md*a*(w^2*sin(theta+phi1)+alph*cos(theta+phi1)); %N,
    Forcing funtion at disk 2
% Mx = -w^2*(Ip - Id)*Ki*cos(theta+phi2); %N, Forcing funtion
     at disk 1
% My = w^2*(Ip - Id)*Ki*sin(theta+phi2); %N, Forcing funtion
    at disk 2;
end
```

```
function [ Kb,Cb ] = Bear(obj,kx,ky,c,DOF)
%% Creates bearing nodal stiffness matrix in the form:
% disp1y disp1z ang1y ang1z disp1x ang1x
% ---------------------------------------
%|                                       |disp1y
%|                                       |disp1z
%|                                       |ang1y
%|                                       |ang1z
%|                                       |disp1x
%|---------------------------------------|ang1x
%% Begin function
switch DOF
    case 6
        Kb = diag([kx,ky,0,0,0,0]);
        Cb = diag([c*kx,c*ky,0,0,0,0]);
    case 4
        Kb = diag([kx,ky,0,0]);
        Cb = diag([c*kx,c*ky,0,0]);
```

```
    case 2
        k = mean([kx,ky]);
        Kb = diag([k,k]);
        Cb = diag([c*k,c*k]);
end
end
```

```
function RootLocus(Model_obj,Omega,plotmodes, ax, linetp,
   color)
%CAMPBELL Summary of this function goes here
%   Detailed explanation goes here
zci = @(v) find(v(:).*circshift(v(:), [-1 0]) <= 0);
if nargin < 6
    color = [0,0,0];
    if nargin <5
    linetp = '.';
    end
    if nargin < 4
        figure
        ax = axes;
    end
    if nargin < 3
        plotmodes = 1:2;
    end
    if nargin < 2
        return
    end
```

```
20
21 end
22
23 for ii = 1:1:length(Omega)
24     w = Omega(ii)/60*2*pi;
25     Mnew = Model_obj.M;
26     Cnew = real(Model_obj.C) + w.*imag(Model_obj.C);
27     Knew = real(Model_obj.K) + w.*imag(Model_obj.K);
28     Zer = zeros(size(Mnew));
29     ey = eye(size(Mnew));
30     A = [-Mnew^-1*Cnew, -Mnew^-1*Knew;
31         ey, Zer];
32     v1=eig(A);
33 %     AA=[Cnew Mnew;Mnew Zer];
34 %     B=[Knew Zer;Zer -Mnew];
35 %     v1=eig(B,-1i*AA);
36     [~, I] = (sort(abs((v1))));
37     eiv(:,ii) = v1((I));
38 end
39 % while min(abs(imag(eiv(1,:)))) == 0
40 %     eiv(1:2,:) = [];
41 % end
42 % eiv = eiv( ~any( isnan( eiv ) | isinf( eiv ), 2 ),: );
43
44 hold on
45 for jj = 1:1:length(plotmodes)
46
```

```
47 %       plot(ax,real(eiv(plotmodes(jj)*4-1,:)),(imag(eiv(
       plotmodes(jj)*4-1,:))),linetp,'Color
       ',[0.8500,0.3250,0.0980])
48 %       plot(ax,real(eiv(plotmodes(jj)*4-3,:)),(imag(eiv(
       plotmodes(jj)*4-3,:))),linetp,'Color',[0,0.4470,0.7410])
49         plot3(real(eiv(plotmodes(jj)*4-1,:)),abs(imag(eiv(
               plotmodes(jj)*4,:))),Omega,linetp,'Color',color,'
               MarkerSize',1);%,'o','Color',[0.8500,0.3250,0.0980],'
               MarkerSize',3)
50         plot3(real(eiv(plotmodes(jj)*4-3,:)),abs(imag(eiv(
               plotmodes(jj)*4-2,:))),Omega,linetp,'Color',color,'
               MarkerSize',1);%,'.','Color',[0,0.4470,0.7410],'
               MarkerSize',4)
51 %       plot3(real(eiv(plotmodes(jj)*4-0,:)),imag(eiv(plotmodes
       (jj)*4-0,:)),Omega,'.','Color',[0,0.4470,0.7410])
52 %       plot3(real(eiv(plotmodes(jj)*4-2,:)),imag(eiv(plotmodes
       (jj)*4-2,:)),Omega,'.','Color',[0,0.4470,0.7410])
53 %       r(1,:) = real(eiv(plotmodes(jj)*4-1,:));
54 %       r(2,:) = real(eiv(plotmodes(jj)*4-3,:));
55 %       ZeroCross1 = zci(r(1,:));
56 %       ZeroCross2 = zci(r(2,:));
57 %       if isempty(ZeroCross1)
58 %       else
59 %       strcross1 = [num2str(Omega(ZeroCross1(1)),4) ' (RPM) '
       newline];
60 %       text(ax,0,abs(imag(eiv(plotmodes(jj)*4-1,ZeroCross1(1))
       )),strcross1,'HorizontalAlignment','right','
```

```
    VerticalAlignment','bottom','FontWeight','bold');
%       plot(ax,0,abs(imag(eiv(plotmodes(jj)*4-1,ZeroCross1(1))
    )),'*k');
%       end
%       if isempty(ZeroCross2)
%       else
%       strcross2 = [ num2str(Omega(ZeroCross2(1)),4) ' (RPM) '
     newline];
%       text(ax,0,abs(imag(eiv(plotmodes(jj)*4-3,ZeroCross2(1))
    )),strcross2,'HorizontalAlignment','right','
    VerticalAlignment','bottom','FontWeight','bold');
%       plot(ax,0,abs(imag(eiv(plotmodes(jj)*4-3,ZeroCross2(1))
    )),'*k');
%       end
end
hold off
ax.YAxisLocation = 'origin';
axis([-inf,inf,0,inf])
xlabel('Real(s)')
ylabel('Imag(s)')
end
```

```
function Campbell(Model_obj,Omega,plotmodes,ax,linetp )
%CAMPBELL Summary of this function goes here
%   Detailed explanation goes here
if nargin < 5
    if nargin == 2
```

```
6           plotmodes = 1:2;
7       elseif nargin < 2
8           return
9       end
10      linetp = '.';
11      if nargin < 4
12          ax = [];
13      end
14  end
15  for ii = 1:1:length(Omega)
16      w = Omega(ii)/60*2*pi;
17      Mnew = Model_obj.M;
18      Cnew = real(Model_obj.C) + w.*imag(Model_obj.C);
19      Knew = real(Model_obj.K) + w.*imag(Model_obj.K);
20      Zer = zeros(size(Mnew));
21      ey = eye(size(Mnew));
22      A = [-Mnew^-1*Cnew, -Mnew^-1*Knew;
23          ey, Zer];
24      v1=eig(A);
25      [~, I] = sort(abs((v1)));
26      eiv(:,ii) = v1(I);
27  % eiv(:,ii)=v1;
28  end
29  if isempty(ax)
30      figure
31      ax = axes;
32  end
```

```
33 % while min(abs(imag(eiv(1,:)))) == 0
34 %     eiv(1:2,:) = [];
35 % end
36 % eiv = eiv( ~any( isnan( eiv ) | isinf( eiv ), 2 ),: );
37
38 hold on
39 for jj = 1:1:length(plotmodes)
40     plot(ax,Omega,abs(imag(eiv(plotmodes(jj)*4-2,:)))/2/pi
       *60,'.k');%,'Color',[0,0.4470,0.7410],'LineWidth',1)
41     plot(ax,Omega,abs(imag(eiv(plotmodes(jj)*4,:)))/2/pi*60,'
       .k');%, 'Color',[0.8500,0.3250,0.0980],'LineWidth',1,'
       MarkerSize',4)
42 %         plot(ax,Omega,(imag(eiv(plotmodes(jj)*4-3,:)))/2/pi
   *60,linetp,'Color',[0,0.4470,0.7410],'LineWidth',1)
43 %     plot(ax,Omega,(imag(eiv(plotmodes(jj)*4,:)))/2/pi*60,
   linetp, 'Color',[0.8500,0.3250,0.0980],'LineWidth',1)
44 %
45 %     plot(ax,Omega,imag(eiv(plotmodes(jj),:))/2/pi*60,linetp
   ,'Color',[0,0.4470,0.7410],'LineWidth',1)
46
47 end
48 plot(Omega,Omega,'--k','LineWidth',2)
49 % plot(Omega,-Omega,'--k','LineWidth',2)
50 hold off
51 xlabel('Spin speed [RPM]')
52 ylabel('Whirl speed [RPM]')
53 title('Campbell Diagram')
```

```
54
55
56 end
```

```
1  function Stability( Model_obj, Omega,ax,linetp )
2  %STABILITY Summary of this function goes here
3  %   Detailed explanation goes here
4  zci = @(v) find(v(:).*circshift(v(:), [-1 0]) <= 0);
5  if nargin < 4
6      linetp = '-';
7      if nargin < 3
8          figure
9          ax = axes;
10     elseif nargin < 2
11         return
12     end
13
14 end
15
16 for ii = 1:1:length(Omega)
17     w = Omega(ii)/60*2*pi;
18     Mnew = Model_obj.M;
19     Cnew = real(Model_obj.C) + w.*imag(Model_obj.C);
20     Knew = real(Model_obj.K) + w.*imag(Model_obj.K);
21
22     Zer = zeros(size(Mnew));
23     ey = eye(size(Mnew));
```

```
24      A = [-Mnew^-1*Cnew, -Mnew^-1*Knew;
25           ey, Zer];
26      v1=eig(A);
27      eiv(:,ii) = sort(v1);
28  end
29  while min(abs(imag(eiv(1,:)))) == 0
30      eiv(1:2,:) = [];
31  end
32  eiv = eiv( ~any( isnan( eiv ) | isinf( eiv ), 2 ),: );
33  hold on
34  plot(Omega,max(real(eiv)),'LineWidth',1,'LineStyle',linetp);
35  ZeroCross = Omega(zci(max(real(eiv))));
36  if ~isempty(ZeroCross)
37      strcross = ['  Threshold: ' num2str(ZeroCross(1),4) 'RPM'
            ];
38      text(ZeroCross(1),0,strcross,'HorizontalAlignment','left'
            ,'VerticalAlignment','middle','FontWeight','bold','
            Rotation',90);
39      plot(ZeroCross(1),0,'*k'); hold off
40  end
41  ax.XAxisLocation = 'origin';
42  xlabel('Speed (RPM)')
43  ylabel('Maximum \Re(s)')
44  title('Stability region')
45  end
```

```
1  function Damping(Model_obj,Omega,plotmodes,ax,linetp,ch)
```

```
2  %CAMPBELL Summary of this function goes here
3  %   Detailed explanation goes here
4  zci = @(v) find(v(:).*circshift(v(:), [-1 0]) <= 0);
5
6  if nargin < 6
7      if nargin == 2
8          plotmodes = 1:2;
9      elseif nargin < 2
10         return
11     end
12     ch = 'dec';
13     if nargin < 5
14         linetp = '-';
15     end
16     if nargin < 4
17         figure
18         ax = axes;
19     end
20 end
21
22 for ii = 1:1:length(Omega)
23     w = Omega(ii)/60*2*pi;
24     Mnew = Model_obj.M;
25     Cnew = real(Model_obj.C) + w.*imag(Model_obj.C);
26     Knew = real(Model_obj.K) + w.*imag(Model_obj.K);
27
28     Zer = zeros(size(Mnew));
```

```
29      ey = eye(size(Mnew));
30      A = [-Mnew^-1*Cnew, -Mnew^-1*Knew;
31           ey, Zer];
32      v1=eig(A);
33           [~, I] = (sort(abs((v1))));
34      eiv(:,ii) = v1((I));
35  end
36
37  while min(abs(imag(eiv(1,:)))) == 0
38      eiv(1:2,:) = [];
39  end
40  eiv = eiv( ~any( isnan( eiv ) | isinf( eiv ), 2 ),: );
41
42  hold on
43  for jj = 1:1:length(plotmodes)
44      idf = plotmodes(jj)*4-1; %forward mode index location
45      idb = idf - 2; %backward mode index location
46      zeta = -real(eiv([idb,idf],:))./abs(eiv([idb,idf],:));
47  %       delta = 2*pi.*zeta./sqrt(1-zeta.^2); %Logarithmic
        Decriment
48  %       delta = -2*pi*real(eiv([idb,idf],:))./imag(eiv([idb,idf
        ],:));
49      plot(Omega,zeta(1,:),linetp,'Color',[0,0.4470,0.7410],'
            LineWidth',1);
50      plot(Omega,zeta(2,:),linetp,'Color'
            ,[0.8500,0.3250,0.0980],'LineWidth',1);
51      ZeroCross1 = Omega(zci(zeta(1,:)));
```

```
52      ZeroCross2 = Omega(zci(zeta(2,:)));
53      if isempty(ZeroCross1)
54      else
55      strcross1 = [num2str(ZeroCross1(1),4) newline];
56      text(ZeroCross1(1),0,strcross1,'HorizontalAlignment','
            left','VerticalAlignment','bottom','FontWeight','bold'
            );
57      plot(ZeroCross1(1),0,'*k');
58      end
59      if isempty(ZeroCross2)
60      else
61      strcross2 = [ num2str(ZeroCross2(1),4) newline];
62      text(ZeroCross2(1),0,strcross2,'HorizontalAlignment','
            left','VerticalAlignment','bottom','FontWeight','bold'
            );
63      plot(ZeroCross2(1),0,'*k');
64      end
65
66  end
67  hold off
68  ax.XAxisLocation = 'origin';
69  xlabel('Speed (RPM)')
70  ylabel('\zeta')
71  title('Damping Characteristics')
72
73  end
```

```
function Shape(Model_obj,Omega,plotmodes,ax,linetp )
%CAMPBELL Summary of this function goes here
%   Detailed explanation goes here
if nargin < 5
    if nargin < 2
        return
    end
    linetp = '-';
    if nargin < 4
        figure
        ax = axes;
    end
end

syms x;
l=1;
z=x/l;
alph=.25;
Tt1 = (1/(1+alph))*(2*z^3 - 3*z^2 - alph*z + 1 + alph);
Tt2 = (1/(1+alph))*(-2*z^3+3*z^2+alph*z);
Tr1 = (l/(1+alph))*(z^3 - (2+1/2*alph)*z^2 + (1+1/2*alph)*z);
Tr2 = (l/(1+alph))*(z^3 - (1-1/2*alph)*z^2 - 1/2*alph*z);
cpsi = [Tt1   0     0   Tr1   Tt2   0     0   Tr2;
        0   Tt1   -Tr1   0     0   Tt2   -Tr2   0];
% psi = [1 - 3*(x/l)^2 + 2*(x/l)^3, x - 2*l*(x/l)^2 + l*(x/l)
    ^3, 3*(x/l)^2 - 2*(x/l)^3, -l*(x/l)^2 + l*(x/l)^3];
% cpsi = [psi(1),       0,        0, psi(2), psi(3),       0,
```

```
          0, psi(4);
%      0, psi(1), -psi(2),       0,       0, psi(3), -psi(4),
          0];
ipts = 4;
d = (0:ipts-1)/ipts;
for ii = 1:1:length(d)
    Nx(ii,:) = subs(cpsi(1,:),x,d(ii));
    Ny(ii,:) = subs(cpsi(2,:),x,d(ii));
end
Nx = double(Nx);
Ny = double(Ny);
w = Omega/60*2*pi;
Mnew = Model_obj.M;
Cnew = real(Model_obj.C) + w.*imag(Model_obj.C);
Knew = real(Model_obj.K) + w.*imag(Model_obj.K);
nM = length(Mnew);

% Zer = zeros(nM);
% AA=[Cnew Mnew;Mnew Zer];
% B=[Knew Zer;Zer -Mnew];
    Zer = zeros(size(Mnew));
    ey = eye(size(Mnew));
    A = [-Mnew^-1*Cnew, -Mnew^-1*Knew;
         ey,Zer];

[V,D] = eig(A,'vector');
% ind=find( (imag(D) > 0) & (abs(D)>1e-3) );     % take
```

```
    positive frequencies only
% l1=D(ind);
% v1=V(nM+1:end,ind);
l1=D;
v1=V(nM+1:end,:);
% v1=V(1:nM,:);
[~, I] = sort(abs((l1)));
l2 = D(I);
v2 = V(:,I);
v = v2(:,plotmodes);
v=v/norm(v);
for ii = 1:1:length(Model_obj.M)/4-1
    Li = Model_obj.npos(ii+1)-Model_obj.npos(ii);
    Nxnew = Nx*diag([1 1 1 Li 1 1 1 Li]);
    Nynew = Ny*diag([1 1 Li 1 1 1 Li 1]);
    pos(ipts*(ii-1)+1:ipts*(ii-1)+ipts+1) = linspace(
        Model_obj.npos(ii),Model_obj.npos(ii+1),ipts+1);
    pos(end)=[];
    shapex(ipts*(ii-1)+1:ipts*(ii-1)+ipts) = Nxnew*v(4*(ii-1)
        +1:4*(ii-1)+8);
    shapey(ipts*(ii-1)+1:ipts*(ii-1)+ipts) = Nynew*v(4*(ii-1)
        +1:4*(ii-1)+8);
end
pos = [pos, Model_obj.npos(end)];
shapex = [shapex, v(nM-3)];
shapey = [shapey, v(nM-2)];
plot(ax,[pos;pos]',real([shapex; shapey])')
```

```
75 hold on
76 for ii = 1:length(Model_obj.npos)
77     plot([Model_obj.npos(ii);Model_obj.npos(ii)]',real([
           shapex(ipts*(ii-1)+1); shapey(ipts*(ii-1)+1)])','.k','
           MarkerSize',8)
78 end
79 hold off
80 figure
81 cpts = 20;
82 theta = linspace(0,2*pi,cpts);
83 for ii =1:length(shapex)
84     xx(:,ii)=real(shapex(ii))*cos(theta) - imag(shapex(ii))*
           sin(theta);
85     y(:,ii)=real(shapey(ii))*cos(theta) - imag(shapey(ii))*
           sin(theta);
86 end
87 N = repmat(pos,cpts,1);
88 hold on
89 plot3(real(shapex),pos,real(shapey),'-k')
90
91 plot3(xx,N,y,'Color',[0,0.4470,0.7410])
92
93 for ii = 1:length(Model_obj.npos)
94     plot3(real(shapex(ipts*(ii-1)+1)),Model_obj.npos(ii),real
           (shapey(ipts*(ii-1)+1)),'.k','MarkerSize',8)
95 end
96
```

```
97  hold off
98  mx = max([abs(shapex),abs(shapey)]);
99  axis([-mx, mx, -inf, inf,-mx, mx ]);
100 disp(['Damping: ' num2str(real(l2(plotmodes))) '. Frequency:
        ' num2str(imag(l2(plotmodes))/2/pi*60) '(RPM).'])
101 ax=gca;
102 ax.XDir='reverse';
103 ax.Title.String={(['\Re(s): ' num2str(real(l2(plotmodes)),2)
        ', \Im(s): ' num2str(imag(l2(plotmodes))/2/pi*60,4) '[RPM]
        ']);(['\Omega: ' num2str(Omega,4) '[RPM]'])};
104 %
105 % [V, D] = eig(Knew, Mnew,'vector');
106 % D = sqrt(D)*60/2/pi;
107 % [D, ind] = sort(abs(D));
108 % D(plotmodes)
109 % V = V(:,ind);
110 % v2 = (V(:,plotmodes));
111 % v3 = reshape(v2,4,[]);
112 % v4 = bsxfun(@times, v3, 1./sqrt(sum(v3.^2, 2)));
113 % v2 = reshape(v4,1,[])';
114 % for ii = 1:1:length(Model_obj.M)/4-1
115 %     shape(8*(ii-1)+1:8*(ii-1)+8) = N*v2(4*(ii-1)+1:4*(ii-1)
        +8);
116 % end
117 % shape = [shape, v2(end-3)];
118 % plot(real(shape))
119
```

```
120
121 % if isempty(ax)
122 %     figure
123 %     ax = axes;
124 % end
125 %
126 % hold on
127 % for jj = 1:1:length(plotmodes)
128 %     pv(1,:) = real(eivect(speed,[4.*(1:14)-3],plotmodes(jj)
    ));
129 %
130 %     plot(pv)
131 % end
132 % hold off
133
134
135 end
```

```
1 function FreqResponse(Model_obj, Omega, node, plottype, fi,
    linetp )
2 if nargin < 6
3     if nargin == 2
4         node = 1;
5     elseif nargin < 2
6         error('Not enough input arguments.\n Provide: Omega(
            required), node #s(optional), axes(optional),
            linetype(optional)',class(Model_obj))
```

```
7       end
8       linetp = '-';
9       if nargin < 5
10          fi = figure;
11          ax = axes(fi);
12          if nargin < 4
13              plottype = 'Bode';
14          end
15          if strcmp(plottype,'Bode') == 1
16              ax(1)=subplot(2,1,1,ax);
17              ax(2)=subplot(2,1,2);
18          end
19      end
20
21  end
22
23  for ii = 1:1:length(Omega)
24      w = Omega(ii)/60*2*pi;
25      Fnew = w^2.*(Model_obj.F);
26      Mnew = Model_obj.M;
27      Cnew = real(Model_obj.C) + w.*imag(Model_obj.C);
28      Knew = real(Model_obj.K) + w.*imag(Model_obj.K);
29      n=length(Mnew);
30      I=kron(eye(n/2),diag([1,1i]));
31      Z = I*(Knew + 1i*w.*Cnew - w^2.*Mnew);
32      X(ii,:) = Z^-1*Fnew;
33  end
```

```
34 switch plottype
35     case 'FreqResponse'
36         hold on
37         for jj = 1:1:length(node)
38             ax=fi.Children;
39             plot(ax, Omega,(abs(X(:,node(jj)*4-3))),linetp)
40             plot(ax, Omega,(abs(X(:,node(jj)*4-2))),linetp)
41             ax.YScale = 'log';
42         end
43         hold off
44         ax.XLabel.String='Spin Speed \Omega[RPM]';
45         ax.YLabel.String='Amplitude[m]';
46     case 'Bode'
47         hold on
48         for jj = 1:1:length(node)
49             subplot(211); hold on
50             ax(1)=fi.Children(1);
51 %             plot(Omega,abs(X(:,node(jj)*4-3)),linetp)
52 %             plot(Omega,abs(X(:,node(jj)*4-2)),linetp)
53             plot(ax(1),Omega,abs(39370.1*X(:,node(jj)*4-3)),
                   linetp)
54             plot(ax(1),Omega,abs(39370.1*X(:,node(jj)*4-2)),
                   linetp)
55             ax(1).YScale = 'log';
56             ax(1).XLabel.String='Spin Speed \Omega[RPM]';
57 %             ax(1).YLabel.String='Amplitude[m]';
58             ax(1).YLabel.String='Amplitude[mils]';
```

```
59                subplot(212); hold on
60                ax(2)=fi.Children(2);
61 %                 plot(Omega,unwrap(mod(angle(X(:,node(jj)*4-3))
       ,2*pi)),linetp)
62 %                 plot(Omega,unwrap(mod(angle(X(:,node(jj)*4-2))
       ,2*pi)),linetp)
63                plot(ax(2),Omega,180/pi*unwrap(mod(angle(X(:,node
                      (jj)*4-3)),2*pi)),linetp)
64                plot(ax(2),Omega,180/pi*unwrap(mod(angle(X(:,node
                      (jj)*4-2)),2*pi)),linetp)
65                ax(2).XLabel.String='Spin Speed \Omega[RPM]';
66 %                 ax.YLabel.String='Phase Angle[Rad]';
67                ax(2).YLabel.String='Phase Angle[deg.]';
68 %                 ax.YTick=[-3*pi/2:pi/2:0];
69 %                 ax.YTickLabel={'-3\pi/2','-\pi','-\pi/2','0'};
70                ax(2).YTick=[-360:90:0];
71                ax(2).YTickLabel={'0','-270','-180','-90','0'};
72           end
73           hold off
74
75
76 end
77 % plot(Omega,max(abs(X)'))
78 % ax = gca;
79 % ax.YScale = 'log';
```

```
1 classdef RotorData < handle
```

```
2       properties
3           X %Horizontal Signal
4           Y %Vertical Signal
5           ref %Keyphasor Signal
6           Fs %Sampling Rate (Samp/Sec)
7           Fres %Frequency Resolution
8           n %filter synchronous multiplier: 1X, 2X, 3X, ... nX
                the running speed
9       end
10      properties (SetAccess = private)
11          Zf %Total Amplitude
12          Phase %Phase
13          Amp %Property that holds X and Y amplitudes
14          Speed %RPM
15      end
16      properties (Access = private)
17          refchop %%%%%%%%%%
18          xchop   %% Organizes the data arrays into matrices
                based on windows
19          ychop   %%%%%%%%%%
20      end
21      properties (Dependent, Access = private)
22          NW %Number of windows
23          freq %Frequency
24          nspw %Number of samples per window
25
26      end
```

```
27      methods
28          function obj = RotorData(x, y, r, f, fres)%Fills
               properties with data
29              if nargin == 5
30                  obj.X = x;
31                  obj.Y = y;
32                  obj.ref = r;
33                  obj.Fs = f;
34                  obj.Fres = fres;
35              end
36          end
37          function set.X(obj, val)
38              obj.X = val;
39          end
40          function set.Y(obj, val)
41              obj.Y = val;
42          end
43          function set.ref(obj, val)
44              obj.ref = val;
45          end
46          function set.Fs(obj, val)
47              obj.Fs = val;
48              if isempty(obj.X) || isempty(obj.Y) || isempty(
                   obj.ref) || isempty(obj.Fs) || isempty(obj.
                   Fres)
49              else
50                  obj.update;
```

```
51              end
52          end
53          function set.Fres(obj, val)
54              obj.Fres = val;
55              if isempty(obj.X) || isempty(obj.Y) || isempty(
                    obj.ref) || isempty(obj.Fs) || isempty(obj.
                    Fres)
56              else
57                  obj.update;
58              end
59          end
60          function set.n(obj, val)
61              obj.n = val;
62              if isempty(obj.X) || isempty(obj.Y) || isempty(
                    obj.ref) || isempty(obj.Fs) || isempty(obj.
                    Fres)
63              else
64                  obj.update;
65              end
66          end
67          function nspw = get.nspw(obj)
68              nspw = ceil(obj.Fs/obj.Fres);
69          end
70          function freq = get.freq(obj)
71              df = obj.Fs/obj.nspw;
72              f = df*(0:obj.nspw-1);
73              Q = ceil((obj.nspw+1)/2); % M/2+1 for M even
```

```
74              fQ = df*(Q-1);
75              freq = f-fQ;
76          end
77          function NW = get.NW(obj)
78              NW = floor(length(obj.X)/obj.nspw); %Rounds
                    number of windows down to closest integer
79          end
80          function filter(obj)
81              disp('filtering')
82              for i = 1:1:obj.NW
83                  Fpass1 = obj.Speed(i)*obj.n/60-5; %Upper
                        frequency of bandpass filter
84                  Fpass2 = obj.Speed(i)*obj.n/60+5; %Lower
                        frequency of bandpass filter
85                  if i == 1
86                      h  = fdesign.bandpass('N,Fp1,Fp2,Ast1,Ap,
                            Ast2', 10, Fpass1, Fpass2, 50, .1, 50,
                             obj.Fs);
87                      Hd(i) = design(h, 'ellip');
88                      Hd(i).persistentmemory = true;
89                      obj.xchop(:,i) = filter(Hd(i),obj.xchop
                            (:,i)); %Apply filter to data
90                      xf = Hd(i).states;
91                      reset(Hd(i));
92                      obj.ychop(:,i) = filter(Hd(i),obj.ychop
                            (:,i)); %||
93                      yf = Hd(i).states;
```

```
94                  else
95                      h  = fdesign.bandpass('N,Fp1,Fp2,Ast1,Ap,
                            Ast2', 10, Fpass1, Fpass2, 50, .1, 50,
                             obj.Fs);
96                      Hd(i) = design(h, 'ellip');
97                      Hd(i).persistentmemory = true;
98                      Hd(i).states = xf;
99                      obj.xchop(:,i) = filter(Hd(i),obj.xchop
                            (:,i)); %Apply filter to data
100                     xf = Hd(i).states;
101                     Hd(i).states = yf;
102                     obj.ychop(:,i) = filter(Hd(i),obj.ychop
                            (:,i)); %||
103                     yf = Hd(i).states;
104                 end
105             end
106         end
107         function update(obj)
108             obj.xchop = zeros(obj.nspw,obj.NW);
109             obj.ychop = zeros(obj.nspw,obj.NW);
110             obj.refchop = zeros(obj.nspw,obj.NW);
111             obj.Speed = zeros(obj.NW,1);
112             x = obj.X(1:obj.nspw*obj.NW);
113             y = obj.Y(1:obj.nspw*obj.NW);
114             r = obj.ref(1:obj.nspw*obj.NW);
115             obj.xchop = reshape(x,obj.nspw,obj.NW);
116             obj.ychop = reshape(y,obj.nspw,obj.NW);
```

```
117             obj.refchop = reshape(r,obj.nspw,obj.NW);
118             for i = 1:1:obj.NW
119                 pp = pulseperiod(obj.refchop(:,i),obj.Fs,'
                        Tolerance',7);
120                 obj.Speed(i) = 1./mean(pp)*60;
121             end
122             if ~isempty(obj.n) && ~obj.n == 0
123                 filter(obj)
124             end
125
126             obj.Amp.XAmp = max(obj.xchop) - min(obj.xchop); %
                    Calculates Amplitude by subtracting min and
                    max from each column
127             obj.Amp.YAmp = max(obj.ychop) - min(obj.ychop); %
                    Calculates Amplitude by subtracting min and
                    max from each column
128             Zwin = hanning(obj.nspw, 'Periodic');
129             Z = obj.xchop + 1i*obj.ychop;
130             for i = 1:1:obj.NW
131                 Z(:,i) = Zwin.*Z(:,i);
132             end
133             obj.Zf = 2*abs(fft(Z)/obj.nspw);
134             obj.Zf = fftshift(obj.Zf',2); %Shifts graph to
                    center on the x axis
135
136             obj.Phase.PhaseX = zeros(obj.NW,1);
137             obj.Phase.PhaseY = zeros(obj.NW,1);
```

```
138             distance = .5*obj.Fs/100;
139             threshold = .5*(max(obj.refchop(:,ceil(end/2))) -
                    mean(obj.refchop(:,ceil(end/2))));
140             for i = 1:1:obj.NW
141                 [~, locsref] = findpeaks(obj.refchop(:,i),'
                        MinPeakHeight',threshold,'MinPeakDistance'
                        ,distance);
142                 [~, locsX] = findpeaks(obj.xchop(:,i),'
                        MinPeakProminence',1,'MinPeakDistance',
                        distance);
143                 [~, locsY] = findpeaks(obj.ychop(:,i),'
                        MinPeakProminence',1,'MinPeakDistance',
                        distance);
144                 if length(locsref) < 2 || length(locsX) < 2
                        || length(locsY) < 2
145                     obj.Phase.PhaseX(i) = NaN;
146                     obj.Phase.PhaseY(i) = NaN;
147                 else
148                     if length(locsX) ~= length(locsY)
149                         if length(locsX) < length(locsY)
150                             if abs(locsX(1) - locsY(1)) < abs
                                    (locsX(end) - locsY(end))
151                                 locsY(end) = [];
152                             else
153                                 locsY(1) = [];
154                             end
155                         else
```

```
156                     if abs(locsX(1) - locsY(1)) < abs
                           (locsX(end) - locsY(end))
157                         locsX(end) = [];
158                     else
159                         locsX(1) = [];
160                     end
161                 end
162             end
163             if locsref(1) > locsX(1) || locsref(1) >
                   locsY(1)
164                 locsX(1) = [];
165                 locsY(1) = [];
166             end
167             if length(locsref) > length(locsX)
168                 locsref(length(locsX):end) = [];
169             end
170             phx = zeros(length(locsref)-1,1);
171             phy = zeros(length(locsref)-1,1);
172             for j = 1:1:length(locsref)-1
173                 phx(j) = mod((locsX(j) - locsref(j))
                       /(locsref(j+1) - locsref(j))*2*pi
                       ,2*pi);
174                 phy(j) = mod((locsY(j) - locsref(j))
                       /(locsref(j+1) - locsref(j))*2*pi
                       ,2*pi);
175             end
176             obj.Phase.PhaseX(i) = 180/pi*mod(mean(phx
```

```
                    (:)),2*pi);
177                 obj.Phase.PhaseY(i) = 180/pi*mod(mean(phy
                    (:)),2*pi);
178                 clear locsref locsX locsY j
179             end
180         end
181
182     end
183     function acqListener(obj, src, event)
184         obj.newData = [event.TimeStamps, event.Data]';
185         obj.ref = [obj.ref, event.Data(1,:)];
186         obj.X = [obj.X, event.Data(2,:)];
187         obj.Y = [obj.Y, event.Data(3,:)];
188         obj.update;
189
190     end
191     %Plotting functions below
192     bode(obj)
193     cascade(obj)
194     obj = downsample(obj,r)
195     orbit3(obj)
196     orbitAnimation(obj)
197     mainplot(obj)
198 end
199 end
```

```
1 function bode(obj)
```

```
figure('Name','Bode Plot')
subplot(211)
plot(obj.Speed,obj.Amp.XAmp,obj.Speed,obj.Amp.YAmp)
xlabel('Running Speed (RPM)');
ylabel('Amplitude (mils)');
legend('Horizontal Plane','Vertical Plane');
subplot(212)
plot(obj.Speed,obj.Phase.PhaseX,obj.Speed,obj.Phase.PhaseY)
xlabel('Running Speed (RPM)');
ylabel('Phase lag (deg.)');
set(gca,'ytick',-720:45:720,'YTickLabel',{'0','45','90','135'
    ,'180','225','270','315'})
end
```

```
function cascade(obj)
figure('name','Cascade Plot')
waterfall(obj.freq, obj.Speed, obj.Zf)
xlabel('Frequency of Vibration (Hz)');
ylabel('Running Speed (RPM)');
zlabel('Amplitude of Vibration (mils)');
axis([-100 100 -inf inf 0 inf])
end
```

```

function orbit3(obj)
N = length(obj.X(:));
F = (obj.Speed(end) - obj.Speed(1))/N*(0:N-1) + obj.Speed(1);
s = fix(sqrt(N));
```

```
Xlin = obj.X(1:s^2);
Ylin = obj.Y(1:s^2);
w = F(1:s^2);
x = reshape(Xlin,s,s);
y = reshape(Ylin,s,s);
o = reshape(w,s,s);
C = sqrt(x.^2+y.^2);
h = mesh(o,x,y,C);
axis([1000 2000 -inf inf -inf inf]);
xlabel('Running Speed (RPM)');
ylabel('Horizontal Amplitude (mils)');
zlabel('Vertical Amplitude (mils)');
h.FaceColor = 'none';
h.MeshStyle = 'column';
end
```

```
function orbitAnimation(obj)

distance = .5*obj.Fs/100;
threshold = .5*(max(obj.refchop(:,ceil(end/2))) - mean(obj.
    refchop(:,ceil(end/2))));
[~, loc] = findpeaks(obj.ref,'MinPeakHeight',threshold,'
    MinPeakDistance',distance);
pksx=obj.X(loc);
pksy=obj.Y(loc);
Fsh = obj.Fs;
maxlm = max(obj.X);
```

```
10 speedarray = (obj.Speed(end)-obj.Speed(1))/length(pksy)*(0:
       length(pksy)-1)+obj.Speed(1);
11 for i = 1:1:length(pksx)-1;
12     plot(obj.X(loc(i):loc(i+1)-fix((1/10)*(loc(i+1)-loc(i))))
           ,obj.Y(loc(i):loc(i+1)-fix((1/10)*(loc(i+1)-loc(i)))),
           '-k',pksx(i),pksy(i),'.','markersize',15)
13     text = [' Running Speed: ',num2str(fix(speedarray(i)),4),
           ' (RPM)'];
14     uicontrol('Style', 'text',...
15         'String',text,...
16         'Units','normalized',...
17         'Position', [.25 .9 0.5 .05]);
18     axis([-maxlm maxlm -maxlm maxlm]);
19     axis square
20     xlabel('Horizontal Amplitude (mils)');
21     ylabel('Vertical Amplitude (mils)');
22 %      pause(1/Fsh)
23     pause
24
25 end
26 end
```